



Sustainable steels for direct deposition of photovoltaic solar cells

(STEELPV)

FINAL REPORT

Sustainable steels for direct deposition of photovoltaic solar cells (STEELPV)

European Commission

Directorate-General for Research and Innovation

Directorate D - Industrial Technologies

Unit D.4 — Coal and Steel

Contact Hervé Martin

E-mail RTD-PUBLICATIONS@ec.europa.eu

European Commission

B-1049 Brussels

Manuscript completed in 2019.

This document has been prepared for the European Commission however it reflects the views only of the authors, and the Commission cannot be held responsible for any use which may be made of the information contained therein.

More information on the European Union is available on the internet (<http://europa.eu>).

Luxembourg: Publications Office of the European Union, 2019

PDF

ISBN 978-92-79-98303-0

ISSN 1831-9424

doi: 10.2777/453905

KI-NA-29-523-EN-N

© European Union, 2019.

Reuse is authorised provided the source is acknowledged. The reuse policy of European Commission documents is regulated by Decision 2011/833/EU (OJ L 330, 14.12.2011, p. 39).

For any use or reproduction of photos or other material that is not under the EU copyright, permission must be sought directly from the copyright holders.

All pictures, figures and graphs © Fundación ITMA, RFSR-CT-2014-00014 STEELPV

European Commission

Research Fund for Coal and Steel

Sustainable steels for direct deposition of photovoltaic solar cells **(STEELPV)**

Pascal Sanchez

Fundación ITMA

Parque Tecnológico de Asturias, ES-33428 Llanera (Spain)

Yun Lan

MK Metallfolien GmbH

Volmarsteiner strasse 1-9, DE-58089 Hagen (Germany)

José María Delgado

Abengoa Solar New Technologies SA

Calle energía solar 1 campus palmas altas, ES-41014 Sevilla (Spain)

Jeffrey Kettle

Bangor University

College road, GB-LL57 2DG Bangor (United Kingdom)

Stefano Lionetti

Centro Sviluppo Materiali SPA

Via di castel romano 100, IT-00128 Roma (Italy)

David Gethin

University of Wales Swansea

Singleton park, GB-SA2 8PP Swansea (United Kingdom)

Grant Agreement RFSR-CT-2014-00014
01/07/2014 – 31/12/2017

Final report

Directorate-General for Research and Innovation

Table of contents

Table of contents.....	3
Final summary	5
Scientific and technical description of the results	15
1. Objectives of the project	15
2. Description of activities and discussion	17
2.1. WP1: Selection of low cost steels for PV applications	17
2.1.1. Steel substrates specifications and steel selection (01/07/2014-30/06/2015_Task 1.1).....	17
2.1.2. Manufacture cost-efficient flexible steel substrates (01/01/2015-31/03/2017_Task1.2)	19
2.1.3. Inspection methodology (01/04/2015 -31/12/2015 _ Task1.3)	21
2.2. WP2: Preparation of low cost steels substrates for PV applications: intermediate layers developments at lab scale level.....	25
2.2.1. Tasks 2.1, 2.2 and 2.3. Lab-scale intermediate layers developments and characterizations (01/04/2015-30/09/2016).....	26
a) ILs developed through the wet route	26
b) ILs developed through the vacuum route	41
c) ILs developed through the hybrid route	46
2.2.2. Intermediate layers characterization through the back contact PV cell deposition (01/10/2015 - 30/09/2016 _ Task2.3).....	51
2.2.3. Lab-scale roll-to-roll (01/10/2015 - 30/09/2016 _ Task2.4)	53
2.3. WP3: Demonstrator of direct thin film PV depositions on steel/IL at lab scale level.....	57
2.3.1. Deposition of small solar cells on steel/ILs substrates (01/01/2016-30/09/2016_Task 3.1)	57
a) Amorphous silicon (a-Si) TFSC.....	57
b) OPV TFSC.....	59
c) CZTS (Kesterite) TFSC	61
d) Perovskite TFSC.....	61
2.3.2. Steel/ILs protection during the storage (01/01/2016-31/12/2016_Task3.2).....	62
2.3.3. Encapsulation of the steel and aging tests (01/01/2016-31/12/2016_Task3.3)	65
2.4. WP4: Up-scaling of steel/ILs at pilot line level: validation and viability (WP leader_ SU).....	67
2.4.1 In-house SiO _x sol-gel.....	67
2.4.2. Commercial Blue ink IL up-scaling.....	75
2.4.3. ILs based on hybrid sol-gel/ vacuum	81
3. Exploitation and impact of the research results	93
3.1. Actual applications.....	93
3.2. Technical and economic potential for the use of the results.....	93
3.3. Publications/conferences.....	100
3.4. Other aspects concerning the dissemination of the results.....	103
4. Conclusions	105
List of figures.....	107
List of tables.....	111
List of acronyms and abbreviations used in the report.....	113
List of references.....	115

Final summary

The main purpose of STEELPV project was to propose technical and economic feasible alternatives to the stainless steel solar grade (SSSG) currently used as substrate for direct deposition of thin film solar cells (TFSC). In this way, low cost industrial steels were functionalized by applying intermediate layers (IL) and coating technologies compatible with an industrial implantation. Furthermore, the economic objective was to propose steel/IL prototypes with a cost below 8€/m² (direct comparison with the SSSG) and below 0.1€/W (6€/m², 10€/m² and 15€/m², respectively for OPV, a-Si and CIGS) making a direct comparison with the maximum affordable substrate cost for each TFSC technology considered in STEELPV.

It can be point out that the SSSG cost is higher than the maximum affordable substrate cost for OPV and may explain why the SSSG is only currently commercially used for a-Si and CIGS TFSC.

As main innovation, it was expected to:

- Propose new market niche for structural steel grades.
- Reduce the cost of steel substrate for TFSC application.
- Make economically feasible a range of steel thicknesses in order to propose several classes of building integrated photovoltaic (BIPV) modules: flexible foil (≤ 0.1 mm); semi-flexible modules (> 0.1 mm); semi-rigid modules (> 0.5 mm).

The below summary addresses the most significant aspects on a task by task basis.

WP1_ Steel selection

Task1.1

Based on TFSC and IL requirements (wet and vacuum processes, maximum temperatures of 500°C, coefficient of thermal expansion (CTE), etc.) and the objective to work with 'low cost' structural steels, four steels were selected:

- AISI430 stainless steel,
- DX51D + Z (zinc hot-dip metallic coated) low carbon steel,
- DX51D + AS (aluminium/silicon hot-dip metallic coated) low carbon steel,
- DC01 (bare) low carbon steel.

Task1.2

Before the IL deposition, a mechanical preparation of the four steels was carried out in order to:

- Reduce the native steel roughness to a range technically and economically affordable for the IL approaches (It was established maximum average roughness_R_a of 0.2µm and peak-to-valley roughness_R_z of 1.5µm).
- Improve the homogeneity of the native steel substrates.
- Reduce the native thickness to a one suitable for lab-scale and pilot plant experiments (it was decided to work with 0.3mm thick steels what is 10 times thicker than current commercial SSSG).

For this selected thickness, different cold rolled processes have been tested from the lower cost, high steel speed (HSS) grinding to a higher cost, hardened finishing process. Although significant improvements were expected after first iterations, it was finally decided to work only with the cold rolled steels by HSS grinding process, as supplementary expensive rolling treatments did not drive to an effective improvement in surface quality.

To avoid an increase of the process cost, no post annealing treatment was initially applied to recover the native mechanical properties of the steel substrates. Indeed, the steel substrates would not have to endure bending process before and after TFSC manufacturing. However, during STEELPV developments, a severe oxidation of the AISI430 substrate at high IL and TFSC air atmosphere temperatures was detected. This problem was solved applying a reductive annealing treatment after the rolling process and a 20% increase of the AISI430 cost was estimated.

The Figure 1 reports the evolution of the cost (€/m²) of the four steels through the rolling process. The cost reference of the SSSG is represented by the black point and the black lines show the maximum affordable substrate costs for each TFSC technologies.

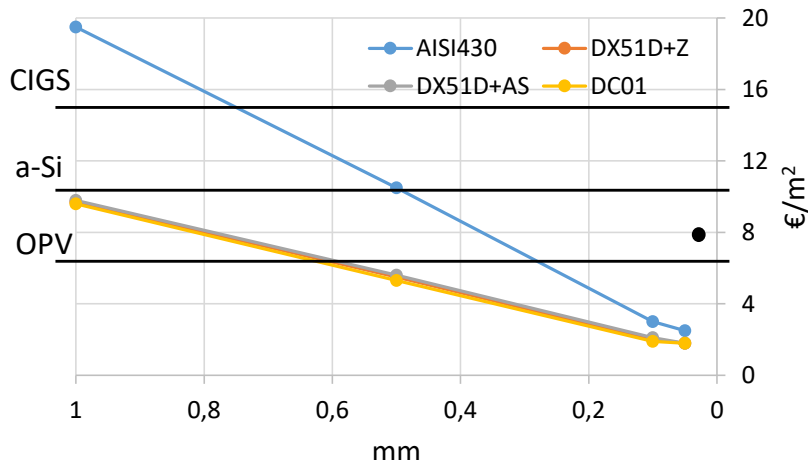


Figure 1. Steel substrates costs (€/m²) depending on the rolling final thickness. Comparison with the SSSG cost (at 25 μm) and the maximum affordable substrate cost depending on the TFSC technology.

Task1.3

The behaviour of the four HSS cold rolled steel substrates was studied through different thermal treatments that simulate IL and TFSC annealing processes considered in later work-packages. A deep characterization before and after these treatments were carried out in terms of superficial oxidation/corrosion, mechanical properties, roughness, chemical diffusion.

It was observed that the thermal treatments do not seem to have negative influence on most of steel substrate properties. However, superficial oxidation was detected for the AISI430 and DC01 steel substrates at high temperatures and air atmosphere thermal treatments. This formation of superficial oxides could pose challenges for high quality IL depositions and could form a delamination fault line for ILs due to the lack of adhesion.

Possible solutions to solve this problem could be carrying out the non-vacuum annealing treatments under inert atmosphere (e.g. a mixture of H₂/N₂), or in the case of the AISI430 steel, by applying an annealing treatment under reductive conditions (100% H₂, temperature of 1000°C in continuous furnace 10.5m/min) after the HSS rolling process.

WP2_ Intermediate layer developments at lab-scale level

Tasks2.1, 2.2 and 2.3

The development of the IL were based on wet and vacuum processes taking into account both the steel substrates and TFSC technologies. The following requirements were first established; i) **Levelling (Ra<40nm and Rz<350nm)**, to guarantee high quality TFSC deposition and to enable the monolithic TFSC serial interconnection, ii) **act as a dielectric barrier (>40V)**, to avoid shunts between the steel substrate and the TFSC and enable the monolithic TFSC serial interconnection, iii) **act as a diffusion barrier**, to avoid the steel element diffusion during the TFSC deposition and iv) **stability**, during the TFSC deposition and the storage step. The developments of the ILs were carried out taking in mind the use of scalable coating techniques and that the steel/rolling/IL prototypes have to fulfil a cost below 0.1€/W.

Looking at the **wet research line**, the challenge was to fulfil the above requirements using 'low cost' and good shelf life dissolutions using a single layer strategy. In-house SiO_x sol-gels were synthetized based on the following matrix; Methyltriethoxysilane (MTES 99%, Aldrich) and Tetraethylorthosilicate (TEOS 98%, Aldrich) as precursors. Water was incorporated as a solvent, PEG (Polyethilenglycol) as tension releasing agents and HNO₃ as a catalyst. Polyvinylpyrrolidone (PVP) or different PEG

concentrations and molecular weight were taken into account in order to reach ormosil and printing compatible formulations.

Several coating (spin, dip, spray, K-bar, blade, roll) and printing (flexography, screen and gravure) techniques were explored for their applications. In particular, the dip and spray coating methods, using the F1 SiO_x sol-gel formulation (PEG6000), enabled to reach single layers of 3μm giving positive results in terms of levelling, dielectric and antidiiffusion behaviours and stability. SiO_x sol-gels were also successfully applied by roll coating using a lab-scale roll-to-roll machine showing, this IL, a good stability during flexible tests. The F3 SiO_x sol-gel formulation (PEG200000) also gave good results by K-Bar coating.

In parallel, alternative wet commercial coatings to SiO_x sol-gel based on polymeric dielectric inks and epoxy coatings have been experimented. In particular, the 'blue ink' (D2140114D5_GEM) and the SU-8_2050 (Chestech) have shown their great potential in terms of levelling, dielectric and antidiiffusion behaviours and stability. They were applied through spin coating, K-bar and screen printing methods.

Figure 2 reports the levelling effect (R_z parameter is reported) achieved through the application of several wet IL and using different scalable techniques. The F1 and F3 sol-gel thicknesses were about 3μm, the blue ink_ one layer about 8μm, the blue ink_two layers about 20μm and the SU-8 about 50μm.

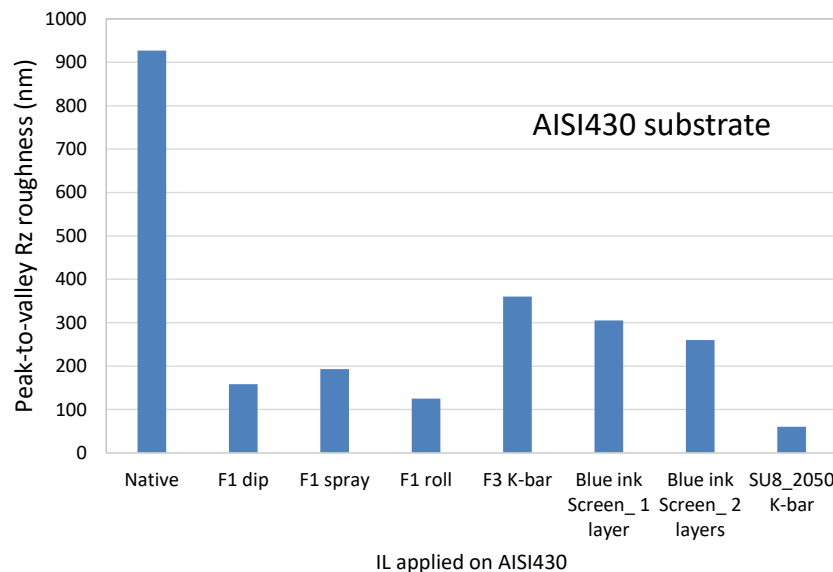


Figure 2. Comparison of the levelling effect depending on the wet IL applied on AISI430 substrate.

Related to ILs deposited by **vacuum technologies**, single and multilayers of ceramic oxides have been deposited by using i) PVD in reactive and non-reactive processes, ii) arc PVD and iii) PECVD. Due to conformal covering of these coatings, these techniques have not fulfilled all of the IL requirements (especially the surface levelling) by itself. A possible alternative corrective solution experimented was to reduce the steel roughness previously to the ILs deposition, but none of the finishing rolled processes tried have reported enough improvements. The options of this route have been then discarded for the up-scaled trials. However, the high quality of vacuum-based coatings constitutes a promising strategy for the achievement of suitable IL in combination with wet routes (hybrid systems).

Finally, **hybrid ILs combining vacuum and sol-gel processes** have shown successful results. Thin SiO_x sol-gel has been included in stack hybrid configurations (bi and tri-layers) combining it with SiO_x and Si₃N₄ layers deposited by PVD or PECVD vacuum techniques. The hybrid ILs have been developed to endure low and high temperature TFSC (up to 500°C). Figure 3 reports the levelling effect comparing it with the native AISI430 one. The thicknesses of the hybrid stacks were about 3-4μm and positive results terms of levelling, dielectric and antidiiffusion behaviours and stability were achieved.

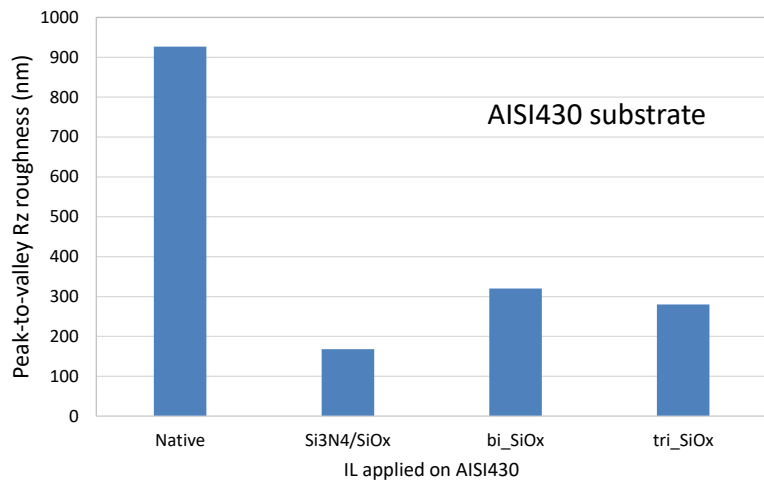


Figure 3. Comparison of the levelling effect depending on the hybrid IL applied on AISI430 substrate

Task 2.4

The different F1, F2 and F3 sol-gels formulations were experimented in the R2R process by using a 'two rolls' coating technique on 0.1mm AISI430, DX51D+Z and DX51D+AS coils. An in-line convection furnace was used to carry out the drying/curing stages. In addition to the characterization tests previously commented, flexible trials (using several working cylinders) were performed in order to evaluate the sol-gel behavior. Dielectric tests were carried out before and after the compression/traction cycles

As it can be observed in Table I, 100% of the metallic pads (18 (1cmx1cm) pads tested_ two samples) passed the dielectric insulation test considering the 90mm working cylinder and, at least 78% passed the dielectric insulation test considering the 50mm working cylinder. F2 IL shows slightly better results probably due to its more elastic formulation.

Table I. Percentage of metallic pad (18 pads tested) that passed the breakdown voltage test before and after flexibility experiments.

	Initial	90mm	50mm
AISI430 + F1	100%	100%	78%
AISI430 + F2	100%	100%	89%
DX51D+Z + F2	100%		89%
DX51D+AS + F2	100%		83%

WP3_ Direct TFSC depositions on steel/IL at lab-scale level

Task3.1

The compatibility of the lab-scale steel/IL systems with different TFSC technologies was studied considering the power conversion efficiency (PCE) of 1cm² solar cells and comparing it with TFSC grown on reference substrates (glass, PET). As reported in Figure 4 and Figure 5, several steel/IL candidates were compatible with, at least, one of the TFSC technologies proposed in STEELPV. Related to a-Si TFSC, sol-gel and hybrid SiO_x showed PCE similar to the reference substrate. Some improvements have to be carried out for the blue ink, but it is important to note that some smart efficiency is registered. No a-Si TFSC worked on the SU-8 IL. Concerning OPV TFSC, both SU-8 and sol-gel showed very similar results to the reference substrates. No OPV TFSC worked on the blue ink.

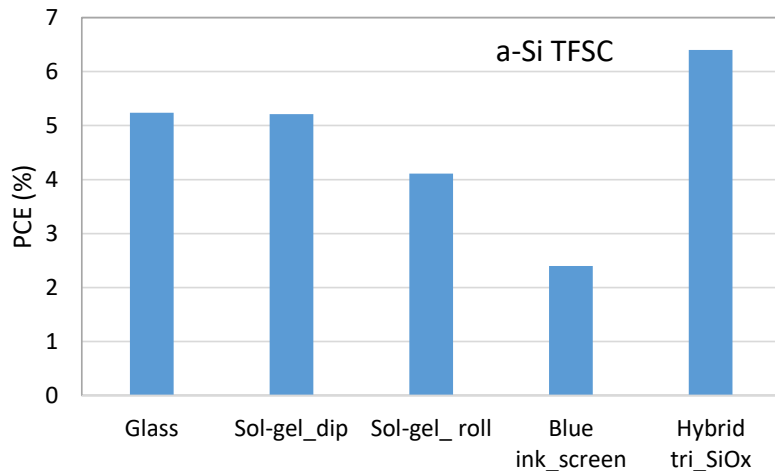


Figure 4. Efficiency (%) of a-Si TFSC deposited on a reference substrate (Glass) and on different steel/IL systems.

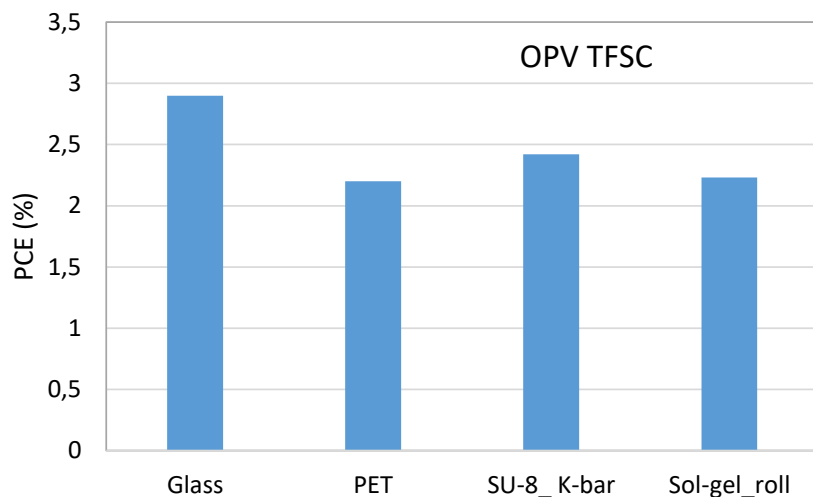


Figure 5. Efficiency (%) of OPV TFSC deposited on a reference substrate (Glass, PET) and on different steel/IL systems.

Task3.2

The study was focused on the IL stability through a simulation of a storage time (3 months). Several protection systems were experiments and the stability of the IL was evaluated through dielectric tests. The following steel/IL systems were considered steels/SiO_x sol-gel for the wet strategy, steels/polymeric ‘blue ink’ for the commercial dielectric inks and AISI430/SiO_x tri-layer for the hybrid approach. Considering the necessity to avoid the corrosion process and to propose cost effective steel/IL products, it was decided to consider specific anti-corrosion storage papers. This strategy has also the advantage that only a very light steel/IL cleaning will be needed before the TFSC manufacture.

Based on the breakdown voltage results, the following conclusions are made:

- Polymeric ‘blue ink’, independently from the steel substrate, shows the best performances.
- The AISI430+hybrid SiO_x samples stored in the VCI paper showed better performances respect to those stored in the no VCI paper.
- The majority of tested samples showed breakdown voltage properties higher than the lower limit requested in the ambit of STEELPV after the three months.
- DC01, even if breakdown voltage properties are satisfactory, could determine instability of the electrical properties. In fact, SEM analysis gave evidence of local detachment of the

coating. However, as the IL integrity seems stable, the deposition of TFSC should not be affected.

Task3.3

The purpose of this task was to give some guidelines about how to encapsulate the steel/IL products. In this way, several protective approaches were tried and tested through the IEC 61646 standard (*Thin-film terrestrial photovoltaic (PV) modules – Design qualification and type approval*). The different steels considered in STEELPV were encapsulated considering several standard transparent polymeric films of Ethylene tetrafluoroethylene (ETFE), polyvinyl butyral (PVB) and Ethylene-vinyl acetate (EVA). Moreover, polyethylene napthalate (PEN) and polyethylene terephthalate (PET) were considered to ensure an extra barrier against humidity and oxygen.

The encapsulation were carried out at two different temperature settings of 100°C and 135°C of the two most corrosion sensitive steels, DX51D+Z and DCO1, with four different combinations of polymer films were carried out (S1 to S8). The lower temperature was used in order not to degrade the OPV samples.

Thermal cycling test of encapsulated samples were carried out in the range -40°C to 85°C for 670h. By visual inspection, only moderate discoloration, delamination and corrosion was observed.

Thermal-humidity test of encapsulated samples was carried out with RH=85% and T=85°C for 1000h hours. High levels of degradation and corrosion were observed after thermal-humidity testing.

- The configuration **S1** (ETFE/PVB/PET/PVB/ DX51D+Z/PVB/PET/PVB/ ETFE) was found as the best encapsulation type for the protection of steel DX51D-Z. The configuration **S8** (ETFE/EVA/DC01/EVA/ETFE) was found to be the most effective protection for DCO1. Both the (ETFE/PVB/PET/PVB/ steel type/PVB/PET/PVB/ ETFE) and the (ETFE/EVA/steel type/EVA/ETFE) configurations were considered for experiments on the other two steels; AISI430 and DX51D+AS.
- As corrosion was noticed after the thermal-humidity cycles, DX51D+AS and AISI430 were also encapsulated at 150°C considering the two best encapsulation configurations from **S1** and **S8**. After 1000 hours of thermal-humidity cycling, it can be concluded that no obvious surface degradation is observed from either encapsulation strategy on either DX51D+AS or AISI430.
- Considering the two best encapsulation configurations, a higher encapsulation temperature of 150°C (max. for a-Si TFSC) was applied on the four steel. After the thermal-humidity tests, the results show no DC01 samples possess moderately improved stability by using the elevated temperature, but no change in the stability of DX51D+Z samples is observed.

WP4_ Up-scaling of steels/ILs at pilot line level

Tasks 4.1, 4.2 and 4.3

From the developments and results achieved in WP2 and WP3, the ILs and deposition processes reported in Table II have been explored at the up-scale pilot plant level. For each IL/process, Table II also reports which steel was used and its size. The up-scale IL have been characterized in terms of roughness, thickness, dielectric and anti-diffusion behaviors.

Table II. ILs, deposition processes and steels' size considered at the up-scale pilot plant level.

IL	Successful Lab-scale process	Up-scale process considered	Steels considered	Steel sizes
SiOx sol-gel F1	Dip, roll, spray	spray	All	30cm x 30cm
SiOx sol-gel F3	K-bar	K-bar	All	30cm x 30cm
Blue ink	Screen printing	Screen printing	All	30cm x 30cm 30cm width coil
Hybrid Si ₃ N ₄ /SiO _x	Hybrid (PVD/sol-gel)	Hybrid (PVD/sol-gel)	AISI430 DX51D+AS	10cm x 180cm
Hybrid SiOx/ SiOx/ SiOx	Hybrid (sol-gel/PVD/sol-gel)	Hybrid (sol-gel/PVD/sol-gel)	AISI430 DX51D+AS DC01	10cm x 10cm
Hybrid SiOx/ SiOx/ SiOx	Hybrid (sol-gel/PECVD/sol-gel)	Hybrid (sol-gel/PECVD/sol-gel)	AISI430 DX51D+AS DC01	10cm x 10cm
Hybrid SiOx/ SiOx		Hybrid (sol-gel/PECVD)	AISI430 DC01	10cm x 10cm

Considering the sol-gel IL, an optimization of the curing process was also studied through, a fast curing step, by means of a near infra-red (NIR) technique. The experiments were carried out in static mode considering the DC01 steel. The sol-gel IL curing grade was evaluated in terms of micro-hardness and desorption behaviour in high vacuum PECVD chamber. The results were compared with a reference sol-gel coating cured using a hotplate and following the standard annealing procedure.

It can be observed (Figure 6) that all the NIR power enable to reach a satisfactory hardness of the SiO_x sol-gel, similar to the one achieved after the hot-plate curing (1h30 time). Related to the desorption sol-gel grade in high vacuum chamber, the vacuum values reached demonstrated that no significant desorption is registered.

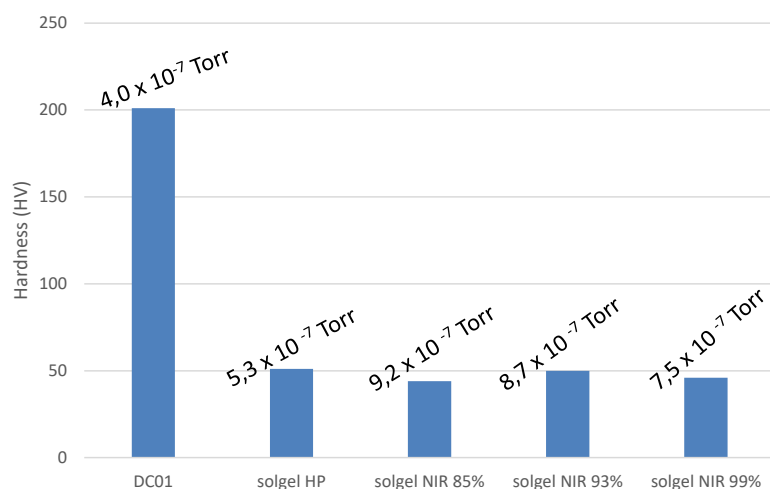


Figure 6. Influence of the NIR power on the sol-gel hardness and desorption in high vacuum chamber (NIR curing time of 2'). Comparison with sol-gel cured by hotplate (HP).

Table III reports the technically feasible steel/IL portfolio.

*Table III. Pilot plant level STEELPV portfolio. *Theoretically, as the ILs have fulfilled all the STEELPV requirements. No TFSC was deposited.**Deposition of a-Si TFSC and CZTS individual layers*

	AISI430	DX51D+Z	DX51D+A S	DC01	Comments
F1 SiO_x sol-gel	✓	✓	✓	✓	<ul style="list-style-type: none"> • 30cm x 30cm prototypes • In-house formulation • Spray coating • Fast curing NIR • Low temperature TFSC
Blue ink	✓	✓	✓	✓	<ul style="list-style-type: none"> • 30cm x 30cm prototypes • Commercial formulation • Screen printing • Low temperature TFSC • Statistical process control
Hybrid Si₃N₄/SiO_x	✓	✗	✓	✗	<ul style="list-style-type: none"> • 10cm x 176cm prototypes • In-house formulation • PVD/Spray coating • All temperature TFSC*
Hybrid tri-SiO_x (PECVD)	✓	✗	✓	✓	<ul style="list-style-type: none"> • 10cm x 10cm prototypes • In-house formulation • Spray coating/ PECVD/ Spray coating • Fast curing NIR (1st layer) • All temperature TFSC**
Hybrid bi-SiO_x (PECVD)	✓	✗	✓	✓	<ul style="list-style-type: none"> • 10cm x 10cm prototypes • In-house formulation • Spray coating/PECVD • Fast curing NIR • All temperature TFSC*

The statistical process control was only performed in the case of the '*blue ink*' IL as this was the unique successful approach that took into account both a commercial deposition technique (flatbed pilot plant screen printer) and a commercial dielectric ink (D2140114D5_GEM, UK).

Task4.4

The economic study was carried out considering the expected two best technically feasible steel/IL prototypes. The in-house sol-gel F1 SiO_x as it enabled to fulfil the IL requirements, was compatible with up-scaling techniques, with a-Si and OPV TFSC. Moreover, very good results were achieved using the NIR fast curing. The dielectric 'blue ink' was also considered in the economic study as, it fulfilled all the IL requirements and, because it is a commercial product, offers the possibility for a faster industrial implantation.

The cost analysis assumed the utilisation of a modern R2R production facility to assure the most efficient and cost effective means to develop the BIPV products. It considered material costs, manufacturing fixed costs (capital investment, labour costs, etc.), estimations of operations and maintenances. After the calculation, the total processing costs (including materials) was 2.60€/m² for Blue Ink and 1.24€/m² for Sol-gel F1.

Figure 7 presents the processed Steel+IL prices (€/m²) considering a) IL= Blue Ink and b) IL= Sol-gel F1 for the different steel types and thicknesses. Figure 7 also reports a comparison with the SSSG reference price (8€/m² _ 25µm) and the maximum affordable substrate costs for the a-Si and OPV TFSC (10€/m² and 6€/m², respectively). It can be notified that, at the SSSG thickness, the steels/sol-gel prototypes enable to decrease the substrate cost in a 50% and the steels/blue ink prototypes in a 40%.

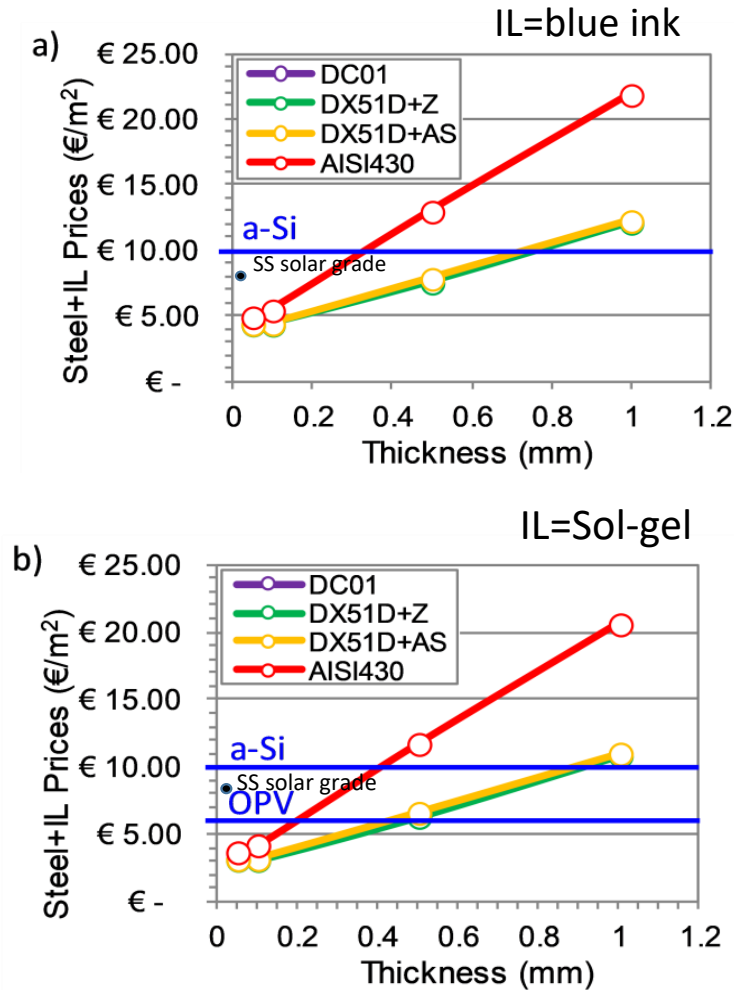


Figure 7. Steel+IL substrate prices. Comparison with the SSSG price and the maximum affordable substrate prices for PV technologies: a) Blue Ink (a-Si only); b) Sol-gel F1 (OPV & a-Si).

Table IV summarises the maximum viable steel thicknesses for each steel/IL prototypes and PV technologies.

Table IV. Maximum viable steel thicknesses for the different IL coatings and suitable PV technologies

IL Material	PV Technology	Steel Type			
		DC01	DX51D+Z	DX51D+AS	AISI430
Blue Ink	a-Si (€10/m ²)	0.75 mm	0.75 mm	0.75 mm	0.35 mm
Sol-gel F1	OPV (€6/m ²)	0.45 mm	0.45 mm	0.45 mm	0.2 mm
	a-Si (€10/m ²)	0.9 mm	0.9 mm	0.9 mm	0.45 mm

The steel substrate thicknesses of STEELPV lend themselves to a number of categories of BIPV applications. As presented in Table V, Blue Ink and Sol-gel F1 IL coatings on all steel types are suitable for flexible foil (thickness $\leq 0.1\text{mm}$) and semi-flexible modules (thickness $>0.1\text{mm}$, $\leq 0.5\text{mm}$) for all suitable PV technologies and IL materials (Blue Ink: a-Si, Sol-gel F1: OPV & a-Si). For the DC01, DX51D+Z & DX51D+AS steels types both ILs with a-Si PV were suitable for semi-rigid modules (thickness $>0.5\text{mm}$).

Table V. STEELPV Suitability of different IL coatings for BIPV module production

IL Material	PV Technology	Steel Type			
		DC01	DX51D+Z	DX51D+AS	AISI430
Blue Ink	a-Si	flexible foil semi-flexible semi-rigid	flexible foil semi-flexible semi-rigid	flexible foil semi-flexible semi-rigid	flexible foil semi-flexible
Sol-gel F1	OPV	flexible foil semi-flexible	flexible foil semi-flexible	flexible foil semi-flexible	flexible foil semi-flexible
	a-Si	flexible foil semi-flexible semi-rigid	flexible foil semi-flexible semi-rigid	flexible foil semi-flexible semi-rigid	flexible foil semi-flexible

Scientific and technical description of the results

1. Objectives of the project.

In the EU, the buildings are responsible for 40% of energy consumption and 36% of the CO₂ emissions, mainly because 35% of the EU's building are over 50 years old [1,2]. EU's 2020 directives aim to reach a 20% share of renewable energy sources in final energy consumption by 2020. In particular the directive 2010/31/EU requires that all new constructions as well as 3% of all old public buildings have to fulfil a nearly zero energy building (NZEB) by 2020 [3].

Photovoltaic (PV) technology is one of the main renewable source to reach the EU's directives and, in the last decade, many researches and developments were and are focussed on how to improve the integration of PV as building attached PV (BAPV) and BIPV systems.

According to the EuroAce 2011 report [4], at least 5 million of old buildings should have to be annually retrofitted to fulfil a complete renovation of the EU's buildings by 2050. Steel, as substrate of PV systems, could play a strategic role although, at this moment, only very high cost stainless steels solar grade are used and only very thin steel/PV products are competitive and proposed in the market (steel thickness about 25µm). As consequence, those flexible products can only be used to cover structures (e.g. roofs).

The STEELPV challenge was to propose cheaper alternatives to the current solar grade stainless steel. More concretely, the technical objective was to functionalize low cost 'rough' industrial steels to be used as direct substrates for TFSC technologies.

As main innovation, it was expected to:

- Propose new market niche for structural steel grades
- Reduce the cost of steel substrate for TFSC application
- Make economically feasible a range of steel thicknesses in order to propose several classes of BAPV/BIPV module production: flexible foil (≤ 0.1 mm); semi-flexible modules (> 0.1 mm); semi-rigid modules (> 0.5 mm)

2. Description of activities and discussion

2.1. WP1: Selection of low cost steels for PV applications

2.1.1. Steel substrates specifications and steel selection (01/07/2014-30/06/2015_Task 1.1)

During photovoltaic devices manufacturing, the selection of the substrate is a critical stage. It has an important impact on the performance of the device and in the final cost of the product. For the first aspect it is needed to consider the following compatibility between steels and the ILs and solar cells, such as:

- The steels have to be chemically inert: compatible with vacuum process, no chemical reaction with other post-chemical treatment (e.g. Selenization step for CIGS/CZTS technologies), etc.
- The steels have to show similar CTE to upper layers to be deposited, either back electrode of the solar cell or ILs to accommodate metallic foils morphology to solar cell requirements. Otherwise, upper layers can be delaminated during post-thermal processes due to the tensile stress accumulated.
- The steels have to take into account TFSC deposition processes, especially thermal conditions. It is particularly important for metallic coated steels in order to be sure that no brittle intermetallic layers will appear during the IL and TFSC depositions. Maximum temperatures are below 200°C for OPV and a-Si and up to 550°C for CIGS/CZTS TFSC technologies.
- The steels have to offer a maximum Rz of 1.5µm. Main limitation to define this design specification is provided by partners interested to demonstrate PVD and CVD capabilities ILs. The ILs' thickness expected for these layers is between 3x-4x times the original surface roughness, which means that maximum surface roughness provided by the steel manufacturer do not over exceed Rz 1.5 µm.
- The steels must be cost effective. The steel selection has to consider the potential cost of the final product: steel+rolling+ILs that should be below 0.1€/W [5].

Based on the above technical requirements, four low cost steels have been selected from the three steel groups of stainless steel, bare steel and hot-dip coated steels as shown in Table VI. Their chemical composition is shown in Table VII.

Table VI. Substrate selected.

Nº.	Material group	Selected steels
1	Stainless steel	AISI430
2	Bare steel	DC01
3	Hot-dip zinc coated Hot-dip Al-Si coated	DX51D+Z DX51D+AS

Table VII. Chemical composition of steels proposed.

Material		Chemical composition % (wt.)						
No.	Material	C	Si	Mn	P	S	Cr	Ti
1	Stainless Steel (AISI430)	≤ 0.08	≤ 1.0	≤ 1.0	≤ 0.04	≤ 0.03	16.0-18.0	
2	Bare steel (DC01)	≤ 0.12	≤ 0.3	≤ 0.6	≤ 0.045	≤ 0.045		
3	Hot-dip zinc coated (DX51D+Z)	≤ 0.18	≤ 0.5	≤ 1.2	≤ 0.12	≤ 0.045		≤ 0.3
4	Hot-dip Al-Si coated (DX51D+AS)	≤ 0.18	≤ 0.5	≤ 1.2	≤ 0.12	≤ 0.045		≤ 0.3

Hot-dip Zn: Zn ≥ 98 % and Hot-dip AS: Al + 9-11%Si + 2.5-3.5%Fe

AISI430 (Alloy430) is the most used ferritic stainless steel grade in the world for different PV-technologies. A chromium content of 16% gives it a good corrosion resistance and this grade is used in wide range of PV-applications because of the cost and its CTE properties. Both DC01 and the core material for Zn and AS coating are low carbon steels.

The Zn and AS coating amounts have been chosen by considering the need for protection against corrosion and the cost efficiency. After rolling to thickness 0.3mm the DX51D+Z exhibits a Zn coating layer thickness of about 5-6µm and the DX51D+AS about 10-12µm (equivalent in both cases to Z100 and AS100) what ensure a long time corrosion protection for the indoor and outdoor applications. Therefore, Z100 and AS100 with 100g/m² Zn or Al-Si-coating are considered as the best coating for this project. Moreover, TFSC devices are always encapsulated (e.g. using flexible polymers, glass, etc.) and, the role of the metallic coating will mainly be to ensure a corrosion protection during steel/IL products storage and previously to the TFSC depositions.

The cost of the steels selected as function of the rolling process is reported in Figure 8. The costs have been calculated taking into account the high steel speed (HSS) grinding rolling process (see task1.2). It can be observed, in a similar tendency for all the selected steels, cost unit per mass (€/ton) increases due to the specific requirements of the processing during the steel fabrication. It is also interesting to note that the bare steel (DC01) has practically the same cost as both metallic coated steels. A comparison between the costs at the beginning (Oct. 2014) and the end (Jun. 2017) of the project is also proposed. It can be seen a cost's increase of between 16% and 20% in this period.

The SSSG reference steel price is included in the €/m² graphs. It is calculated based on the material supplied by MKM to the solar manufacturer Global Solar in 2011. The substrate thickness was 25µm at a cost of 8€/m², which is several €/m² more expensive than the steels selected and rolled in the project. This price's difference lets an important cost margin for the IL developments.

Competitive solar cell manufacturing cost is close to 0.5€/W, the substrate contributing about 20% (0.1€/W) [5,6,7]. Taking into account average PCE of OPV (6%), a-Si (10%) and CIGS/CZTS (15%) and considering the global AM1.5 spectrum (1000W/m²) at 25°C (IEC 60904-3:2003), maximum substrate affordable costs (€/m²) for each TFSC technology is also reported in the €/m² graphs.

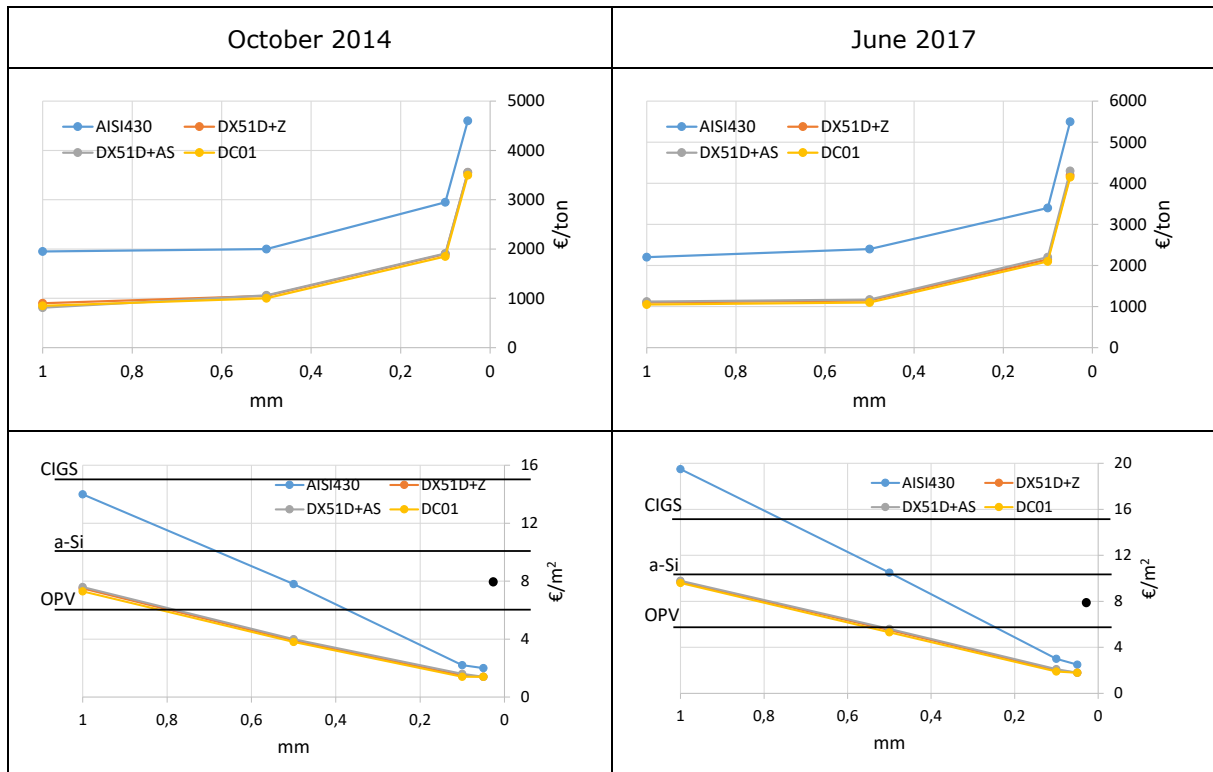


Figure 8. Cost €/Ton and €/m² as function of the HSS rolling process for different types of steels. Evolution of price between Oct. 2014 and Jun. 2017. Prices include the rolling and degreasing and cleaning (15%) of the steels

Considering partners purposes and facilities (lab-scale and up-scale) for IL developments, it was decided to adopt a common position for all partners about steel thickness. The main reason was to be able to compare technical and economic steel/IL products and to make ensure easier interpretation of results across partner sites. The thickness chosen, 0.3mm, has the following advantages:

- It ensures easy handling during experiments at lab-scale level. For example, lower thicknesses could induce sample thermal bending during IL and TFSC annealing treatments.
- It could be used by all the partners developing IL at lab-scale and up-scale levels, being affordable for either roll-to-roll as format up-scaling strategies.
- It proposes a different thickness as the one already used in PV market (increase of 10 times).

2.1.2. Manufacture cost-efficient flexible steel substrates (01/01/2015-31/03/2017_Task1.2)

For the substrate manufacture, different rolling tools, HSS and ASP (powder metallurgy) rolls were considered during the project. Both materials are high-performance special steels offering high hardness at temperatures up to 500°C and high wear resistance. As compared to conventional HSS with the same hardness and alloy content, the ASP steels have better grindability, uniform wear, better wear resistance, smaller regrinding depth and higher strength.

All the production parameters have been so chosen that the manufacturing cost can be as low as possible (e.g. no post annealing treatments were initially applied). Figure 9 reports an estimation cost taking into account HSS and ASP rolling tool materials. To convert €/m² to €/W, an average PCE of 10% was considered.

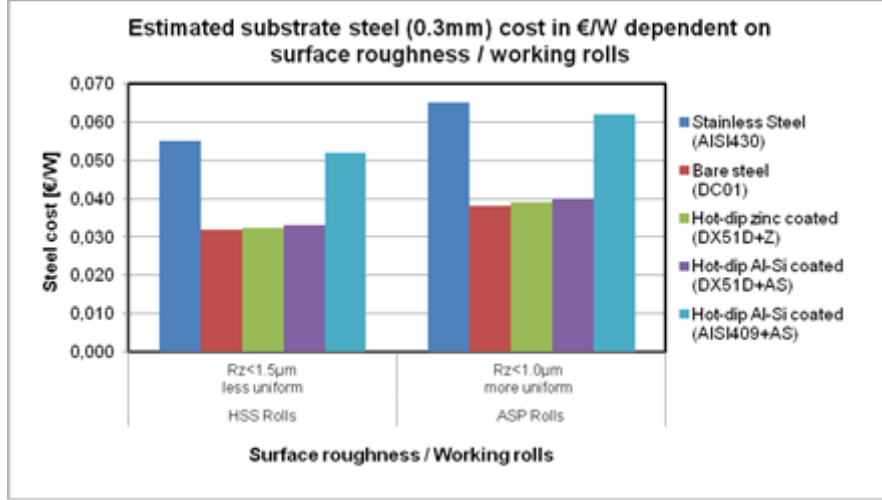


Figure 9. Estimated substrate cost with different qualities

Considering the steel thickness of 0.3mm, an estimation of the steel rolling cost as a function of different finishing working rolls after the HSS grinding process (HSS polished, hardened steel and ceramic rolls) was also performed. The first column reports real costs using HSS grinding. Results are reported in Figure 10.

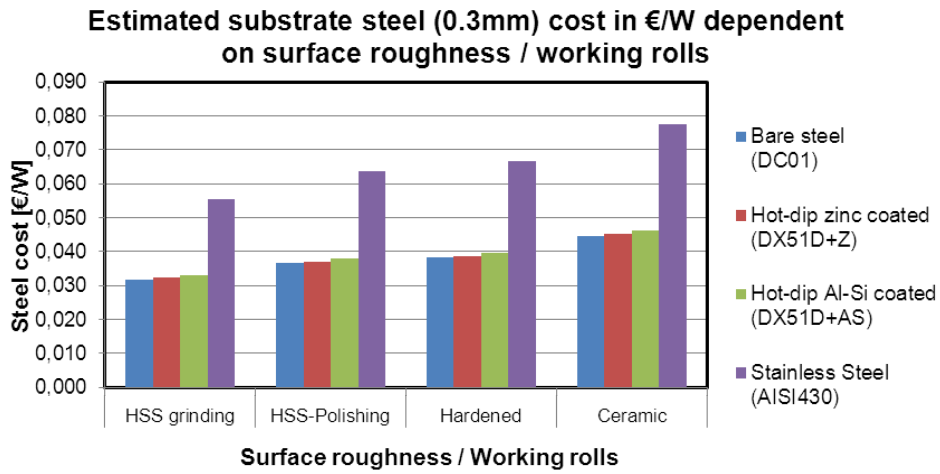


Figure 10. Dependence of substrate cost €/Wp on surface roughness/working rolls for different types of steels

As shown in Figure 10, the substrate produced with standard ground HSS ensures the lowest manufacturing cost but the highest roughness and the poorest surface homogeneity. Based on these estimations and taking into account the necessity to ensure low production cost and to develop economically viable steel+rolling process+IL products, HSS finishing working rolls were considered for lab-scale and up-scale processes. No recrystallization annealing process was applied after the rolling step in order to get the lowest possible cost. As example, Table VIII reports the material properties determined just after the rolling processes for the first lab-scale delivery. The mechanical properties show much more brittle materials compared to their original states. However, for the purpose of the project this state should not be determinant as no cold-formed of the materials is expected (i) only flat substrates will be used for the IL depositions, ii) TFSC manufacturer only use flat substrates in their deposition processes and, iii) no cold-formed of the PV ended products _steel/IL/TFSC_ will be carried out as some brittleness of the TFSC could appear). Moreover, it is expected that the steel/IL/TFSC products will be used in BIPV in façade/roof elements without ensuring a support purpose.

All the sample materials fulfill the requirements: $R_z < 1.5\mu\text{m}$ and cost $< 0.1\text{€}/\text{W}$. For lab-scale experiments, 5cm and 10cm width steel coils were produced and for up-scale trials 30cm x 30cm sheets and 30cm width coils were processed.

Table VIII. Mechanical and physical properties (first lab-scale delivery)

Material	Sample size		Surface roughness		Mechanical properties			Physical
	Thickness [mm]	Width [mm]	R _a [μm]	R _z [μm]	R _{p0,2} [N/mm ²]	R _m [N/mm ²]	A80 [%]	
Stainless Steel (AISI430)	0.3	50, 100	0.127-0.136	0.73-0.87	696-702	734-744	2.1-3.2	10
Bare steel (DC01)	0.3	50, 100	0.112-0.172	1.04-1.36	455-462	496-505	6.5-7.2	11.1
Hot-dip zinc coated (DX51D+Z)	0.3	50, 100	0.076-0.090	0.57-0.83	458-461	493-495	6.1-6.3	11.6
Hot-dip Al-Si coated (DX51D+AS)	0.3	50, 100	0.105-0.132	0.89-1.49	433-456	469-494	5.1-5.8	11.9

As it is explained in the 3.2.1. section (*Lab-scale IL developments*), neither physical vapor deposition (PVD) nor chemical vapor deposition (CVD) techniques were able to level the steel substrate surfaces for TFSC applications. As contingency plan, it was decided, considering a final steel's thickness of 0.3mm, to try to level more the steel surface by ASP rolling process. The objective was to reach a high surface quality (R_a~0.04μm, R_z<0.35μm).

A Cr-coated ASP roll followed by a ASP polished roll were used. The first roll has a higher surface roughness and hardness and can be used for the beginning steps for improving the surface homogeneity during the rolling process by reducing the wear force. The final surface roughness of the substrates was achieved by using a ASP polished roll. Results, considering the DC01 steel are reported in Figure 11. It can be observed a decrease of the roughness comparing to the HSS ground + polished roll process. Ra has decreased from 0.14μm to 0.09μm and Rz from 1.2μm to 0.75μm. However, these roughness results are still too high for being combined with PVD and CVD technologies for the IL depositions. Moreover, it was estimated that the cost of ASP working tools are about 9 times higher than HSS one.

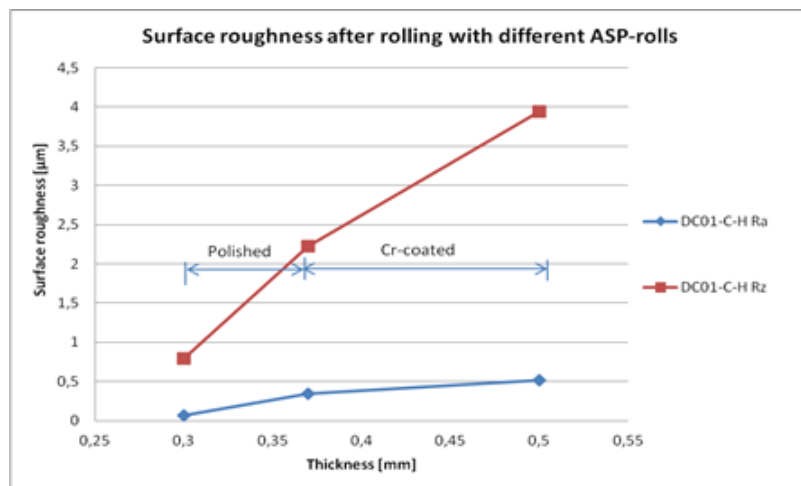


Figure 11. Evolution of surface roughness of DC01 with firstly Cr-coated and then polished ASP-rolls

2.1.3. Inspection methodology (01/04/2015 -31/12/2015 _ Task1.3)

Through the Tasks 1.1 and 1.2, four steels were selected for the project and rolled through a HSS low cost process to 0.3mm thickness. A specific and exhaustive characterization of the four steels is crucial to ensure a high quality of the ILs depositions which have to make compatible these steels with the three TFSC technologies considered in the project (OPV, a-Si and CIGS/CZTS).

It was decided to characterize the four selected rolled steels before and after applying annealing treatments that simulate ILs and TFSC process conditions (Table IX). The following properties were

studied: superficial aspect, roughness, element diffusion for the metallic coated steels, mechanical properties (tensile, hardness, adhesion, CTE), oxidation/corrosion and metallography.

Table IX. Thermal treatments applied on the four rolled steels before their characterizations_ annealing time: 1 hour.

Steels Treatments	AISI 430	DC01	DX51D+Z	DX51D+AS
200°C_ Non-vacuum (air atm_Hot-plate)	✓	✓	✓	✓
500°C_ Non-vacuum (air atm_Hot-plate)	✓	✓		✓
200°C_ Vacuum_ 10 ⁻⁷ mTorr (PECVD)	✓	✓	✓	✓
500°C_Vacuum_ 10 ⁻⁷ mTorr (PECVD)	✓	✓		✓

As main conclusions of this study, it can be reported that:

- The thermal treatments does not seem to have influence on the chemical element diffusion of the metallic coated steel substrates as similar in-depth profiles are found comparing annealed and non-annealed conditions.
- Related to mechanical properties, the 200°C treatment show some bake hardening effect and the 500°C one some restoration process. In both cases, these changes does not have to influence the IL and TFSC behaviors. For the hardness of the three steels grades, no change due to the thermal treatments are detected. However, some softness can be observed in the case of the AS metallic coating. Finally, concerning the steels CTE, almost linear behaviors are achieved, especially for the AISI430.
- Concerning the zinc and AS metallic coatings, good homogeneity without lack of layer is observed after the HSS cold rolled process (Figure 12). In the case of the AS coating, some hole defects (red circles) can be easily detected although it seems that without being determinant for the purpose of the project (it was demonstrated that TFSC were correctly working on DX51D+AS/IL prototypes_ e.g. in Tables XXV, XXVI, XXVII).

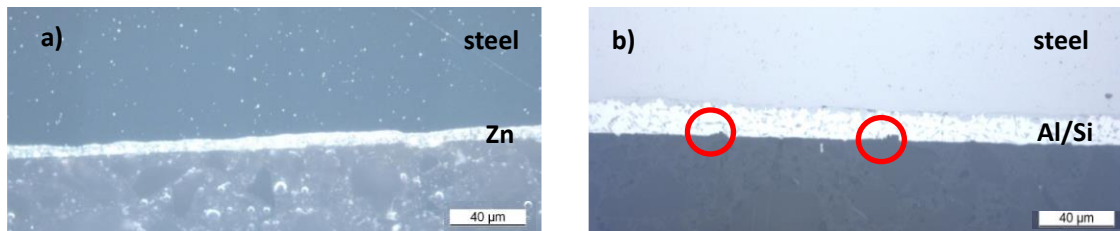


Figure 12. Metallic coatings homogeneity. 500x magnification optical microscopy images. a) DX51D+Z steel coil_outer side, b) DX51D+AS steel coil_outer side.

- Related to the anti-corrosive behavior, it can be observed that the thermal annealed samples present worse results than non-annealed ones. The treatment is especially harmful for AISI430, probably due to the alteration of the passive layer that protects it. However, the final product (steel/IL/TFSC) will have to be encapsulated in order to ensure a protection to the TFSC. At the same time, this encapsulation process will offer an anti-corrosion protection to the steel substrate.
- The superficial aspect is a crucial parameter to be controlled. No degradation was observed for thermal treatments under vacuum after visual inspection. However, a low superficial oxidation at 200°C temperature and a much stronger one at 500°C can be seen for the AISI430 and DC01 steels processed under air atmosphere. This formation of superficial oxides could pose challenges for high quality IL depositions and could form a delamination fault line

for ILs due to the lack of adhesion. Figure 13 shows macroscopy images of the AISI430 and DC01 steels substrates before and after the different annealing steps.

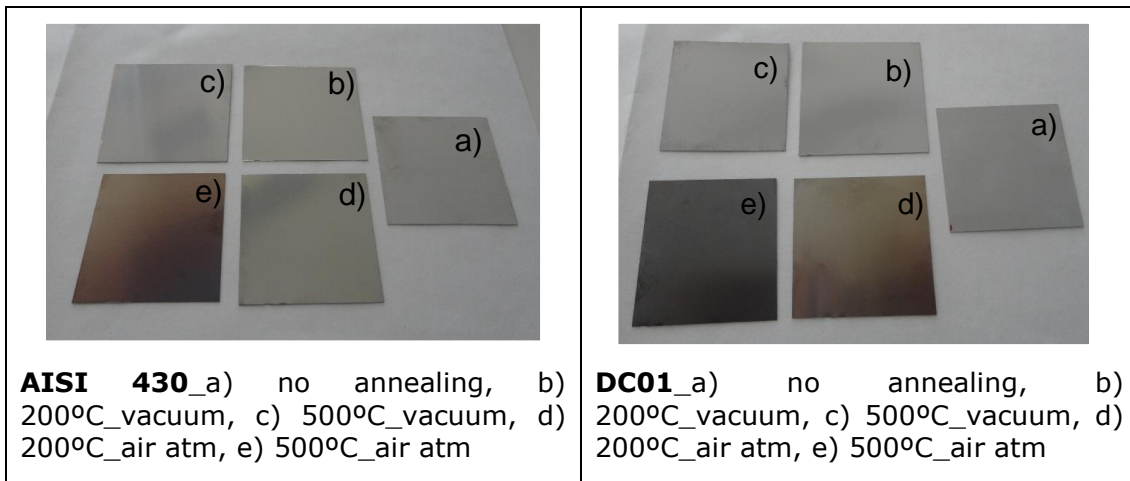


Figure 13. Macroscopic visual aspect of the AISI430 and DC01 steels after the annealing treatments.

A possible solution is to carry out the non-vacuum annealing treatments under reductive inert atmosphere (e.g. H₂/N₂). In the case of the AISI430 steel, it was also found that the oxidation can also be avoided by applying an annealing treatment under reductive conditions after the HSS rolling process (it was estimated a cost increasing of 20%). As reported in Table X, the mechanical properties of the AISI430 substrate are completely modified after the rolling process and are possibly the main reason of the oxidation process at high temperature. It is probable that some deleterious phase precipitation (secondary sigma phase or carbides precipitation) reduces the corrosion resistance of the steel. By applying an annealing heat treatment, a redissolution of the phases could have happened, leaving the steel with better corrosion properties. Indeed, as shown in Figure 14, the oxidation phenomenon is highly decreased (comparison of sample 2 in Figure 14b and sample 3 in Figure 14c).

Table X. AISI430 steel properties considering several process conditions: 1) before the rolling process, 2) after the rolling process, 3) after the rolling and annealing processes.

No.	Thickness [mm]	Experimental condition	R _{p0,2} [N/mm ²]	R _m [N/mm ²]	A80 [%]
1		unprocessed steel	301	488	31
2	0.3	rolled	699	739	2.7
3	0.3	rolled+annealed	353	549	25

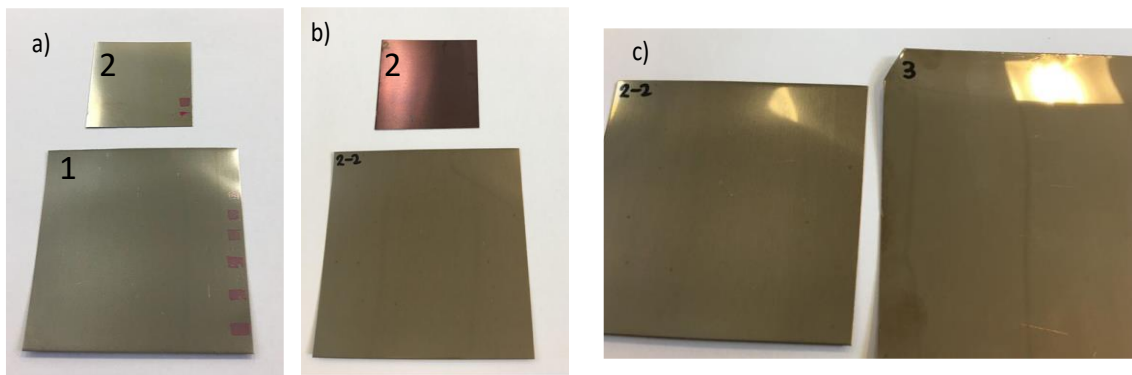


Figure 14. Visual aspect of the AISI430. a) Initial materials; Small sample was rolled, b) after the thermal treatment (425°C – 30min_air), c) after the thermal treatment (425°C – 30min_air), sample 3 is rolled and annealed under reductive atmosphere.

The roughness of the native steels is also an essential factor to be taken into account for the optimum IL deposition. Figure 15 shows a comparison of the roughness of the four steels delivered for

experiments at lab-scale and pilot plant levels. It was initially required the same roughness between lab-scale and up-scale formats in order to make much easier the IL up-scaling processes.

In all case, the roughness was measured by mechanical profilometry (Ambios Technology, XP1). According to the standard EN ISO 4288:1996 (*Geometrical product specifications_GPS surface texture: Profile method. Rules and procedures for the assessment of surface texture*), the evaluation length (L_n) and the cut-off (λ_c) considered were 4.0mm and 0.8mm, respectively.

As it can be observed in Figure 15, some differences, especially for the AISI430 substrate, were registered. In this particular case, both the R_a and the R_z are practically divided by two for the up-scale format. The DC01 and DX51D+Z substrate also show some slighter decreases. The DX51D+AS presents very similar results between the lab-scale and up-scale native steels.

This decrease of the roughness could be a serious problem for IL such as sol-gel. Indeed, the critical cracking thickness (CCT) of a sol-gel is highly influenced by the roughness of the substrate. At lab-scale level, it was found that a minimum of $3\mu\text{m}$ of SiO_x sol-gel was necessary to fulfil all the requirement to match the steel with the TFSC. Reducing the steel roughness (up-scaled steels Figure 15) could reduce the CCT and, without modifying the lab-scale sol-gel formulation, could make more difficult a successful IL up-scaling for the purpose of STEELPV project.

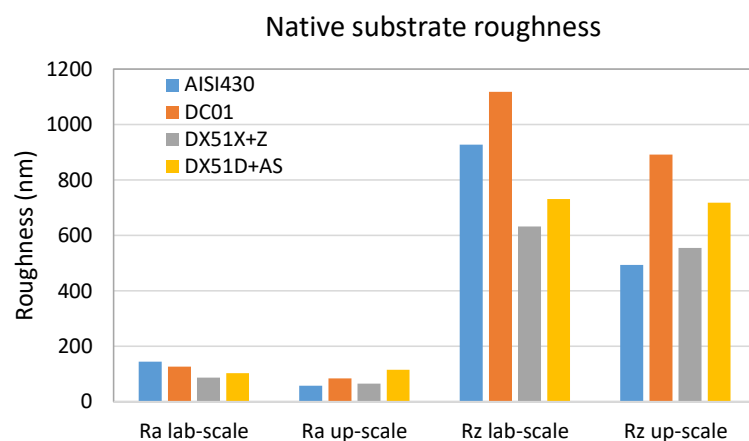


Figure 15. Comparison of the steel substrates roughness between the lab-scale and up-scale formats.

The homogeneity of the rolled steels was also studied. As example, Figure 16 shows the deviation observed in 50 AISI430 samples. All samples have a R_z below $1.5\mu\text{m}$ but with a higher deviation. From these results, it was suggested that each sample must be characterized before and after the IL deposition process, in order to evaluate the impact of this step on the surface roughness; otherwise, there is no clear information about which is the benefit of the barrier layer on the metallic substrate.

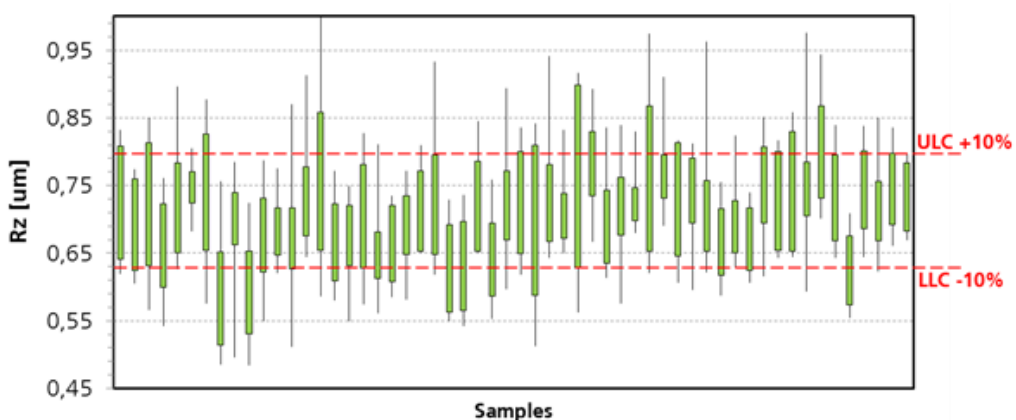


Figure 16. Surface roughness comparison with 50 identical samples, each of them measured at 10 points.

Finally, Figure 17 shows examples of roughness profiles achieved for each steel substrates after the rolling step. It can be observed different surface aspects depending on the steel studied. The AISI430 shows a quite regular texture of peaks and valleys without deep hole or high sharp peaks defects. The DC01, DX51D+Z and DX51D+AS shows similar properties; very closely packed peaks and valleys with frequent narrow and deep valleys (up to $1.5\mu\text{m}$ deep). However, no high sharp peak defects are observed. The DX51D+AS also shows wide and deep defects (up to $5\mu\text{m}$ deep) that could influence the ILs quality.

It can be also noticed, looking at Figure 17 profiles, that the lack of high sharp peaks is a positive information. In fact, these kind of defects are the most problematic ones in order to achieve high quality IL and TFSC devices. From Figure 17, it can be observed that the peaks heights are around 500nm-600nm for the four steels. Considering that the IL thickness expected should be between 3x-4x times the original surface roughness, compact IL of about $2\mu\text{m}$ should be enough to ensure an electrical insulation of these steels.



Figure 17. Examples of roughness profiles of the four steel substrates.

2.2. WP2: Preparation of low cost steels substrates for PV applications: intermediate layers developments at lab scale level.

The objectives of this WP consisted on developing IL based on wet and vacuum processes taking into account both the steel substrates and PV technologies. The IL developed have to fulfill the following requirements:

- **Levelling:** The roughness after the HSS rolling process is too high to guarantee the good performance and reliability of all solar technologies to be developed in the project. Moreover, a levelled surface is essential to enable a high quality monolithic integration process.

The IL objective is to reach a Ra roughness below 40nm and a Rz one below 350nm.

- **Electrical insulation:** the IL must be able to electrically insulate the back contact of the solar cell from the metallic substrate. Otherwise, it would not be possible to use the monolithic integration process to transfer the lab scale concept (solar cell) to the industrial environment (module with interconnected solar cells).

The objective is not to register a breakdown voltage of the IL below 40V.

- **Diffusion barrier:** the IL has to inhibit the steel element diffusion during the TFSC deposition in order to prevent its degradation.

- **Mechanical and thermal stability:** the IL has to be compatible with the TFSC process, enduring TFSC temperatures manufacturing and vacuum conditions. No lack of adhesion and desorption of the ILs have to be registered.

Furthermore, the ILs were studied in terms of:

- **Surface integrity:** The presence of defects (e.g. cracks, bubbles, etc.) was evaluated by exposing the steel/IL systems to indoor and outdoor real atmospheres during several months. As the IL deterioration could be difficult to detect visually or by using optical microscopy technique, it was decided to evaluate it through the breakdown voltage behavior.
- **Monolithic cell interconnection:** This process was evaluated through the P1 scribing test through a marking ablation laser process.

The thermal and climate tests through standard IEC 61646:2008 (*Thin-film terrestrial photovoltaic (PV) modules – Design qualification and type approval*), originally proposed in task2.2 were not carried out as they concern finished solar devices (including the encapsulation step). Some work has been carried out in this way in task3.2.

Three processing routes have been explored for the development of the ILs: wet, vacuum and hybrid strategies. The developments and achievements are extensively reported in the Deliverables D2.1 (*Lab-scale intermediate layer routes*) and D2.2 (*Intermediate layer characterizations*).

2.2.1. Tasks 2.1, 2.2 and 2.3. Lab-scale intermediate layers developments and characterizations (01/04/2015-30/09/2016)

a) ILs developed through the wet route

Wet solutions based on SiO_x sol-gel

The first strategy for the IL has been focused on wet processes based on SiO_x sol-gel technology. Sol-gel based on a SiO_x precursor is a well-established technology for the development of coatings on metals with many applications [8]. It consists in a chemical route based on a hydrolysis-condensation of the precursors (Figure 18), and enables coatings through low cost deposition techniques.

Hydrolysis



Condensation

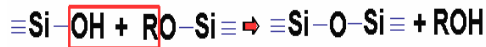
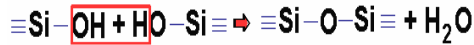


Figure 18. Hydrolysis-condensation_sol-gel mechanisms.

However, the main drawback of most of current sol-gel coatings is found in their maximum achievable thickness being free of cracks, around 1µm. Cracks are mainly produced due to osmotic stresses generated during the evaporation of the solvent and mechanical stresses due to the CTE difference with the substrate, during the densification, especially when the substrate is a metal [9,10]. The concept of CCT is then defined as the maximum thickness that can be carried out after the heat treatment without any cracks forming in the coating layer [11]. The CCT can be subject to small variations, as it depends on factors such as the roughness of the substrate, the application technique, the formulation and viscosity of the sol-gel, etc.

As no high cost rolling processes or other physic-chemical treatments were contemplated for the different 'rough' substrates, thick sol-gel layers will have to be applied through sol-gel stacks or by the addition of chemical agents that ensure both the increases of the thickness and the elasticity. Sol-gels were developed taking into account:

- The nature of the steel substrates; the galvanized steel, due to its zinc protection cannot be annealed over 300-350°C; otherwise the Fe will diffuse through the Zn making a brittle Zn-

Fe alloy. For stainless steel, aluminized and bare low carbon steel substrates, the annealing sol-gel stage can be carried out at higher temperatures.

- To develop low cost formulations (few precursors, room temperature formulations, etc.) as well as a low cost application (a single layer strategy was considered).
- Viability for a possible future industrial implantation. So, the solutions have to be stable, mainly looking at the viscosity parameter.

The different sol-gel formulations developed in STEELPV have the same following matrix: Methyltriethoxysilane (MTES 99%, Aldrich) and Tetraethylorthosilicate (TEOS 98%, Aldrich) as precursors. Water was incorporated as a solvent, PEG (Polyethilenglycol) as tension releasing agents and HNO_3 as a catalyst. All the sol-gel dissolutions were based on a one step acid catalysis.

The **F1 formulation** was optimized with the following molar ratios: TEOS/MTES: 1.35, $\text{H}_2\text{O}/(\text{MTES}+\text{TEOS})$: 4.7, and PEG-6000/(MTES+TEOS): 0.02. This formulation was successfully applied by dip, spray and roll coating and was finally selected for the up-scaled trials. Its lifetime was stable during several hours as shown in Table XI, and was compatible with ethanol in case a dilution is needed. Moreover, this formulation endures the STEELPV high temperatures requirements (500°C).

Table XI. Evolution of the sol-gel viscosity at a speed rate of 100rpm.

	1hour	10 hours	24 hours	96 hours
Viscosity (Pa.s)	0.0057	0.0084	0.0082	0.013

In the **F2 formulation** an additional tension releasing agent (polyvinylpyrrolidone _PVP10000, 99%, Aldrich) was introduced in order to increase the sol-gel CCT. The purpose of this *ormosil* (organic modified silicate) is to avoid the mechanical stresses due to the CTE difference with the substrate during the densification. The optimized molar ratio used was PVP10000/(MTES+TEOS): 0.02. This formulation was successfully used for the first trials by spin coating and also by roll coating. However, no good results were achieved in case a dilution was needed and a degradation of the coating was observed for temperatures higher than 250°C . So, this formulation was not selected for the up-scaling experiments.

Finally, the **F3 formulation** was developed to match with printing and coating technologies. Printing methods require an increase in sol-gel viscosity. Several ILs processing routes such as flexography, screen, and gravure printing methods as well as blade, bar and roll coating methods were explored in STEELPV. The increase of the viscosity was studied by varying the PEG molecular weights (PEG6000, PEG10000, PEG200000 and PEG400000) and a range of concentrations from 2% to 55% were explored for this study to cover as wide a range of viscosities as possible.

Figure 19 displays the effect of PEG concentration and molecular weight on viscosity of PEG solutions. It can be seen that the viscosity of PEG solution increased by three orders of magnitude from 0.007Pa.s to 7.33Pa.s with an increase in the molecular weight from 6000 to 400000.

This is a very promising result as it might be possible to tune the sol-gel solutions to both the low viscosity printing processes such as flexography, gravure, bar, blade and roll coating processes (about 0.1Pa.s) as well as the high viscosity printing process such as screen (2-100Pa.s).

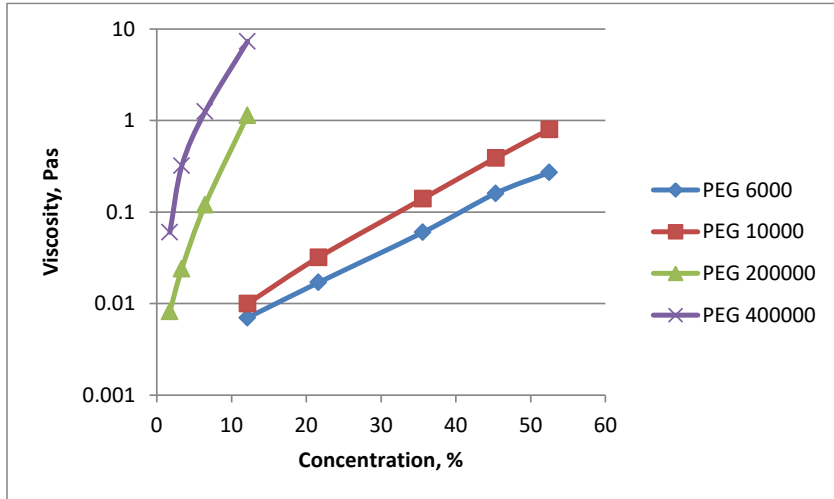


*Figure 19. Effect of PEG concentration and molecular weight on viscosity of PEG solutions
—shear rate of 230 1/s.*

The different sol-gel formulations have been applied, at lab-scale level using techniques such as spin-coating, dip, spray, K-bar and roll coating in roll-to-roll (R2R) process and flexography, gravure and screen printing. Table XII summarizes the compatibility of the different sol-gel developed in the project with the selected steels depending on the coating/printing techniques tried at lab-scale level. It can be observed that all the sol-gel are viable for the four steels although, depending on the application method, not all are suitable due to the two thin or thick and cracked single layer applied.

The F1 sol-gel formulation was finally selected to carry out the up-scale experiments by spray coating technique and the F3 (PEG200000) sol-gel formulation for the K-Bar ones.

The printing techniques (flexography, gravure and screen) were not suitable due to lack of levelling, heterogeneity of the layer or crack appearance

Table XII. Compatibility of the different sol-gel solutions depending on the coating/printing techniques experimented at lab-scale level.

Sol-gel	Precursors	COATING TECHNIQUES							
		Spin coating	Dip coating	Spray coating	Roll coating	K-bar coating	Flexo printing	Gravure printing	Screen printing
F1	TEOS, MTES, PEG, HNO ₃	No	Yes	Yes	Yes	---	No	---	No
F2	TEOS, MTES, PEG, HNO ₃ , PVP	Yes	No	No	Yes	---	---	---	---
F3	TEOS, MTES, PEG, HNO ₃	---	---	---	Yes	Yes	No	No	No

Coating applications

F1 and F2 formulations have been mainly considered for coating techniques due to their relative low viscosity. Successful native steel levelling with thickness above 3µm were achieved considering potentially scalable technique such as dip, spray and roll coatings.

Figure 20 shows a sum up of the IL maximum thicknesses that were achieved with a SiO_x single layer depending on the coating technique. It can be pointed out that the two potential scalable techniques are able to solve the main drawbacks of F1 solution applied by spin coating; the low thickness.



Figure 20. Maximum IL SiO_x thickness with no delamination/crack and good homogeneity in 5cmx5cm samples: Influence of the coating technique

Figure 21 reports the roughness determined through mechanical profilometer scans for two steels before and after the application of the sol-gel by dip and spray coating. It can be observed that the IL thickness enables to successfully level the surface of the two steels and a compatibility with the TFSC can be expected.

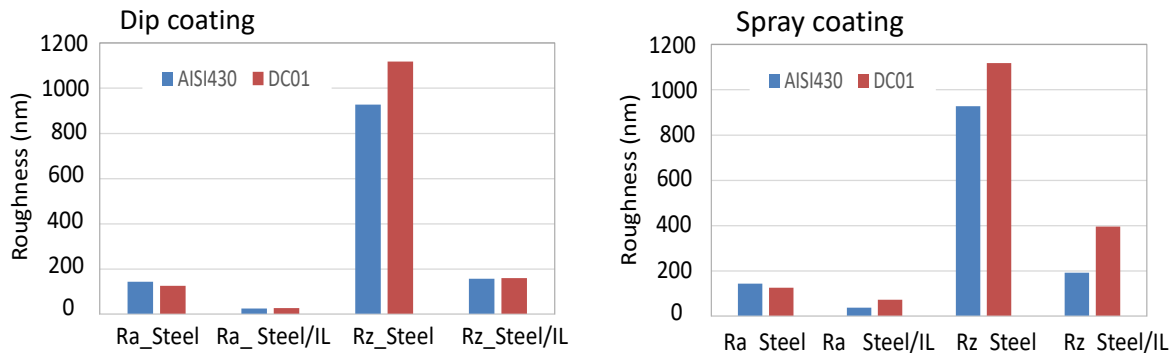


Figure 21. Roughness measured before and after the application of the F1 sol-gel IL by dip and spray coating.

Related to **F3 sol-gel**, several molecular weights were tried; F3_PEG10000, F3_PEG200000 and F3_PEG400000. The applications have been carried out on the four steels using different K-bar wire diameters (K-Bar 0 - 50 μm, K-Bar 1 - 80 μm, K-Bar 2 - 150 μm and K-Bar 3 - 310 μm_ humid weight).

F3 sol-gel layers using K-bar0 and K-bar2 were uniform and free of cracks. However, the IL thicknesses achieved were too low ($0.68 \pm 0.24 \mu\text{m}$ to $2.00 \pm 0.38 \mu\text{m}$) and, therefore, would not provide sufficient insulation required by TFSC technologies.

Considering K-bar3 some positive results were obtained on the AISI430 and DX51D+Z substrate (Figure 22). The sol-gel layers were uniform and free of cracks and the thicknesses about 3μm ($2.88 \pm 0.50 \mu\text{m}$ for F3_PEG200000 sol-gel).

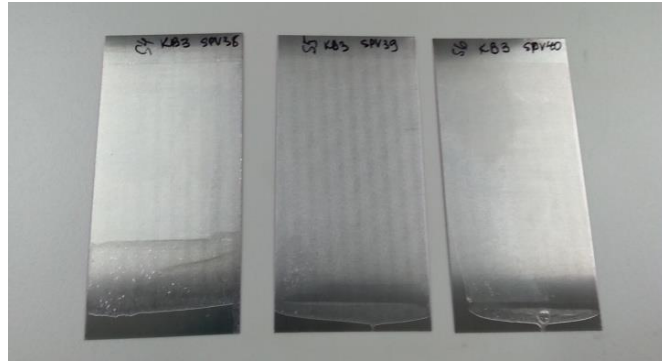


Figure 22. Visual aspect of IL sol-gel single layer applied by K-Bar 3 coating onto AISI430: SPV38: F3-PEG10000, SPV39: F3-PEG200000, SPV40: F3-PEG400000.

Related to the roughness, Figure 23 shows the results determined using mechanical profilometer scans for four steels before and after the application of the F3_PEG200000 sol-gel by the K-Bar3 coating. It can be seen that the printed IL successfully levelled the native steel surfaces making them compatible with TFSC technologies.

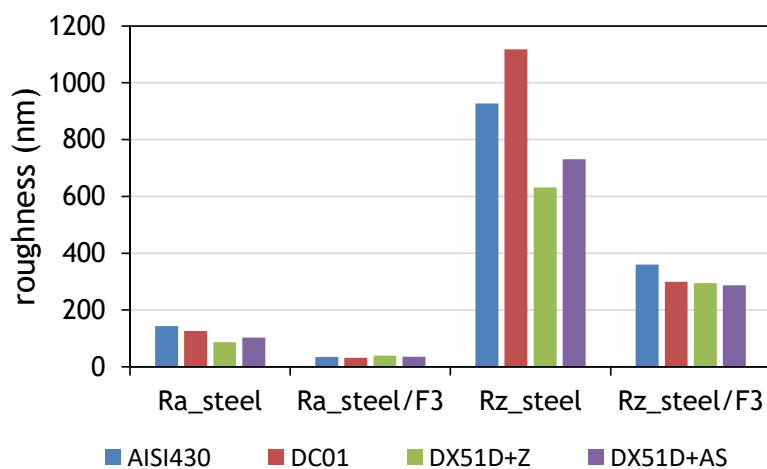


Figure 23. Roughness measured before and after the application of the F3_PEG200000 sol-gel by K-Bar3 coating

Flexography, gravure and screen printing applications

Several printing techniques were explored using different F1 and F3 formulations. None of the sol-gel formulations / printing techniques combinations' were found to fulfil all the STEELPV ILs' requirements.

Flexography print trials were performed using IGT F1 where the plate was mounted using a standard double-sided backing tape. Five micropatterned solid areas were chosen to increase F1 and F3 sol-gel volumes and improve sol-gel transfer and hence, the thickness of the F1 and F3 sol-gel layers.

The visual aspect of the prints was very good (Figure 24) with homogeneous layers free of cracks and delamination.

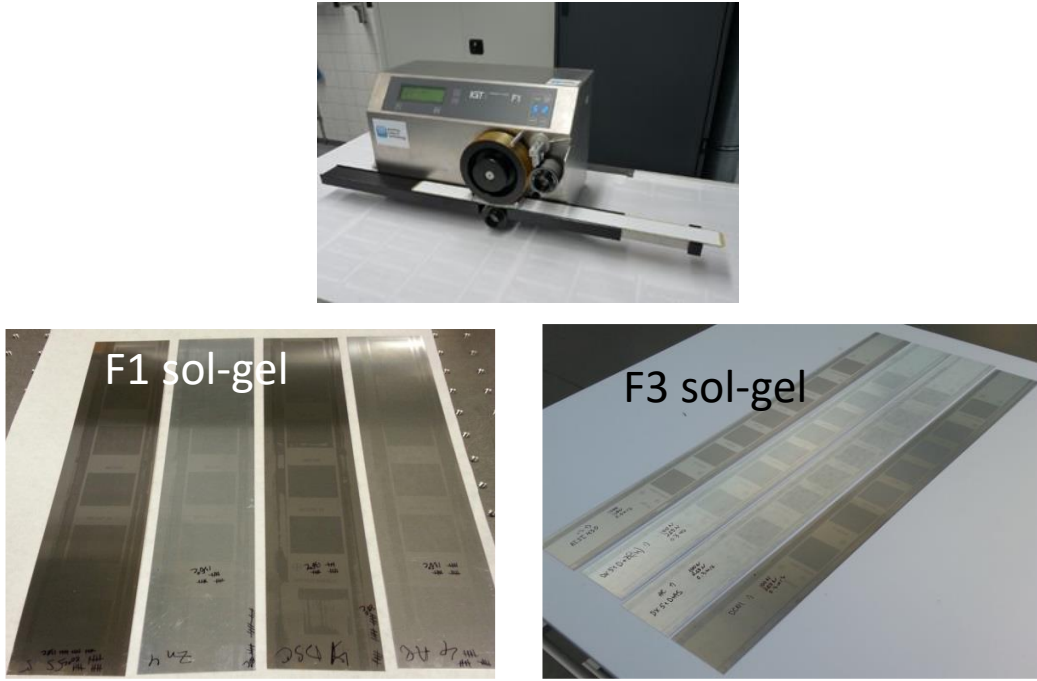


Figure 24. Lab scale flexo tester IGT F1 and flexo prints of F1 and F3 sol-gel IL on four steel substrates.

The sol-gel flexo prints were characterized in terms of roughness and thickness. Figure 25 displays R_z of sol-gel layers for all steel substrates printed with five microcell patterns. As it can be observed related to the surface levelling, only the mc09p_l pattern enables a significant reduction for AISI430, DX51D+Z and DX51D+AS substrates using F1 sol-gel and for DX51D+AS using F3 formulation. Other conditions are not suitable with TFSC.

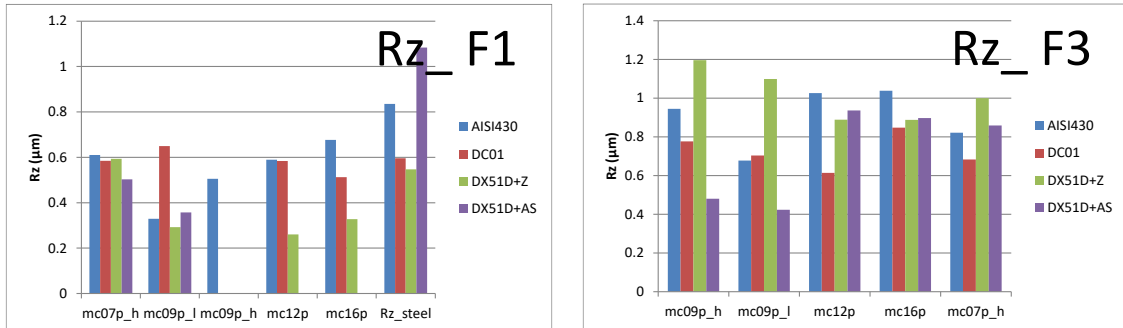


Figure 25. Roughness (R_z) of flexo printed F1 sol-gel IL.

Concerning the thickness, maximum values of 650nm and $1.4\mu\text{m}$ were achieved using F1 and F3 sol-gel. Dielectric tests reported breakdown voltages at about 20-25V what is too low to ensure the proper dielectric IL requirement.

Regarding the gravure printing, the optimum parameters to achieve a continuous sol-gel layer without defects were 100 N gravure cylinder force, 150 N printing force, 0 revolutions, and speed of 1.5 m/s. At these conditions one layer of the F3 sol-gel was printed onto four steels and dried in two steps using a convection oven. The visual aspect of all prints was very good with homogeneous layers free of cracks and delamination. Figure 26 shows an example of the roughness determined for the DX51D+AS steel before and after the application of the F3 sol-gel by the two offsets gravure printing. It can be seen that the printed ILs successfully levelled the DX51D+AS native steel surfaces making them compatible with TFSC technologies. However, the offset gravure printed F3 sol-gel ILs had thickness levels in the range of 0.6-1.5 μm which were below the target value of 3-4 μm and, hence, did not pass the breakdown voltage test.

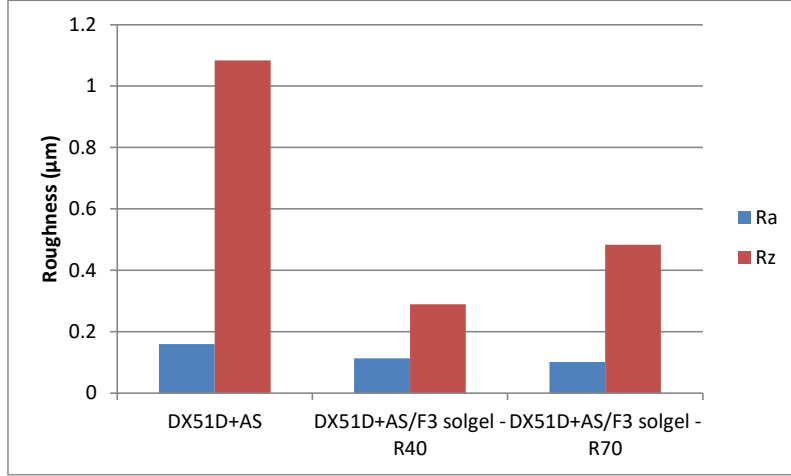


Figure 26 . Roughness measured before and after the application of the F3 sol-gel by offset gravure printing

Screen print trials were performed using F3_PEG200000 and F3_PEG400000 sol-gel formulation. Figure 27 shows the roughness determined through mechanical profilometer scans for all steels before and after the application of the F3_PEG200000 and F3_PEG400000 sol-gels. It can be seen that the screen printed F3_PEG200000 sol-gel IL levelled all but DC01 native steel surfaces in terms of R_z . On the other hand, the roughness of the screen printed F3_PEG400000 sol-gel IL was much higher than that of native steels most likely due to levelling issued of the thicker sol-gel.

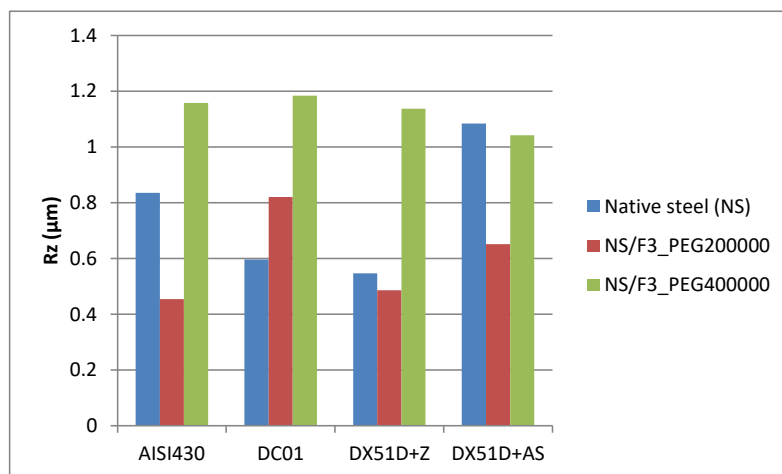


Figure 27. Roughness measured before and after the application of the F3 sol-gels by screen printing

However, many cracks were developed after the curing step (Figure 28).

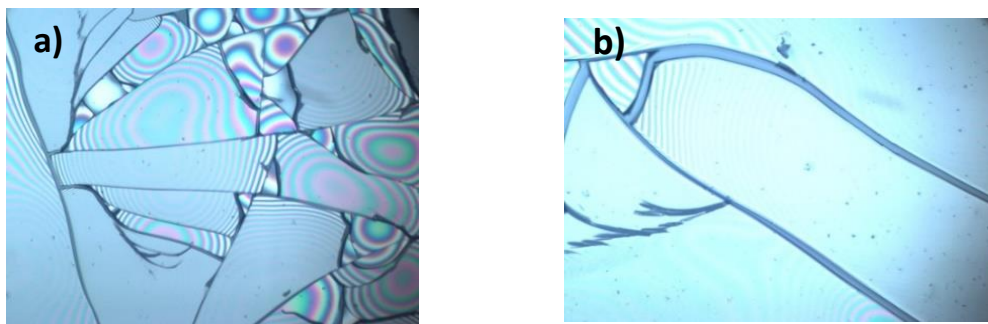


Figure 28. Cracks developed during annealing for screen printed IL: a) F3_PEG200000 and b) F3_PEG400000 sol-gels.

Anti-diffusion barrier behavior of the SiO_x sol-gel

The anti-diffusion behavior of the SiO_x sol-gel single layer was studied using solid state glow discharge mass spectrometry (GD-MS) method. GD-MS provides a fast and direct solid analysis of conducting and non-conducting materials with high depth resolution of comparatively large sample areas ($\sim \text{mm}^2$) [12-13].

Figure 29 shows qualitative in-depth profiles of the hot-dip coated steels covered by the SiO_x sol-gel single layer and an Al coating simulating a TFSC back contact. For each steel/SiO_x/Al system, a comparison between a not-annealed and an annealed process simulating the time and temperature needed for an amorphous silicon TFSC deposition (2h30 – 210°C) is carried out. The Al coating was deposited in order to study if some diffusion from TFSC back contact into the SiO_x layer was happening.

Each qualitative depth profiles reports intensities of the element lines (count per second - cps) versus sputtering time. For each qualitative depth profiles, it can be first observed the Al layer, next the SiO_x coating. At the same sputtering time of the Si and O lines a C one is observed. This is probably due to the PEG releasing agent that is not degraded at 210°C curing temperature.

Related to the DX51D+AS substrate, it is clearly observed that no steel element (Fe, Cr) and Al/Si metallic coating are going through the SiO_x sol-gel, demonstrating the good anti-diffusion behaviour of this IL. Concerning the DX51D+Z substrate, a possible slight diffusion of the Zn may be observed although without interfering with the Al back contact what demonstrate the good anti-diffusion behaviour of the SiO_x sol-gel.

Finally, no diffusion from the Al back contact into the steel substrates was observed, so it appears that the SiO_x sol-gel does indeed act as an ionic blocking layer.

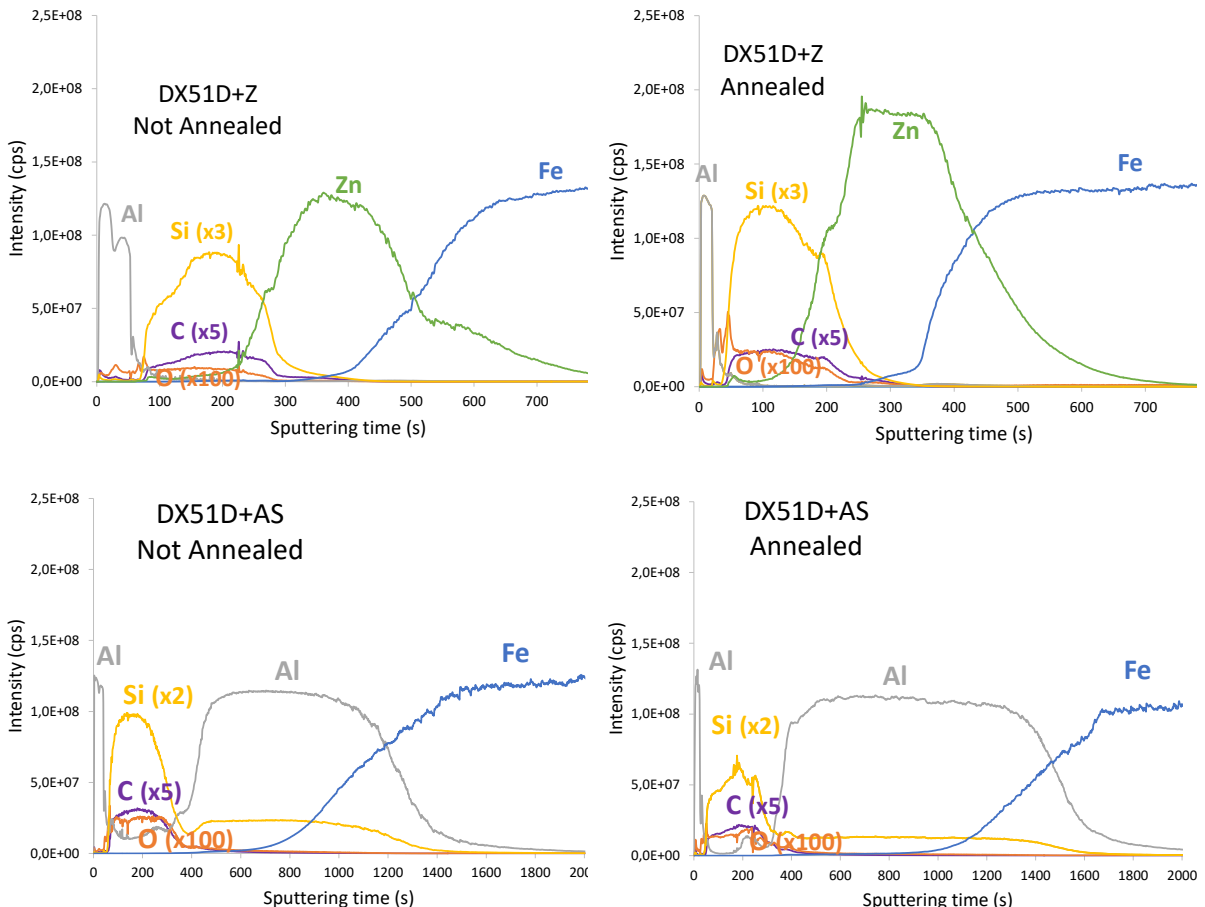


Figure 29. Qualitative depth profiles of not annealed and annealed steels/SiO_x sol-gel samples.

Monolithic cell interconnection: P1 scribing

Serial interconnection strategy has been carried out by laser scribing with conventional industrial marking laser (ROFIN, nanosecond pulsed, Nd:YAG, repetition rates in the KHz range and wavelength of 532 nm). The P1 scribe has been developed in a similar way than followed in superstrate configuration (p-i-n structure) by a-Si thin film solar modules manufacturers considering the Al/ITO TFSC back contact. Related to OPV TFSC, a Al/ZnO back contact has been tested (Figure 30). The laser scribing process enables to avoid the silk printing or “cut & paste” approaches for PV cells serial interconnections [14]. Due to the use of non-transparent substrates, P1 scribes have been applied directly on the TFSC back contacts.

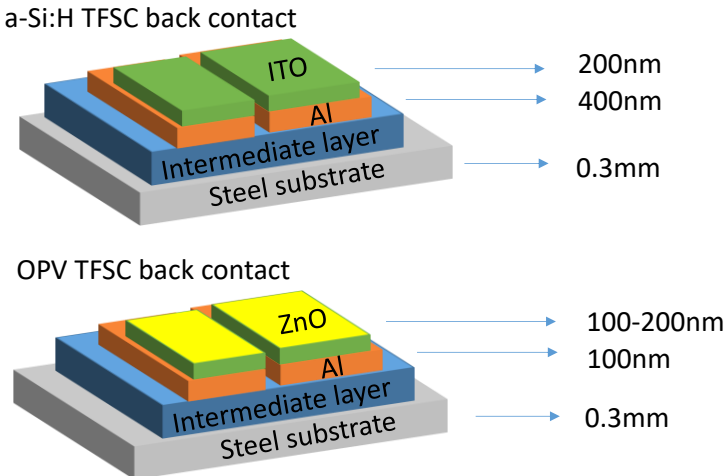


Figure 30. P1 laser scribing considering a-Si and OPV TFSC back contacts.

The laser source parameters (current intensity, scan speed and repetition rate) have been optimized, while the wavelength (532 nm) and the focal length were kept constant.

The optimum parameters to achieve a continuous P1 scribe without defects were 20.5A, 1500mm/s and 50Hz for the current intensity, the scan speed and repetition rate, respectively. At these conditions the mechanical profile shows a cut about 600nm depth what is agreement with the a-Si TFSC back contact deposited.

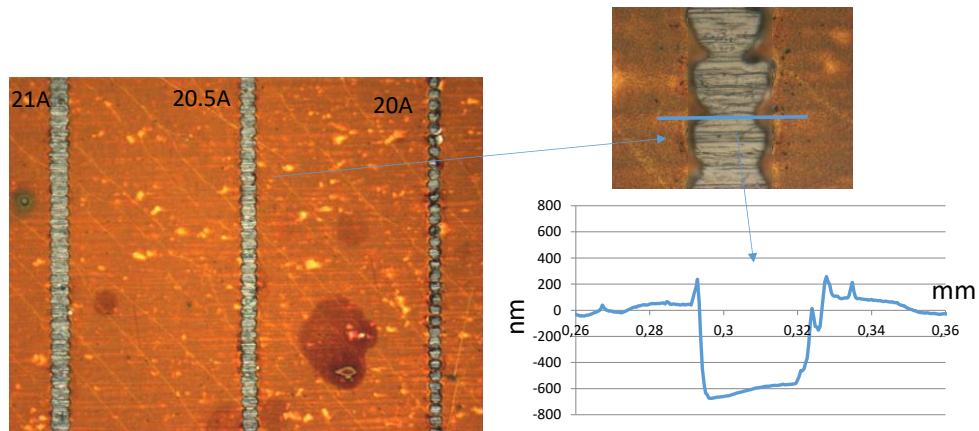


Figure 31. Influence of the current intensity on the P1 scribe (a-Si TFSC back contact).

Related to the OPV back contact (Figure 32), optimum conditions were achieved at 21.5A, showing a mechanical profile of 200nm depth in agreement with the OPV back contact.

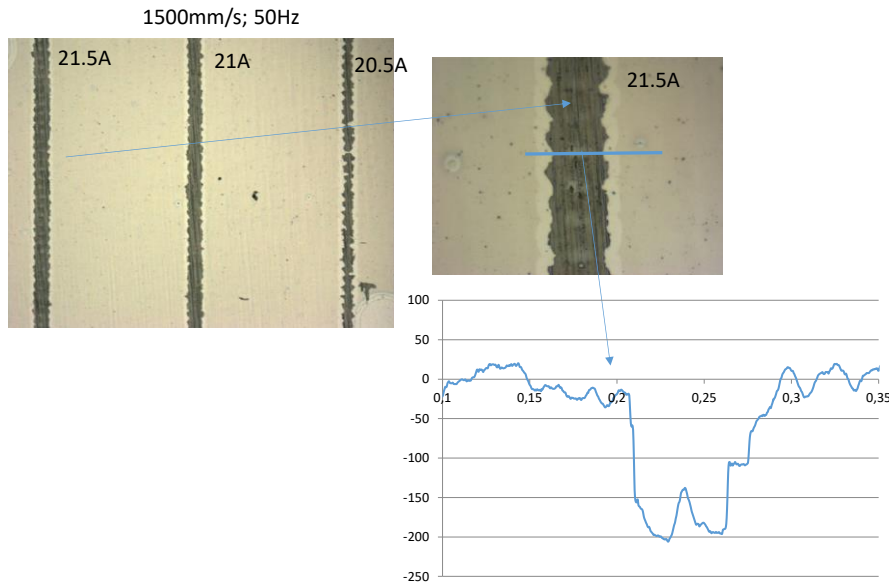


Figure 32. Influence on the current intensity on the P1 scribe (OPV TFSC back contact).

After the characterization tests carried out on the SiO_x sol-gel single-layer, it can be concluded that the SiO_x sol-gel approach fulfill all the requirements established in the project to make compatible the 'rough' steels selected and rolled in WP1 for TFSC devices. Dip, roll and spray techniques are suitable to up-scale the F1sol-gel and K-bar to up-scale the F3 sol-gel.

Wet solutions alternatives to SiO_x sol-gel

The alternatives to sol-gels were identified with the following priorities: low cost, proven dielectric material in electronics, printability/coatability, good insulation, good adhesion to underlying steel, can act as diffusion barrier, etc.

Three solvent based screen inks such as solvent resistant blue dielectric paste (D2140114D5), white dielectric paste (D2070209P6) and UV curable dielectric ink (D2150901D1) from GEM, UK were tried. Screen printing was chosen for printing these dielectric layers as a wide range of well establish dielectric inks is commercially available. Also, a wide range of the layer thicknesses (1-30 μm) could be achieved by screen printing depending on process parameters.

A-second alternative route of IL development was based an epoxy material; SU-8. It is widely used in the microelectronics and MEMs industry as it crosslinks under UV irradiation and can be used for patterning. The SU-8 epoxy layer (the formulation used is SU-2050, supplied from Chestech Ltd., UK) was doctor bladed onto the steel samples (size 18x18mm) and then spin or K-bar coated at 2000 rpm. The film was then cured at 150°C for 15 minute then hard baked at 250°C for 10 minute.

Table XIII summarizes the polymeric commercial coating and the application techniques experimented. This table reports which steel/IL/application technique combination has technically fulfilled the requirements established for an intermediate layer (in green) and is a good candidate to be compatible with a TFSC deposition and to be up-scaled.

Table XIII. Combination of Steel/Polymeric commercial IL/application techniques successful for TFSC depositions and IL up-scaling.

Solutions	Reference	K-Bar coating	Screen printing
SU8	SU-2050, Chestech Ltd.	All steels	---
Blue ink	D2140114D5, GEM	---	All steels
White ink	D2070209P6, GEM	---	All steels
UV curable	D2150901D1, GEM		All steels

Figure 33 reports the average roughness of the three dielectric inks (single layer) applied by screen printing onto the AISI430 steel. It can be observed that the blue ink one enables to drastically reduce the steel native roughness ($R_a=36\text{nm}$ was achieved) whereas the other two inks increase it (up to 2400nm considering the UV curable ink). Similar results were achieved with the other steel substrates.

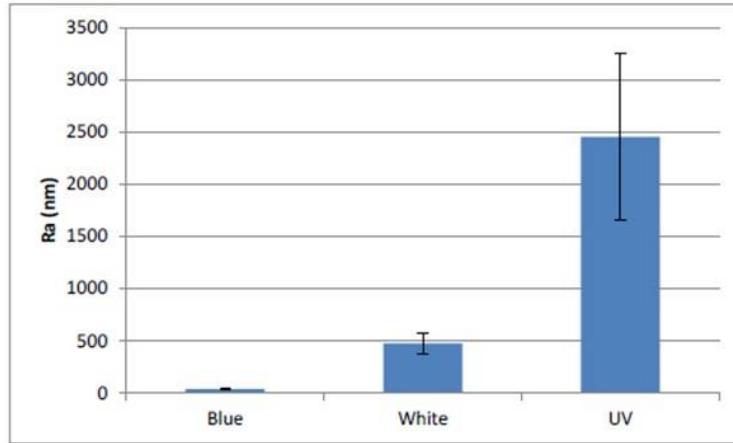


Figure 33. Roughness (R_a) determined after applying the different dielectric inks

Considering the 'blue ink', the influence of several layers on the roughness was studied. Figure 34 shows that the roughness does not decrease from the two layers deposits to the three layers' one. The thickness of 'blue ink' samples was about 8\mu m for one layer deposits, about 20\mu m for two layers deposits, and about 27\mu m for three layers deposits.

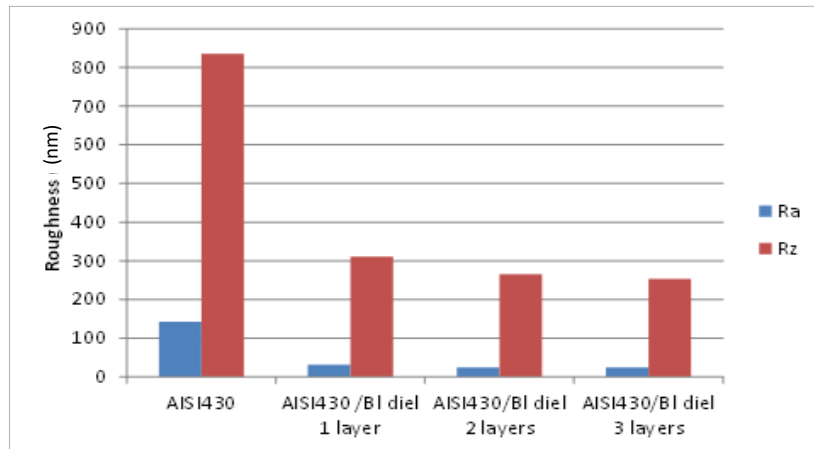


Figure 34. Screen prints of blue dielectric IL on AISI430.

Integrity of the 'blue ink'

The integrity aging tests were first of all performed through outdoor real atmospheres ($12^\circ\text{C}-30^\circ\text{C} - >70\text{HR}$ [15]) and the integrity behavior evaluated through the breakdown voltage test after 3 months of exposition. Figure 35 shows AISI430 and DX51D+Z steels covered by the 'blue ink' coating after 3 months of exposition in outdoor atmosphere. The visual aspect of the 'blue in' is, in all cases perfect. Considering those systems the anti-diffusion behavior of the 'blue ink' coating was studied by the solid state GD-MS method and no diffusion were registered.

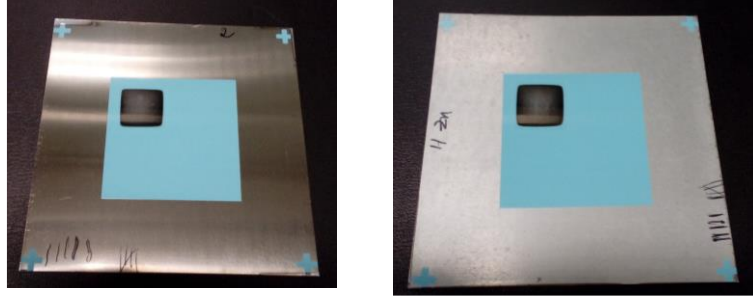


Figure 35. Visual aspect of the four AISI430 and DX51D+Z with blue ink _ Outdoor test after 3 months.

Monolithic cell interconnection: P1 scribing

Serial interconnection strategy has been carried out by laser scribing with conventional industrial marking laser (ROFIN, nanosecond pulsed, Nd:YAG, repetition rates in the KHz range and wavelength of 532 nm). The P1 scribe has been developed in a similar way as explained in the SiO_x sol-gel section and considering the a-Si and OPV TFSC back contacts (Al/ITO and Al/ZnO).

Related to a-Si back contact, the optimum parameters to achieve a continuous P1 scribe without defects were 21.5A, 1500mm/s and 50Hz for the current intensity, the scan speed and repetition rate, respectively. The wavelength (532 nm) and the focal length were kept constant.

At these conditions the mechanical profile shows a cut about 600nm depth (Figure 36) what is agreement with the a-Si TFSC back contact deposited.

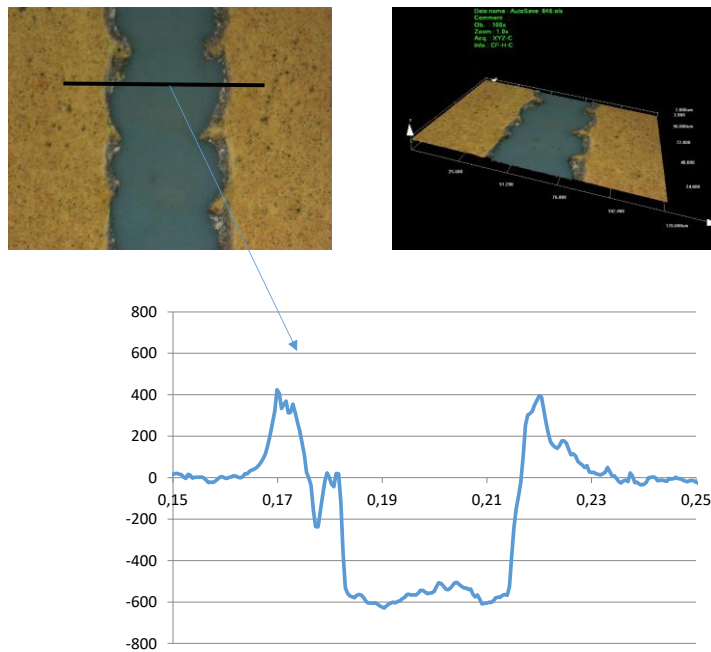


Figure 36. P1 scribe aspect and mechanical profile (a-Si back contact).

Concerning the OPV back contact, the optimum current intensity was 21.A to achieve a continuous P1 scribe without defects. The mechanical profile shows a cut about 300nm depth (Figure 37) what is agreement with the OPV TFSC back contact deposited

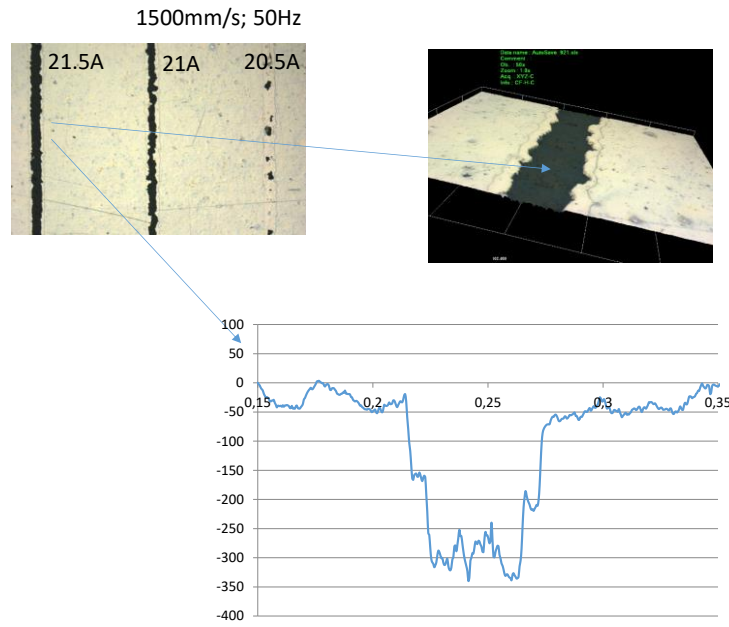


Figure 37. P1 scribe aspect and mechanical profile (OPV back contact)

After the characterization tests, it can be concluded that Screen Printing is a viable technique to apply the dielectric 'blue' ink and to fulfil the requirements to make compatible the steels selected in the project for TFSC applications.

Commercial SU-8 epoxy layer

The formulation used, SU-2050, supplied from Chestech Ltd., was doctor bladed onto the four steel and then applied using either spin coating or K-Bar coating and offered a high levelling quality ($R_a < 15\text{nm}$ and $R_z < 70\text{nm}$). Thicknesses about $50\mu\text{m}$ were determined. Figure 38 shows a comparison of the steel substrates before and after IL treatment using SU-8, which were measured using White Light Interferometry (WLI). For each sample, a map of the surface topography was obtained first using WLI microscope (Micro-XAM from KLA-Tencor, Milpitas, CA).

It is clear that the application of SU-8 dramatically reduces the surface roughness of the steel. Table XIV shows the measured roughness from WLI measurements and using mechanical profilometer, what confirm the high levelling achieved.

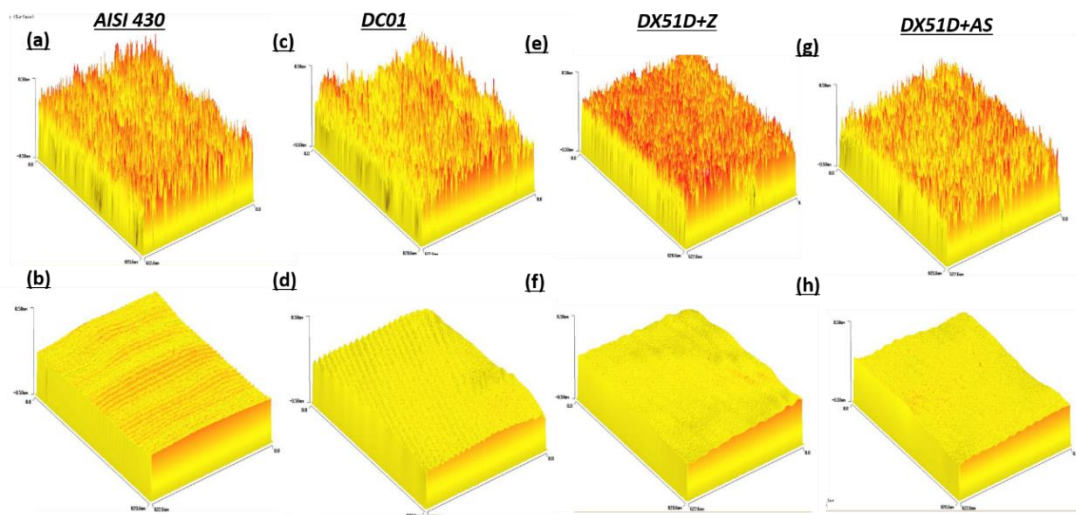


Figure 38. White light interferometry measurements of (a) AISI430 before and (b) after application of SU-8 IL, (c) DC01 before and (d) after application of SU-8 IL, (e) DX51D+Z before and (f) after application of SU-8 IL and (g) DX51D+AS before and (h) after application of SU-8 IL. Area size is $6 \times 8\text{mm}$, with a z-axis scale of -50 to $50\mu\text{m}$

Table XIV. Measure surface roughness (nm) by WLI and mechanical profilometry (MP) of steel grades selected in WP1 before and after IL coating with SU-8.

	AISI430			DX51D+Z			DX51D+AS			DC01		
	No IL WLI	With IL WLI	With IL MP	No IL WL	With IL WLI	With IL MP	No IL WLI	With IL WLI	With IL MP	No IL WLI	With IL WLI	With IL MP
R _a	100	12	7	97	15	11	83	10	15	83	10	8
R _z	710	63	60	630	57	70	710	55	90	590	49	66

Monolithic cell interconnection: P1 scribing by the K-Bar coating

Related to a-Si back contact, the optimum parameters to achieve a continuous P1 scribe without defects were 19A, 1500mm/s and 50Hz for the current intensity, the scan speed and repetition rate, respectively. The wavelength (532 nm) and the focal length were kept constant.

At these conditions the mechanical profile shows a cut about 600nm depth (Figure 39) what is agreement with the a-Si TFSC back contact deposited.

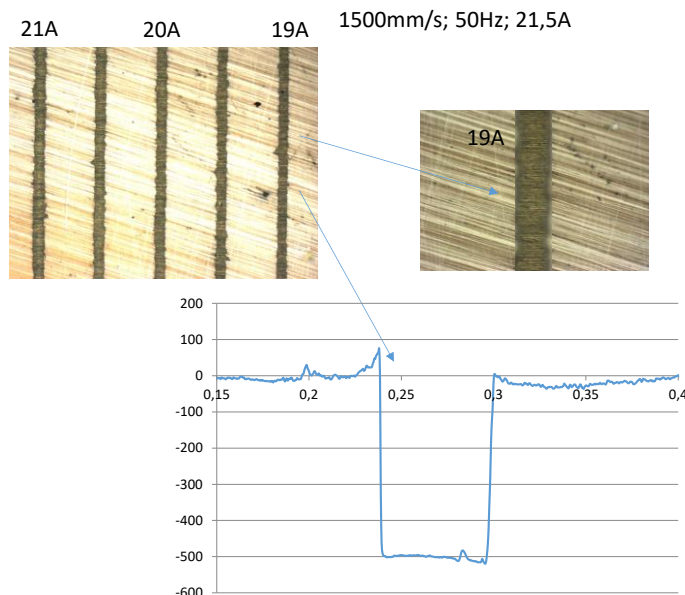


Figure 39. P1 scribe aspect and mechanical profile (a-Si back contact).

Concerning the OPV back contact just Ag was deposited and the optimum current intensity was 20.5A to achieve a continuous P1 scribe without defects. The mechanical profile shows a cut about 100nm depth (Figure 40) which is in good agreement with the OPV TFSC Ag back contact thickness.

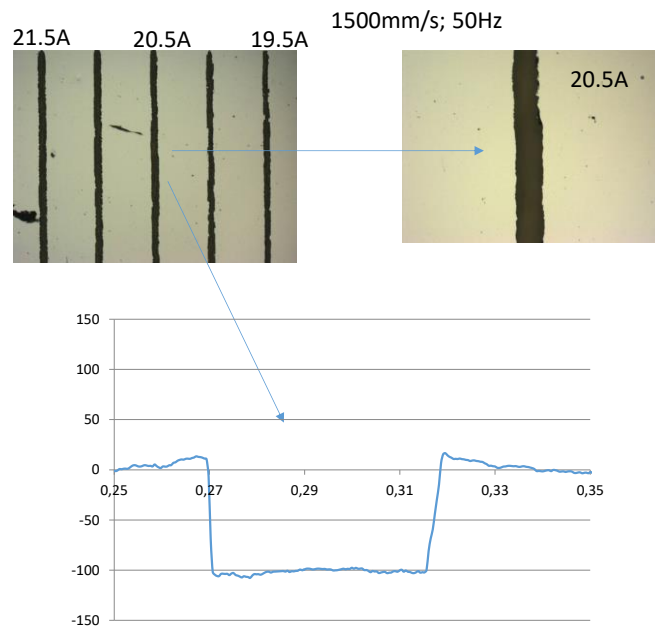


Figure 40. P1 scribe aspect and mechanical profile (OPV back contact)

After the characterization tests, it can be concluded that K-Bar coating is a viable technique to apply the epoxy SU-8 polymer and to fulfil the requirements to make compatible the steels selected in the project for TFSC applications.

b) ILs developed through the vacuum route

The IL layers were based on ceramic oxides and nitrides materials. The main advantage of vacuum technologies for the IL developments is the high quality that can be reached in terms of very low contamination and the high density of the coating, which is crucial for high quality dielectric and anti-diffusion layers. Moreover, the techniques considered in the project are all widely used industrial technologies. Table XV reports the different materials deposited as well as the vacuum techniques used. As it can be observed, same materials have been deposited by different methods in order to compare their influence on the IL quality.

Table XV. Vacuum deposition techniques and materials considered

Materials	Non reactive Sputtering PVD	Reactive Sputtering PVD	Cathodic Arc PVD	PECVD
HfO ₂	AISI430 DC01 DX51D+AS	AISI430 DC01 DX51D+AS		
Al ₂ O ₃	AISI430 DX51D+AS	AISI430 DX51D+AS		
TiO ₂	AISI430 DX51D+AS	AISI430 DX51D+AS	AISI430 DX51D+AS	
Si ₃ N ₄	AISI430 DX51D+AS	AISI430 DX51D+AS		
Cr ₂ O ₃	AISI430 DX51D+AS	AISI430 DX51D+AS		
Al _x N _y	AISI430	AISI430		
TiO _x	AISI430	AISI430		
ZnO _x		AISI430		
SiO _x		AISI430		AISI430
SiAlO _x		AISI430		

Two industrial PVD and a PECVD machines were employed (Figure 41). The PVDs offer the possibility of depositions with both sputtering and cathodic arc. One machine allows a rotation of the sample holder during the deposition in order to get films that show a high uniformity even on substrates with a complex geometry and to realize continuous deposition processes. In the other machine, flat substrates can be processed in a horizontal translation mode (up to three targets).



Figure 41. Illustrations of the PVD and PECVD machines

In **PVD sputtering**, the material to be deposited from a 'target', which is eroded by a low pressure plasma produced by the ionization of gases such as Ar, N₂, O₂, etc. If reactive gases such as N₂ and O₂ are employed, there is the possibility of depositing nitrides or oxides of the selected metals (e.g. titanium oxide is achieved considering a target of Ti and O₂ is used as sputtering gas in the deposition chamber).

In **Cathodic arc mode**, the material to be deposited, is eroded by an electric arc placed onto the cathode. Thus, to employ this variant the material to be deposited must be electrically conductive. The deposition temperature is generally high and the rate of growth is higher respect to the sputtering variant.

In the **PECVD** mode, the material is deposited through the plasma of a mixture of gas. In the project the SiO_x IL was deposited considering the process summarized in Table XVI. With these conditions, the deposition rate was 28nm/min.

Table XVI. Process conditions during SiO_x by PECVD

Pressure [mbar]	Ar Flow [sccm]	N ₂ O Flow [sccm]	SiH ₄ Flow [sccm]	Temp [°C]	Power MW [W]
6.2x10 ⁻²	50	16	34	RT	1100

PVD and PECVD: single layer

The influence of different IL thicknesses deposited by PVD was studied. In Al_xN_y case, its thickness was varied in the range 0.5 to 4 microns, Figure 42 reports that no improvement of the surface quality is observed for any thickness.

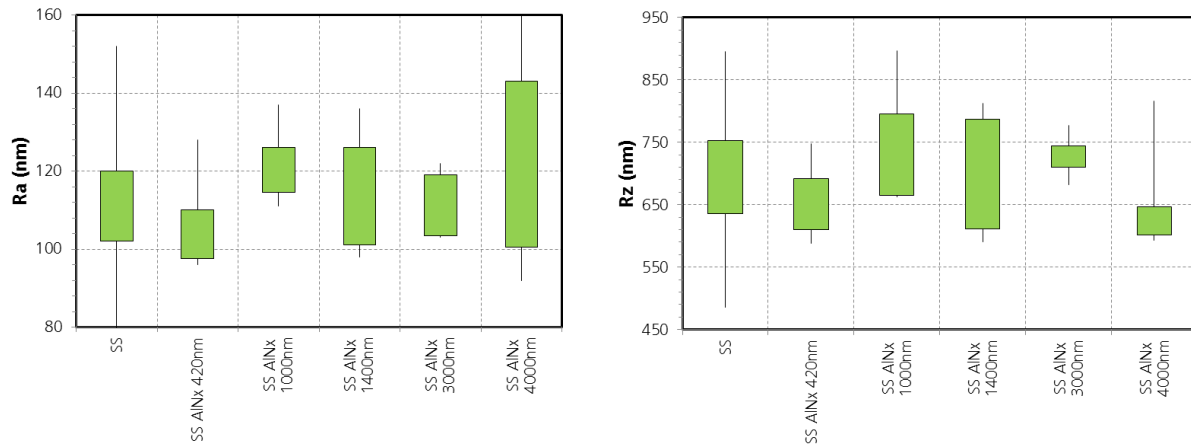


Figure 42. Surface roughness after Al_xN_y deposition with different thickness on AISI430

Considering the PECVD technique, single layers were also deposited varying their thicknesses; 300nm, 700nm and 1200nm. As shown in Figure 43, no clear benefit is observed regarding the surface quality of the AISI430 steel after SiO_x deposition: the roughness is closer to the original steel roughness, and no clear trend with thickness is observed.

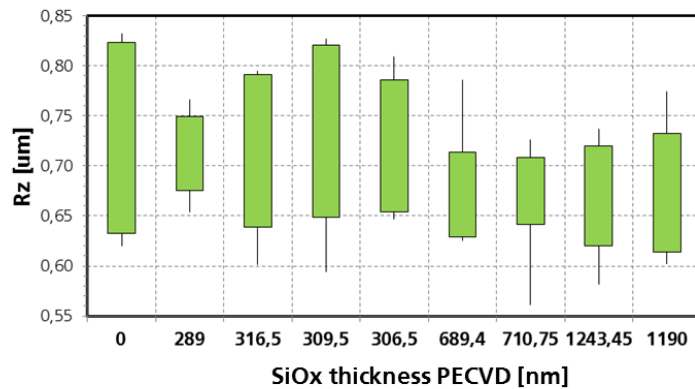
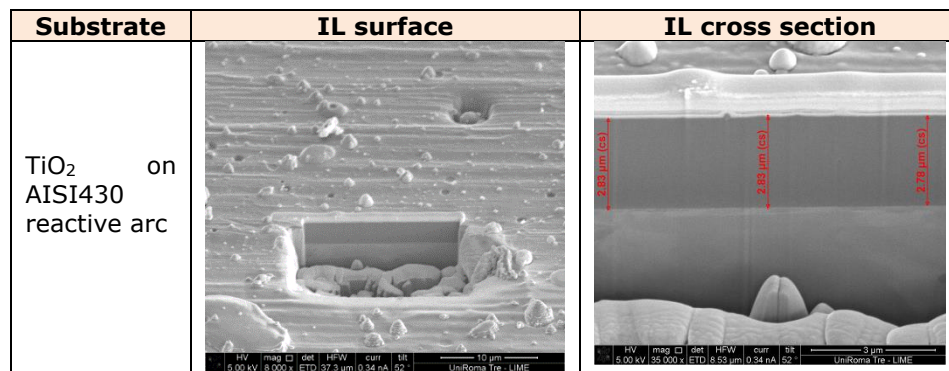


Figure 43. Surface roughness of SiO_x on AISI430 deposited by PECVD

PECVD mode showed very good adhesion coatings and the fastest deposition rates but macro droplets discard this technique for the purpose of the project. This phenomena is probably due to instabilities of the arc current that are determined by the high partial oxygen pressure employed. Table XVII shows an example of characterisation TiO₂ IL deposited on AISI430 steel.

Table XVII. Example of characterization test by SEM and FIB analyser_ Si_3N_4 IL on AISI430 steel.



Related to reactive and non-reactive sputtering modes, Figure 44 shows a comparison of the roughness of IL deposited on AISI430 and DX51D+AS. From the results of the roughness measurements carried out before and after PVD depositions, several considerations can be carried out:

- Specimens coated with non reactive sputtering have shown a lower roughness respect to specimens coated with reactive sputtering. This could be due to the fact that in the reactive sputtering, the optimal oxygen partial pressure as a function of the total pressure is not correct and hence the stoichiometric ratio between sputtered atoms and oxygen atoms impacting on the target is non-optimised.
- Si_3N_4 seems to be the most promising material for surface roughness reduction (Figure 44). It was observed that increasing the pressure in the deposition chamber by a factor 2.5 reduced the surface texture.

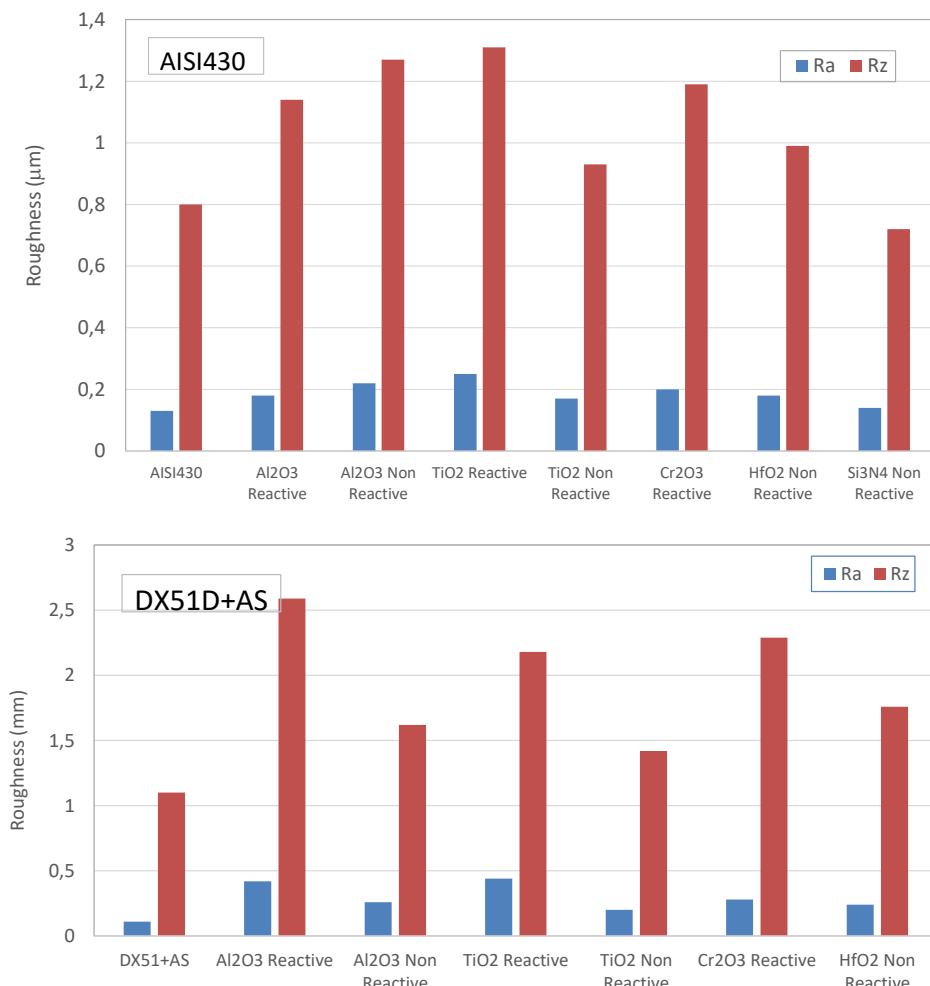
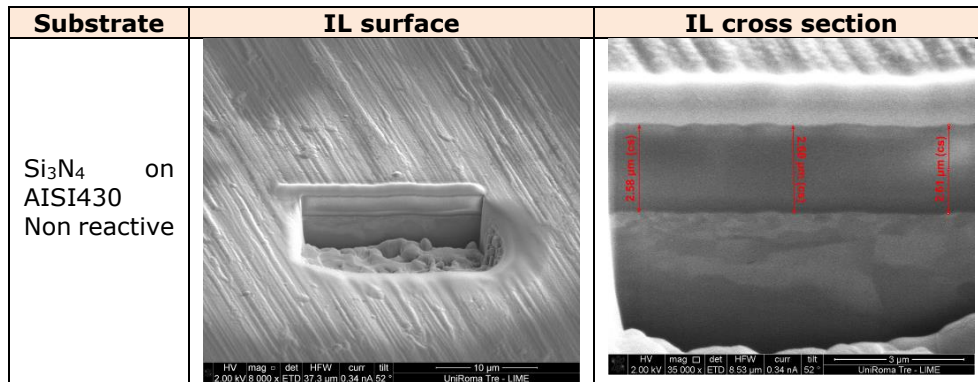


Figure 44. Comparison of R_z and R_a before and after PVD reactive and non reactive modes.

Considering the Si_3N_4 layers, characterization tests were also performed by SEM and a Focused Ion Beam (FIB) analyser. It can be observed a good interface with both the AISI430 and DX51D+AS steel substrates without appreciable defects such as interdiffusion between the coating and the substrate or detaching area of the coating from the substrate. Table XVIII shows an example of characterisation by using the FIB analyser, concretely of the surface and section of a Si_3N_4 IL deposited on AISI430 steel.

SEM analysis of Si_3N_4 shows that its thickness is consistently higher respect to the other materials deposited by non reactive sputtering, even considering that the other deposition parameters have been fixed to values that can justify these differences. So, it is possible to conclude that Si_3N_4 is really suitable to be deposited by sputtering in Ar atmosphere, reaching very high deposition rates.

Table XVIII. Example of characterization test by SEM and FIB analyser_ Si_3N_4 IL on AISI430 steel.



PVD and PECVD: multi-layers

The multilayer approach, using the PVD sputtering process or a combination of PVD/PECVD, has consisted in designing stacks of different materials under the hypothesis that the additional layers are not influenced by the native surface of the steel and it will be able to level the defects. The combinations of materials/techniques are summarized in Table XIX.

Table XIX. Vacuum deposition techniques and materials considered

Materials	Sputtering PVD	PECVD
$\text{SiO}_x/\text{SiO}_x$	AISI430	AISI430
$\text{TiO}_x/\text{Al}_x\text{N}_y$	AISI430	
$\text{SiO}_x/\text{TiO}_x$	AISI430	
$\text{Al}_x\text{N}_y/\text{SiO}_x$	AISI430	AISI430

Concerning stack depositions by PVD mode, it can be observed that no improvements were achieved comparing with single layers experiments when two layers of 2 microns each one are combined to create one bilayer structure. No differences between AISI430/ $\text{Al}_x\text{N}_y/\text{TiO}_x$ and AISI430/ $\text{TiO}_x/\text{Al}_x\text{N}_y$ were observed. In fact, when Al_xN_y is deposited on top of TiO_x , the resulting surface roughness (R_z) was higher than for the AISI430 (Figure 45).

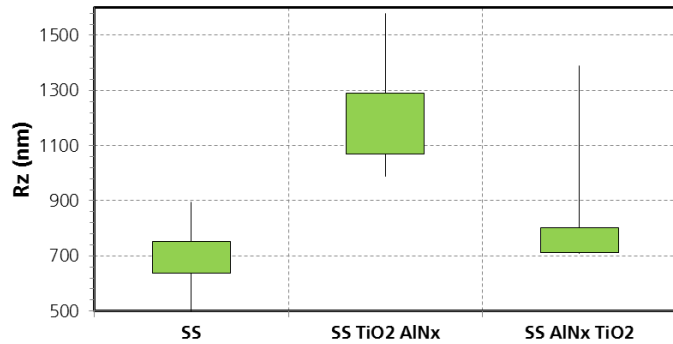


Figure 45. Surface roughness after TiO_x and AlN_x deposition on AISI430

Concerning the combination of SiO_x deposited by PVD and PECVD modes, it can be observed that the roughness does not improve. Although R_a is lower after barrier layer deposition, R_z presented a higher deviation (Figure 46).

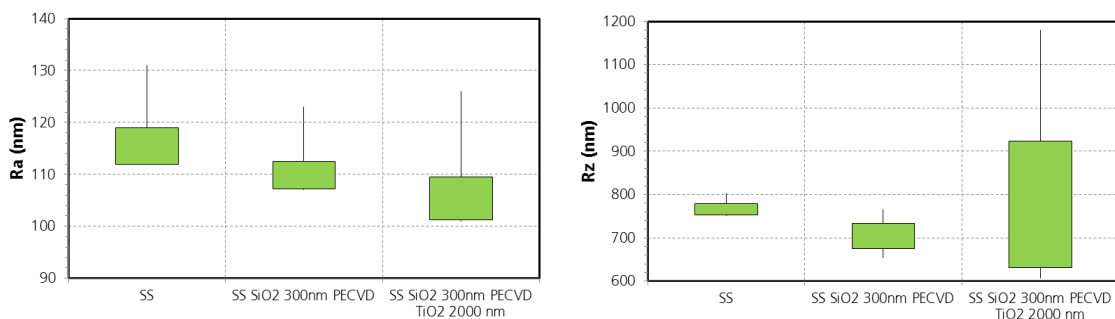


Figure 46. Surface roughness reduction when SiO_x by PVD is deposited on 300nm of $SiO_x/AISI430$ deposited by PECVD

Based on the levelling results, it was concluded that the vacuum approach alone in single or multi-layers strategies is not suitable to fulfil the requirements to be compatible with the deposition of TFSC and will not be considered for the up-scaling part. However, several materials, in particular SiO_x and Si_3N_4 show interesting properties and will be considered for hybrid stacks.

c) ILs developed through the hybrid route

The hybrid route has dealt with the combination of different vacuum techniques with wet sol-gel process for IL stacks developments. The main motivation for those developments was the achievement of high quality ILs as, in wet single layer strategies some cracks and other kind of defects could appear during the deposition and curing processes. In the hybrid strategy, the sol-gel layer was applied only for its high capacity of levelling and the vacuum techniques main purpose was to improve the dielectric property through the deposition of dense and free of defects layers.

Several approaches below described have been carried out. Table XX reports the different materials deposited as well as the techniques used.

Table XX. Deposition techniques and material considered

Reactive Sputtering PVD	PECVD	Sol-gel	Substrates
SiO _x	----	SiO _x	AISI430
----	SiO _x	SiO _x	AISI430
Si ₃ N ₄		SiOx	AISI430

SiO_x/SiO_x hybrid stacks

Levelling property

The first approach has initially considered SiO_x/SiO_x in bi and tri-layers in order to better match the CTE of the layers piled, SiO_x was selected for both the sol-gel solution and the magnetron sputtering. Three alternative stacks were proposed (Figure 47).

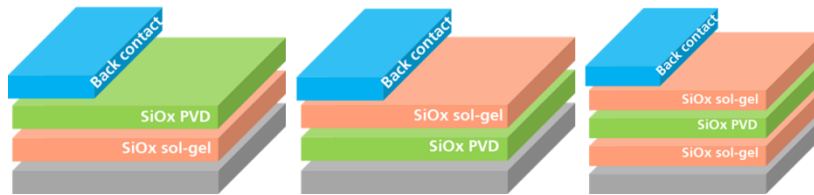


Figure 47. Proposed structures to study combined SiO_x layers deposited from sol-gel and PVD

The aim of these experiments was to reduce the roughness on the native steel surface using the SiO_x sol-gel layer, and to enhance the insulation behaviour of the barrier layer, by sputtering the SiO_x layer. The SiO_x thickness deposited by magnetron sputtering was progressively increased, while SiO_x thickness deposited from sol-gel was kept constant (about 1.5μm).

The main result is that in all cases the roughness was decreased in the range of 20% (R_z), with the majority of the reduction due to the sol-gel layer and almost no impact from the SiO_x material deposited by magnetron sputtering. For the bilayer structure (PVD/sol-gel), the optimum thickness of SiO_x deposited by magnetron sputtering is 600nm, from the point of view of surface quality. However, the electrical behaviour was optimum for 1200nm SiO_x layer, due to the thicker layer being better suited to the rough steel surface (less pinholes and better covering of the substrate).

For the tri-layer, the structure has consisted in a SiO_x by magnetron sputtering sandwiched between two SiO_x from sol-gel and showed the best results in terms of surface levelling (Figure 48). The optimum thickness was also found to be 600nm. When the thickness is increased to 1200nm, cracks and voids are present on the surface of the top SiO_x layer. The mechanical stress accumulated in the sputtered layer during the last sol-gel curing step at 500°C is likely the origin of this failure.

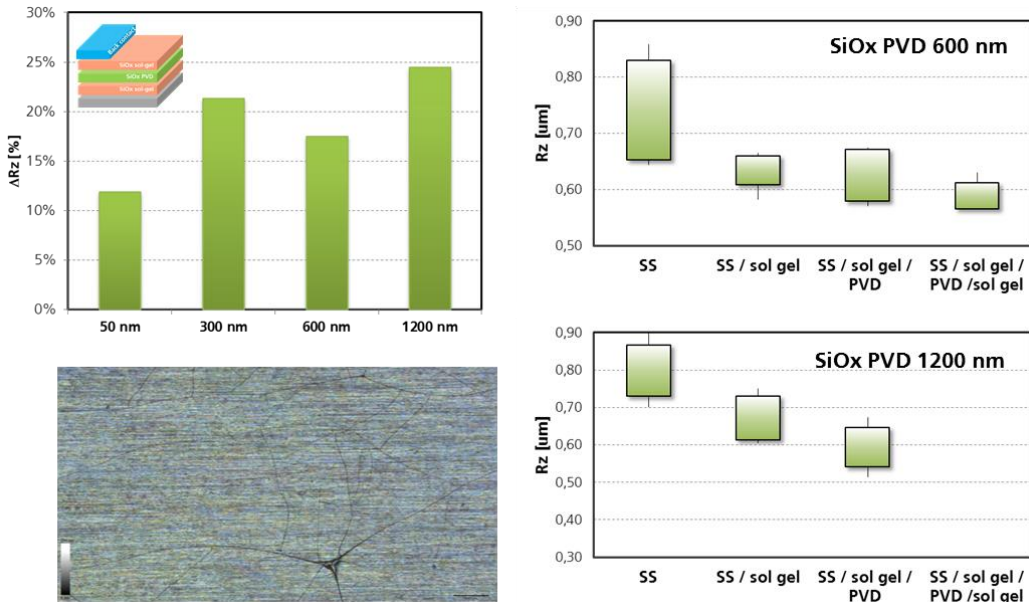


Figure 48. On the left, surface roughness reduction obtained with sandwich structure (sol-gel/PVD/sol-gel) and visual inspection revealing cracks on the surface; on the right, surface roughness measured during the stacking of layers, as function of SiO_x thickness deposited by magnetron sputtering

Anti-diffusion behavior of the solgel/PVD/sol-gel strategy

The anti-diffusion behavior of the SiO_x tri layer hybrid strategy coating was studied by the solid state GD-MS method. Figure 49 shows qualitative in-depth profiles of AISI430 steel covered by the SiO_x hybrid layer and a Mo coating simulating a TFSC back contact. A comparison between a not-annealed and an annealed process simulating the time and temperature needed for CIGS/CZTS TFSC deposition (45min _ 550°C) is carried out. The Mo coating was deposited in order to study if some diffusion from TFSC back contact into the SiO_x layer was happening.

For both qualitative depth profiles, it can be first observed the Mo layer, then the SiO_x hybrid layer and finally the element signal of the AISI430 substrate. It is also important to observe in the annealed sample that the Fe and Cr signal are not penetrating into the SiO_x layer, demonstrating that the hybrid SiO_x acts as anti-diffusion barrier.

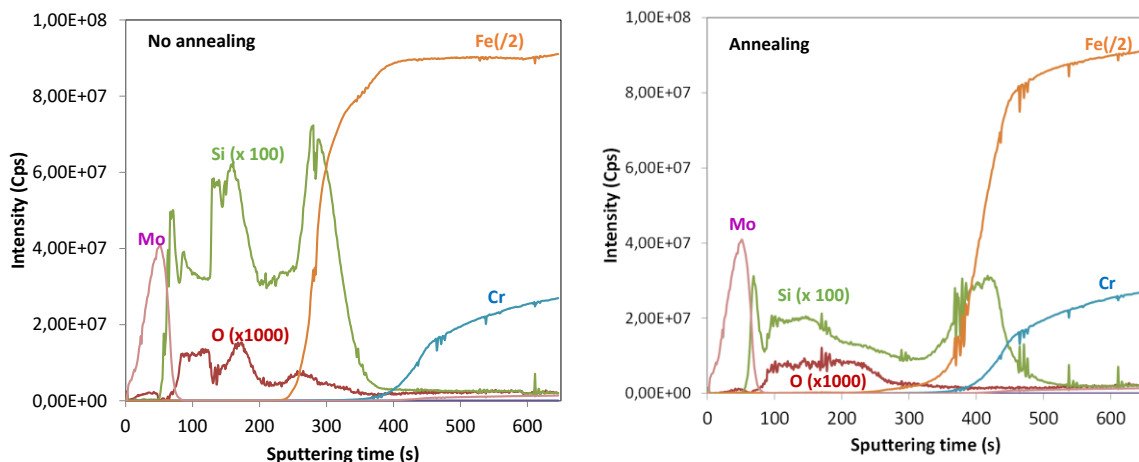


Figure 49. Qualitative in-depth profiles of not annealed and annealed AISI430/hybrid SiO_x samples.

Monolithic cell interconnection: P1 scribing

Serial interconnection strategy has been carried out by laser scribing with conventional industrial marking laser (ROFIN, nanosecond pulsed, Nd:YAG, repetition rates in the KHz range and wavelength

of 532nm). The P1 scribe has been developed in a similar way as explained in the SiO_x sol-gel section and considering a-Si, CZTS and OPV TFSC back contacts (Al/ITO, Mo and Al/ZnO, respectively).

Considering the a-Si back contact, the optimum parameters to achieve a continuous P1 scribe without defects were 20A, 1500mm/s and 50Hz for the current intensity, the scan speed and repetition rate, respectively. The wavelength (532nm) and the focal length were kept constant.

At these conditions the mechanical profile shows a cut about 600nm depth (Figure 50) what is agreement with the a-Si TFSC back contact deposited. It can also be observed that higher conditions (20.5A and 21A) show a deterioration of the hybrid SiO_x layer.

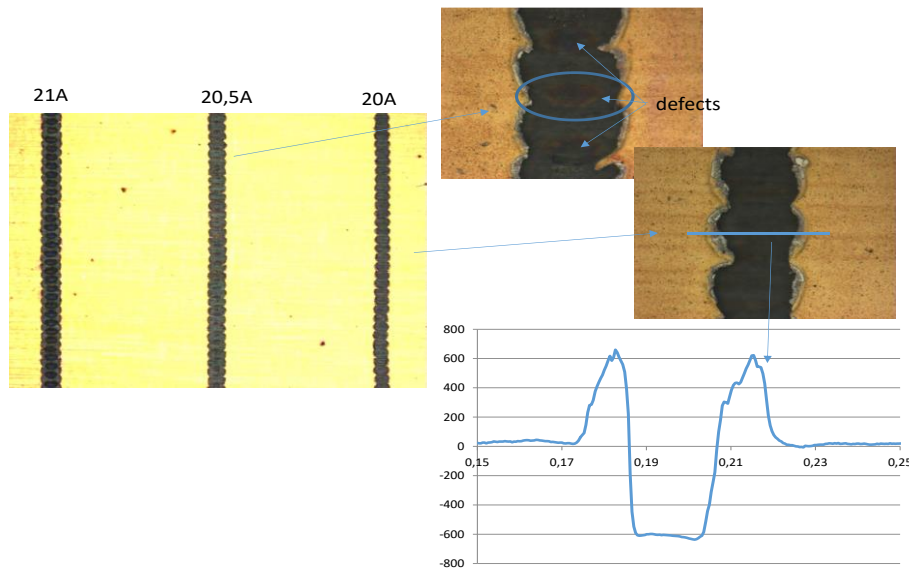


Figure 50. Influence of the current intensity on the P1 scribe.

Related to the CZTS, a Mo back contact of 700nm deposited by PVD technique. Three laser (355, 532 and 1064nm) sources were used to identify best process conditions (Figure 51): Mo layer is removed, scribe produced has square profile, barrier layer is not affected by thermal or mechanical stress. The scribes were also characterized by electronic microscope (Figure 52).

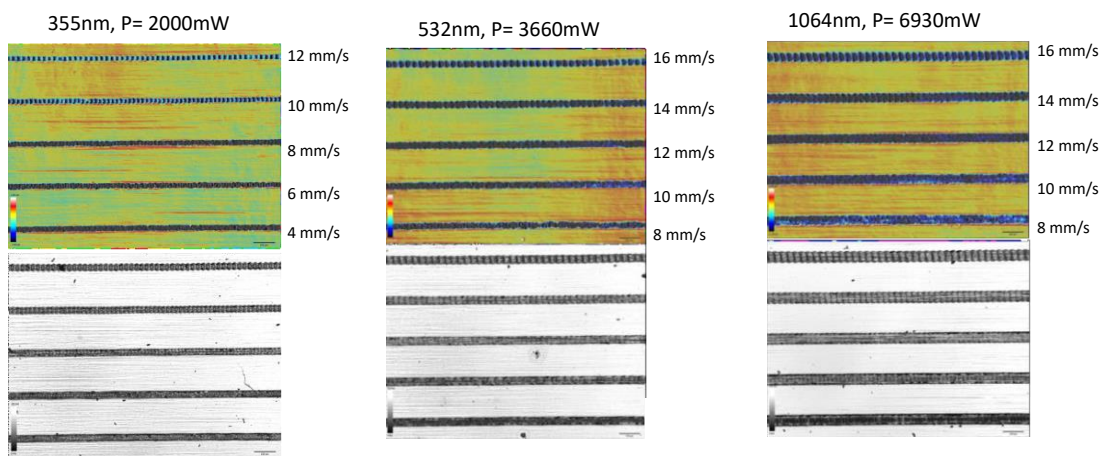


Figure 51. Overlapping study. From left to right, 355nm, 532nm and 1064nm

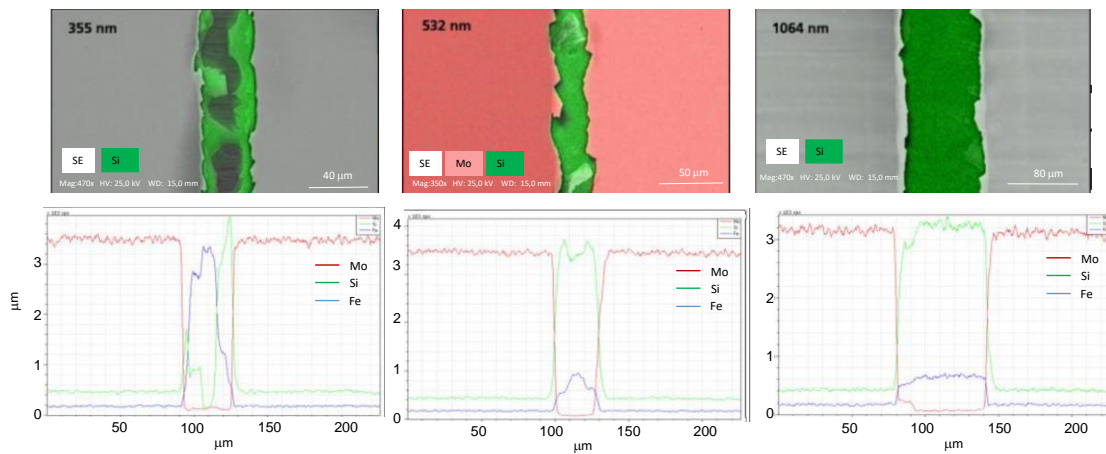


Figure 52. SEM/EDX characterization of P1 scribes: Mo/barrier layer/SS using different laser wavelengths

At the end of the activity, best process window identified for P1 laser scribing on Mo/hybrid SiO_x IL/AISI430, was:

- Laser source recommended: IR 1064 nm
- Speed: 1 mm/s
- HV EOM: 60%
- Power: 2W
- Repetition rate: 200kHz
- Number of pass: 1

Concerning the OPV back contact (Al/ZnO), the optimum current intensity was 20.5A to achieve a continuous P1 scribe without defects. The mechanical profile shows a cut about 300nm depth (Figure 53) what is agreement with the OPV TFSC back contact deposited

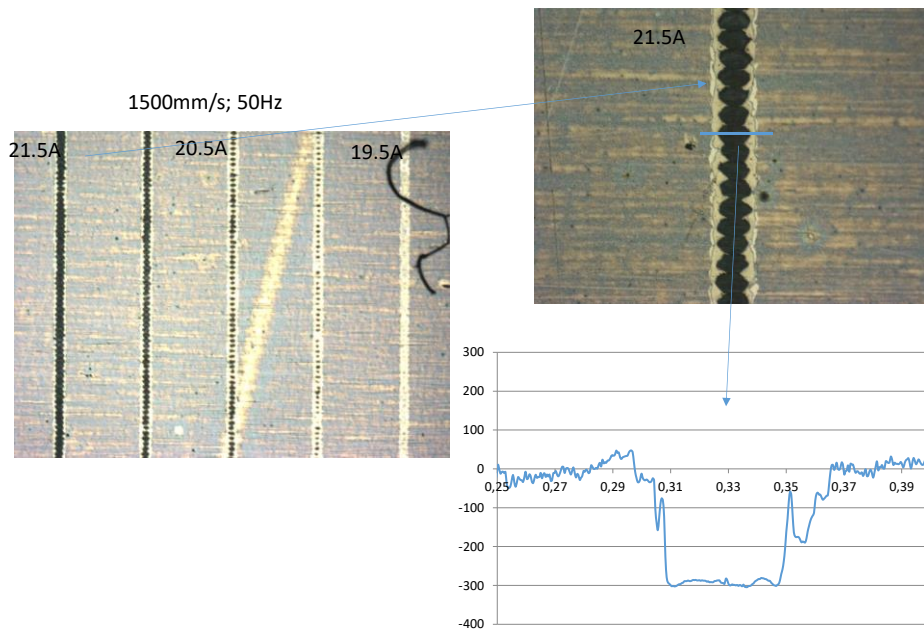


Figure 53. P1 scribe aspect and mechanical profile (OPV back contact)

After the characterization tests, it can be concluded that the hybrid strategy considering SiO_x depositions by sol-gel and vacuum technique is suitable to fulfil all the requirements to make compatible the AISI430 steel selected in the project for TFSC applications.

Si₃N₄/SiO_x hybrid stacks

Levelling property

Following the results achieved with the Si₃N₄ single layer deposited by PVD, it was decided to combine it with SiO_x sol-gel. The experiments were carried out using the F1 diluted sol-gel formulation and the spray coating as application method. Figure 54 shows the superficial view of the SiO_x sol-gel deposited on the Si₃N₄ layer. It can be observed a good homogeneity of the SiO_x without cracks or other kind of defects. One part of the sample was not covered and used for the SiO_x thickness measurement. This one, carried out using the mechanical profilometry method, show values of 2.5 ± 0.3 μm.

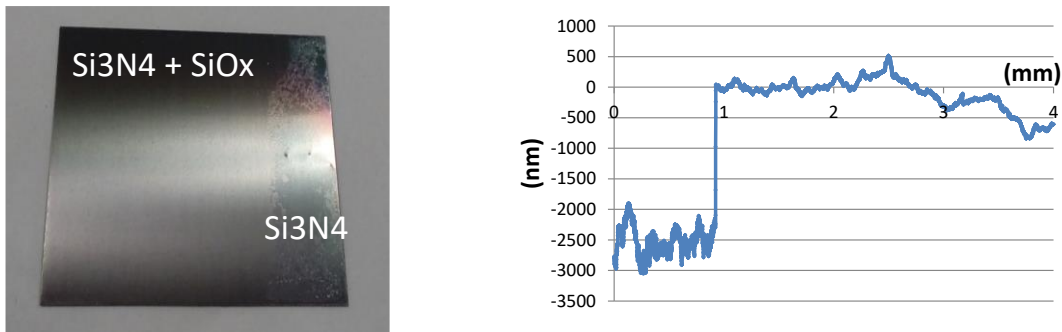


Figure 54. Visual aspect of the Si₃N₄/SiO_x hybrid IL. Mechanical profile of the Si₃N₄ coating (left part) and the Si₃N₄/SiO_x hybrid stack (right part).

Figure 55 reports the roughness determined through mechanical profilometer scans comparing the native AISI430 steel, the AISI430/Si₃N₄ system and the AISI430/Si₃N₄_SiO_x hybrid IL. As it can be observed the roughness decreases in a significant way, especially the R_z parameter with the hybrid IL and is accorded with the levelling requirement for being used for TFSC applications.

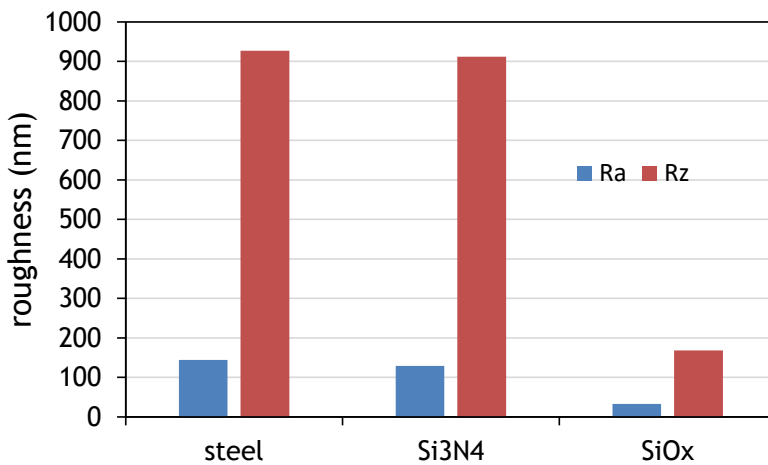


Figure 55. Roughness measured before and after the application of of Si₃N₄ and the SiO_x F1 sol-gel by spray coating.

After the characterization tests, it can be concluded that the hybrid strategy considering SiO_x depositions by sol-gel and Si₃N₄ by vacuum technique is suitable to fulfil all the requirements to make compatible the AISI430 steel selected in the project for TFSC applications.

2.2.2. Intermediate layers characterization through the back contact PV cell deposition (01/10/2015 - 30/09/2016 _ Task2.3)

The main purpose of task 2.3 is to evaluate the dielectric behavior of the ILs on steel. To evaluate the electrical properties fully, a metallic electrode pad needs to be deposited onto the IL. The metallic pad needs to be the same material as the material to be used in the respective TFSC technology (Ag or Al for OPV and a-Si and Mo for CIGS/CZTS). The depositions can be carried out by using the sputtering PVD or thermal evaporation techniques in order to use the same sample geometries for TFSC growing.

Dielectric barrier behavior (Round Robin tests)

It was proposed in STEELPV to evaluate the dielectric behavior of the IL through the breakdown voltage and leakage current analyses. These tests were performed by different partners through several procedures (Round Robin) in order to confirm the suitability of the IL. First procedure was carry out at ITMA, the second one at the University of Bangor and the third one at Abengoa.

Previous to the tests, the maximum voltage that will have to endure the IL was established considering i) the up-scale steel format proposed in WP4; 30cm x 30cm size, ii) that a typical industrial thin film solar module (OPV, CIGS or a-Si) is made of 1cm width serial interconnected cells and, iii) that the open circuit voltage of a a-Si TFSC is about 800mV per cell. Based on these considerations, the total voltage of the module will be about 24V. Taking into account a safety gap, it was established that the IL developed in the project do not have to present any breakdown voltage below 40V.

First procedure

The breakdown voltage was evaluated through a voltage scanning from 0V to 53V (using a DC source_ 53V is the maximum voltage). As shown in Figure 57, one probe is connected to the steel substrate (side without the IL coating) and the other probe has to touch the metallic Al pad. The breakdown voltage occurs when visual shorts suddenly appear at the IL surface (as shown in Figure 57). This test enables, in an easy way, to also check the IL quality in terms of defects detection such as small voids/cracks; in this case, the breakdown voltage occurs at very low voltage. Moreover, it enables to verify if the IL is thick enough to provide an effective insulation. Moreover, the Al pad is also useful to visually observe the compatibility between the IL and the TFSC back contact and to check that no delamination occurs.

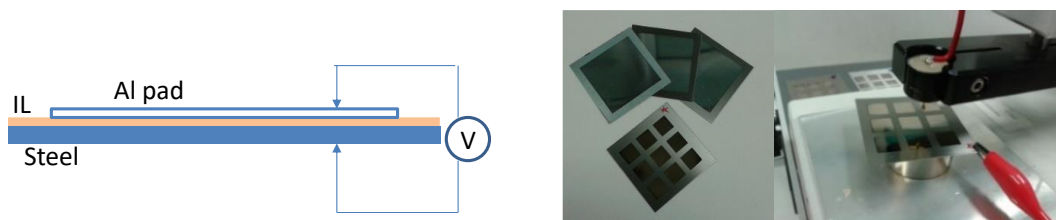


Figure 56. Scheme of IL electric insulation property test proposed and example of a real samples with different Al size pad and trial.



Figure 57. Example of breakdown voltage failure. Crater as results of short. DC01 substrate covered by sol-gel (spin coating) _ thickness $1.3 \pm 0.2 \mu\text{m}$.

Second procedure

Another method to determine the dielectric behaviour of the IL is through the leakage current measurement. Although this test requires a more specific equipment than for the breakdown voltage,

it enables a quantification of the IL insulation. For these tests, the electrodes were thermally evaporated on the IL. Using a Keithley 237 High Voltage Source Measurement Unit (SMU), the leakage current between the back electrode and steel substrate was measured and it was established that the IL have to report nA values to be considered as sufficiently dielectric. The bias range was selected from -40V to +40V and the SMU is capable of measuring leakage down to a value of 10^{-13} A with enclosed Signatone probe station. Small contact areas were used (5mm diameter circle) and contacted using electrical probing. Shown in Figure 58, an example of the leakage current for Al and Ag on F2 sol-gel coated steel substrates. In both cases, an insulation layer exists between the two layers.

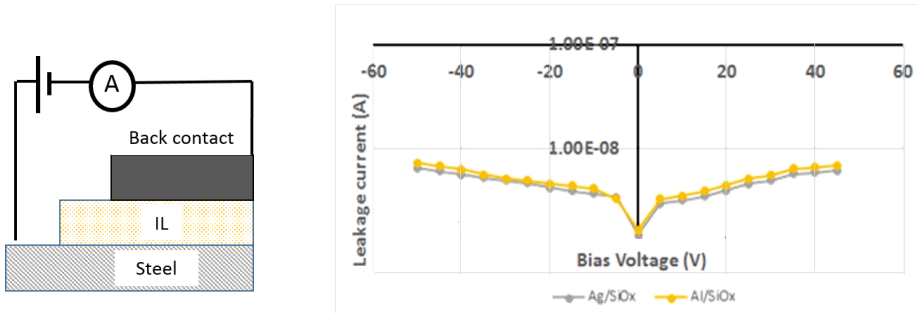


Figure 58. Current Voltage measurement setup (left) to measure the current leakage across the IL by depositing a back electrode directly onto F2 SiO_x sol-gel-coated AISI430 steel

Third procedure

The protocol (Figure 59) consisting in an electrical resistance insulation test using a commercial equipment (Fluke 1550C) sample can be submitted to a progress increment of external voltage; equipment is capable to determine sample resistance stability as one stress test.

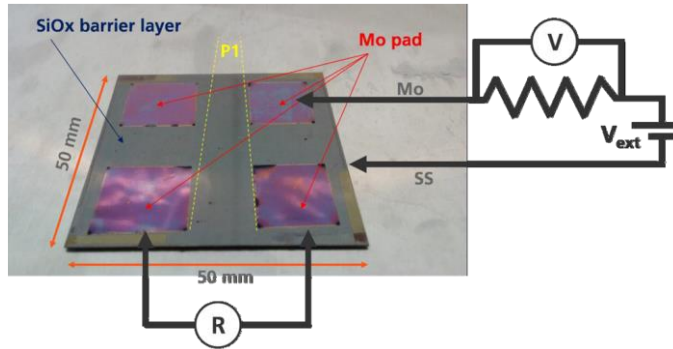


Figure 59. Mo pads onto the AISI430+SiOx hybrid IL and scheme of the test.

Table XXI reports the results of the ILs' behaviour in terms of the dielectric property. All the results take into account IL thicker than 3 μm. The 'third' procedure reports real breakdown voltages whereas following the 'first' procedure no breakdown voltage was registered using the maximum voltage of the DC source (53V). It is important to note that it was established that the IL have to pass 40V.

Table XXI. Summary of the dielectric tests carried out on the different IL.

	Procedures		
	First	Second	Third
Sol-gel F1	> 53V	0.67 nA	
Sol-gel F2	> 53V	6.22-6.97 nA	280V
Sol-gel F3	> 53V		
Blue ink	> 53V		751V
SU8	> 53V	2.77-9.98 nA	
Hybrid tri-SiOx	> 53V		45V
Hybrid Si₃N₄/SiOx	> 53V		278V

2.2.3. Lab-scale roll-to-roll (01/10/2015 - 30/09/2016 _ Task2.4)

The purpose of this task is to undertake trials whereby sol-gel coatings are applied to roll-to-roll processes for scale up. As the R2R lab-scale equipment (Figure 60) is designed for polymeric substrates, 0.3mm thick steel coils were not able to be used in the trials (not enough flexible). Based upon this limitation, thinner AISI430, DX51D+Z and DX51D+AS coils (0.1mm thick) were used. Moreover, the use of this thickness is important to study the suitability of the sol-gel approach on more flexible steel substrates. Although very similar roughness for 0.3mm and 0.1mm steel thicknesses are required, it was determined much lower ones (especially for DX51D+Z and DX51D+AS coils) for 0.1mm coils (Table XXII). These differences might be probably due to the highest pressure applied to reach the thickness of 0.1mm.

Table XXII. Roughness of 0.1mm and 0.3mm steel substrates

Levelling	0.1 mm native steels (nm)	0.3mm native steels (nm)
AISI430	$R_a = 73, R_z = 646$	$R_a = 144, R_z = 927$
DX51D+Z	$R_a = 38, R_z = 329$	$R_a = 87, R_z = 632$
DX51D+AS	$R_a = 58, R_z = 415$	$R_a = 103, R_z = 731$

As no degreasing stage is available in the lab-scale R2R equipment, the 0.1mm steel coils were previously cleaned at the MKM site and used as received in ITMA. Some superficial corrosion could easily appear on DC01 degreased coils and it was decided not to work in this task with this substrate.

The different F1, F2 and F3 sol-gels formulations were applied by using a 'two rolls' coating technique. F1 and F2 sol-gels involved PEG6000 whereas F3 sol-gel was formulated using PEG200000 as releasing agent. As it can be observed in Figure 60, a dipping roll takes the liquid and transfers it to the steel coil. The coating thickness was optimized by varying the gap between the two rolls and the coil speed. An in-line convection furnace was used to carry out the drying/curing stages. The strategy was to fulfil the IL requirements with a single layer. The sol-gel coating were characterized in terms of roughness, thickness, dielectric behavior and flexibility.



Figure 60. Two rolls coating technique in a R2R process.

Levelling property of the SiO_x sol-gel applied by the 'two rolls' coating

Figure 61 shows the roughness determined through mechanical profilometer scans for the three steel before and after the application of the F1, F2 and F3 sol-gels by the 'two rolls' coating. It can be observed that the IL enables to successfully level the native steels surfaces for being compatible with TFSC technologies.

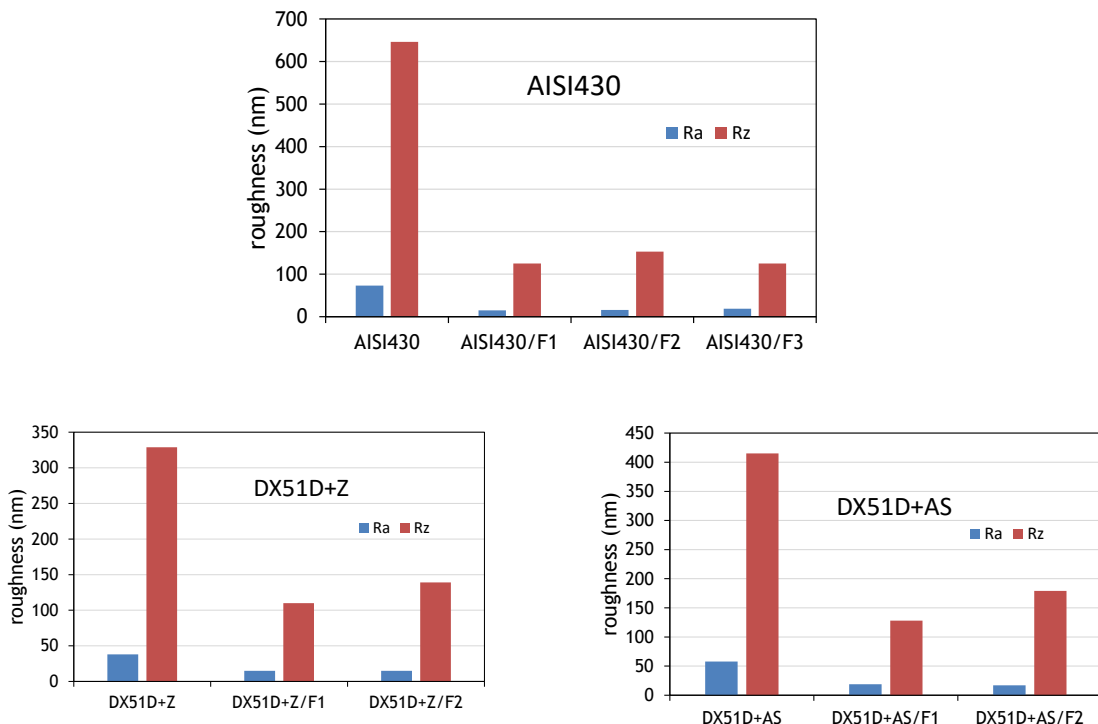


Figure 61. Roughness measured before and after the application of SiO_x sol-gel by two rolls coating in a R2R process. AISI430, DX51D+Z and DX51D+AS are considered.

However, the CCT achieved for DX51D+Z and DX51D+AS covered by F1 SiO_x sol-gel was not successful (Table XXIII). Higher thicknesses free of cracks was not possible probably due to the too low 0.1 mm native steels roughness. On the contrary, F2 SiO_x sol-gel enables to achieve thickness higher than 3.5 microns with the three steels. This increase of CCT is probably due to the addition of the releasing PVP agent.

Table XXIII. Critical thicknesses achieved taking into account the three steels and F1 and F2 formulations.

Thickness (μm)	F1	F2
AISI430	3.2 ± 0.3	3.5 ± 0.8
DX51D+Z	1.6 ± 0.5	3.7 ± 0.8
DX51D+AS	1.7 ± 0.4	3.6 ± 0.6

Hardness, adhesion property of the SiO_x sol-gel applied by the 'two rolls' coating

Related to visual aspect and mechanical property, both F1 and F2 sol-gels IL applied by the 'two rolls' coating shows an acceptable behavior with the all steels in terms of visual aspect (no delamination is observed), adherence (tape pulled-off) and hardness (6H pencil tests).

Dielectric behavior of the SiO_x sol-gel applied by the 'two rolls' coating

The electrical insulation behavior of the SiO_x sol-gel was evaluated in terms of breakdown voltage (First procedure). As established the breakdown voltage target is 40V. As it can be observed in Figure 62, this target is fulfilled for the AISI430 covered by both SiO_x sol-gels and for the other steels with the F2 SiO_x sol-gel. It is also confirmed that when the CCT is not sufficient the breakdown voltage target is not reached.

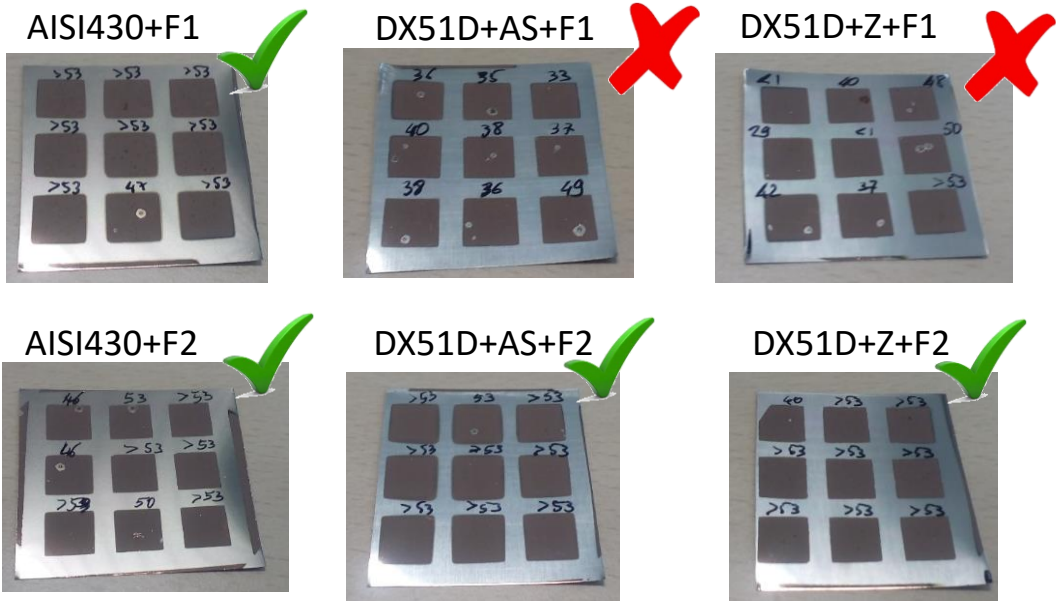


Figure 62. Visual aspect of Al pads deposited on AISI430/SiO_x after applying 53V.

Following the second procedure, the leakage current was measured on the AISI430 covered by the F1 SiO_x. Results of 0.67nA were achieved, what shows the suitable dielectric behaviour of this IL.

Behavior of the SiO_x sol-gel applied by the 'two rolls' coating after shears cut

As this section deals with the production of steel coils covered by the SiO_x sol-gel, it is important to study the SiO_x sol-gel behavior through shears cut process. Indeed, this process will be possibly carried out at production scale before the deposition of the TFSC devices. Figure 63 shows the F1 and F2 SiO_x sol-gel layer deposited on the AISI430 aspect after the cut. The optical micrographs show for both sol-gels a broken zone approximately in the first 40-60 microns from the edge. After that, it can be appreciated that the layer seems to be intact as no cracks or other kind of defects are starting from the broken part.

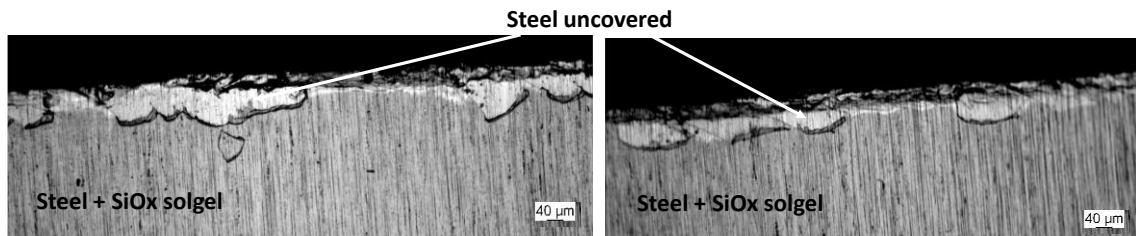


Figure 63. Visual aspect of the SiO_x F1 and F2 sol-gel coatings after shears cut.

Behavior of the SiO_x sol-gels applied by the 'two rolls' coating after flexibility tests

Flexibility test was performed in order to study the behavior of the F1 and F2 IL and to demonstrate if they are suitable for a R2R process. The flexibility test consisted in shaping the steel/IL in compression and traction ways (20 cycles each) using different working cylinders (50mm and 90mm diameters) as it can be observed in Figure 64. The working cylinder diameter of 90mm was chosen as this size could be considered as the lowest standard one for industrial rolling process. The behavior of the F1 and F2 SiO_x IL was determined through breakdown voltage tests (First procedure).

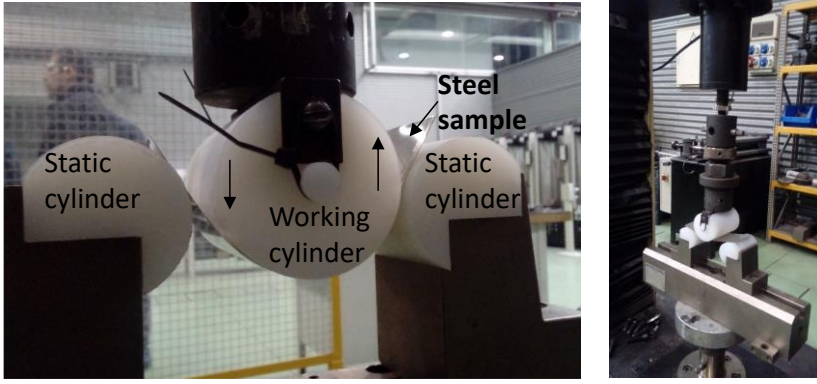


Figure 64. Flexibility test procedure.

As it can be observed in Table XXIV, 100% of the metallic pads (18 (1cmx1cm) pads tested_ two samples) passed the dielectric insulation test considering the 90mm working cylinder. So, a narrower working cylinder was used (50mm) in order to carry out more drastic experiments. As reported in Table XXIV, at least 78% of the metallic pads passed the dielectric insulation test considering the 50mm working cylinder. F2 IL shows slightly better results probably due to its more elastic formulation.

Table XXIV. Percentage of metallic pad (18 pads tested) that passed the breakdown voltage test before and after flexibility experiments.

	Initial	90mm	50mm
AISI430 + F1	100%	100%	78%
AISI430 + F2	100%	100%	89%
DX51D+Z + F2	100%		89%
DX51D+AS + F2	100%		83%

After the characterization tests, it can be concluded that the rolls coating in a R2R process is a viable technique to apply both F1 and F2 sol-gel formulations and to fulfil the requirements to make compatible the steels selected in the project for TFSC applications. Moreover, it can be pointed out that these results were achieved considering a more flexible steel (0.1mm thick).

It is also important to notify that if the native steel surface is too smooth, the SiO_x sol-gels developed (in particular the F1 formulation) are not sufficient alone to reach the suitable critical thickness.

2.3. WP3: Demonstrator of direct thin film PV depositions on steel/IL at lab scale level

2.3.1. Deposition of small solar cells on steel/ILs substrates (01/01/2016-30/09/2016_Task 3.1)

The deposition of TFSC on lab scale steel/IL prototypes constitutes a crucial part of STEELPV, in order to validate the work carried out in WP1 and WP2 and the deposition of the solar cells will ultimately demonstrate the validity of the steel/IL prototypes quality and their compatibility.

a) Amorphous silicon (a-Si) TFSC

Amorphous silicon solar cells (1 cm^2) were based on typical *n-i-p* a-Si single junction [16] as shown in Figure 65, using Ag/Indium tin oxide (ITO) as back electrode and ITO as top electrode. This section summarises the work reported in the deliverable D3.1 'Deposition of small (1 cm^2) solar cells on the steels/ILs systems'.

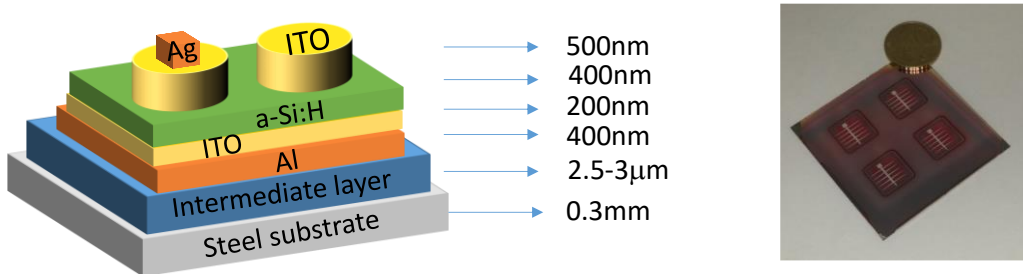


Figure 65. *n-i-p* a-Si TFSC developed on the steel/IL prototype

The Al and ITO layers constituting the back reflector were carried out by radiofrequency (RF) sputtering (AJA International, model ATC Orion 8HV). Both processes were performed at room temperature. The *n-i-p* a-Si layers were deposited by rf-PECVD in a cluster configuration system which have separate chambers for the deposition of intrinsic, n-type and p-type layers in order to avoid cross contamination (Elettrotorava, model V0714).

The performance of the a-Si TFSC were determined in terms of efficiency (PCE) from current-voltage (I-V) curves generated by the TFSC devices under global AM1.5G spectrum (1000W/m^2 , 25°C) solar simulator through the standard IEC 60904-3:2008 (*Photovoltaic devices - Part 3: Measurement principles for terrestrial PV solar devices with reference spectral irradiance data*). The TFSC areas were 1cm^2 and the efficiencies were calculated through the following equation:

$$\eta (\%) = \frac{I_{sc} * V_{oc} * FF}{G * S} * 100$$

where I_{sc} is the short circuit current, V_{oc} the open circuit voltage, FF the fill factor, G the irradiance and S the area of the TFSC.

In parallel to a-Si TFSC grown on the steel/IL samples, cells were also manufactured on glass substrate as a reference.

a-Si TFSC on SiO_x sol-gel deposited by different coating techniques

Table XXV reports the PCE results of a-Si TFSC deposited on the four steel substrates covered by different SiO_x formulations (F1 and F2) and using different application techniques (spin, dip and roll coating). The influence of the curing stage on the TFSC quality was also performed using the hotplate and convection processes.

In all cases, the compatibility of the SiO_x sol-gel with the a-Si TFSC deposition processes was demonstrated as no desorption was detected in the vacuum chambers and no lack of adhesion was observed.

Based upon the results in Table XXV, it can be noticed that both sol-gel formulations applied by the different coating techniques enable to achieve PCE similar to the reference cell using glass as a substrate. Moreover, it is important to notify that the spin and dip coatings were performed on 0.3mm

thick substrates whereas the roll coating used 0.1mm thick coil, demonstrating the viability of the SiO_x sol-gel on different steel thicknesses.

Table XXV. Results of a-Si TFSC PCE on the different steel/ sol-gel IL prototypes. IL deposited by spin, dip and roll coating. Comparison of the influence of the curing method (hot-plate and convection). Comparison with a reference a-Si TFSC deposited on glass. Jsc: short circuit current density, Voc: open circuit voltage, FF: fill factor.

Lab scale prototypes	Jsc (mA/cm ²)	Voc (mV)	FF	PCE (%)	Ag grid
Reference cell on glass	9.3	800	0.57	5.24	Yes
AISI430 F2 SiO _x spin + hot plate	9.9	830	0.64	5.84	Yes
AISI430 F2 SiO _x spin + convection	10.0	790	0.58	5.37	Yes
DX51D+Z F2 SiO _x spin + hot plate	10.4	845	0.63	5.59	Yes
DX51+AS F2 SiO _x spin + convection	10.5	840	0.48	4.70	No
DC01 spin + hot plate	9.6	829	0.61	5.44	Yes
AISI430 F1 SiO _x dip coating + hotplate	9.5	834	0.55	4.90	No
DC01 F1 SiO _x dip coating + hotplate	10.0	839	0.56	5.21	No
AISI430 F1 SiO _x roll coating + convection	10.2	860	0.42	4.11	No
AISI430 F2 SiO _x roll coating + convection	10.0	840	0.40	3.73	No

Figure 66 shows an example of I-V curves obtained through the measurement of a 1cm² a-Si TFSC deposited on DX51D+Z/F2 SiO_x sol-gel deposited by spin coating. It can be observed the good TFSC quality.

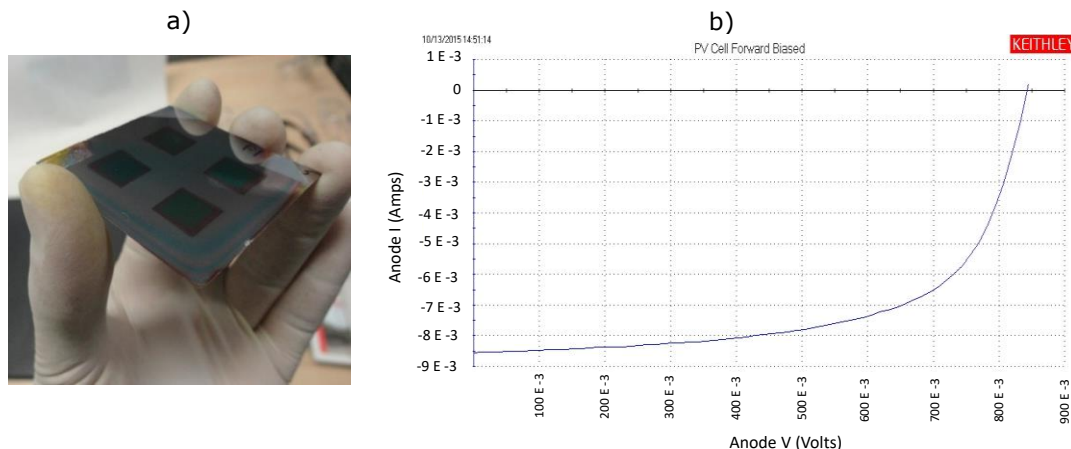


Figure 66. a-Si visual aspect and I-V curve achieved on a a-Si TFSC deposited on DX51D+Z/F2 sol-gel.

a-Si TFSC on commercial polymeric ink

As the coating is organic based, the covered steels were first introduced in a PECVD high vacuum chamber in order to evaluate possible desorption. It was first detected a loss of one vacuum order ($2.1 \cdot 10^{-6}$ Torr instead of $2.0 \cdot 10^{-7}$ Torr). In order to avoid some desorption that could induce future delamination of the a-Si TFSC, a high vacuum treatment at 180°C was carried out for two hours within the chamber. This thermal treatment allowed the improvement of the vacuum in the PECVD chamber to values close to $3.1 \cdot 10^{-7}$ Torr. Subsequently, the a-Si TFSC were deposited using the same procedure as previous devices. Figure 67 shows a photographic image of the a-Si TFSC deposited on the polymeric 'blue ink' IL and the I-V curve. The PCE is 2.4% that is, in this case, lower than the reference cell (5.24%). However, TFSC are working what demonstrate that the polymeric 'blue ink' seems to be a suitable IL for the purpose of the project. Improvements of the

PCE should be achieved by some modifications of the a-Si TFSC (e.g. thickness of back contact, etc.) out of the purpose of STEELPV project.

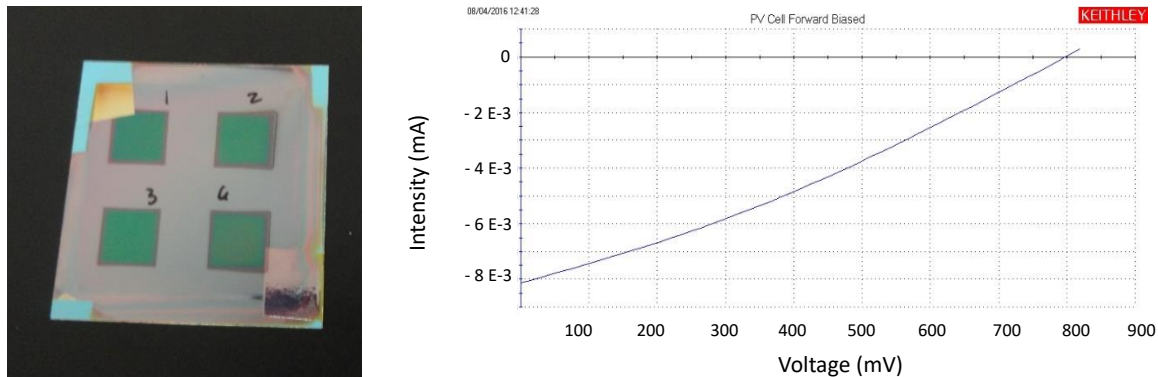


Figure 67 Example of four 1cm² a-Si TFSC grown on steel/polymeric 'blue ink'.

Another potential epoxy ink (SU8) that also passed the characterizations tests in terms of levelling, dielectric behaviour, adhesion, etc, was considered for a-Si trials. In a similar way as for the polymeric 'blue ink', steels covered by SU8 were introduced in PECVD high vacuum chamber. However, a high desorption was registered just after the sample introduction in the PECVD chamber ($1.2 \cdot 10^{-5}$ Torr instead of $4.0 \cdot 10^{-7}$ Torr). In order to avoid the desorption, the samples were heated in a hotplate at 200°C during 2 hours and then introduce in a high vacuum chamber during two hours at 180°C. It was then observed a slight improvement but a huge desorption still happened ($9.5 \cdot 10^{-6}$ Torr). As a result of the poor desorption properties, it was then concluded that the SU8 epoxy, at this stage, was not suitable for a-Si TFSC.

a-Si TFSC on hybrid SiO_x stack

a-Si was deposited on the most promising hybrid SiO_x tri-layer. After the deposition of the a-Si TFSC, no delamination was observed and this is confirmed by the images shown in Figure 68. The best PCE was 6.4% that is, in this case, quite higher than the reference cell (5.24%) demonstrating that the hybrid SiO_x stack is technically viable to make compatible a-Si TFSC and AISI430 substrate.

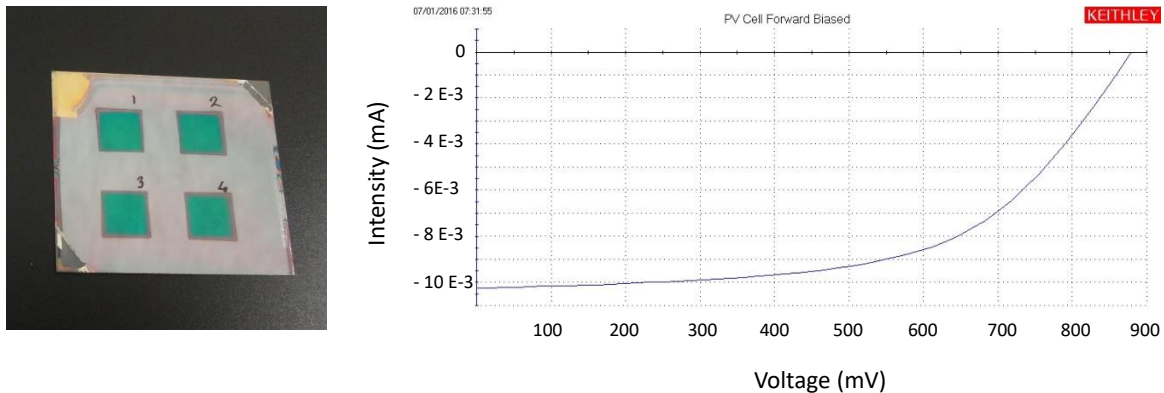


Figure 68 Example of four 1 cm² a-Si TFSC grown on AISI430/ hybrid SiO_x

As summary, it has been shown that a-Si TFSC can be deposited upon all steel/IL prototypes except for steel/SU-8. This IL does not seem well-suited to the vacuum pressure needed for a-Si TFSC deposition.

b) OPV TFSC

Figure 69 provides a representation of the device structure of a top illuminated OPV, which was fabricated onto a steel substrates:

(steel/IL/Al/ZnO/P3HT:PCBM/CLEVIOS™HTL/AgNW).

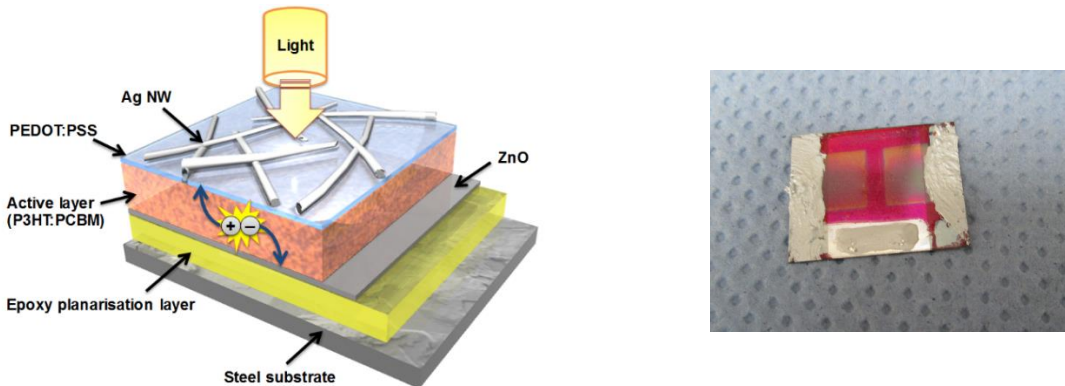


Figure 69 Schematic of the OPV manufactured onto steel and OPV device onto DX51D+Z steel substrate with sol-gel F2

In parallel, OPVs were manufactured onto glass substrates and plastic substrates (PET and PEN). This enables comparison of substrate type and how it affects solar cell performance. OPV solar cells on glass substrates composed of a transparent bottom electrode, a thin-film active layer, and a transparent top electrode have been constructed.

OPV on SU8

Table XXVI reports that glass lead to the best performance in terms of PCE with an efficiency of 2.90% and the plastic substrates (PEN and PET) possess a PCE of 2.31% and 2.2% respectively. By comparison OPVs made on steel have an intermediate PCE; they are not better than glass, but appear to work statistically better than plastic substrates.

Table XXVI. Comparison of OPV performance made on a range of competing substrates. Jsc: short circuit current density, Voc: open circuit voltage, FF: fill factor

Sample	Jsc (mA/cm ²)	Voc (mV)	FF	PCE (%)
Reference cell on glass	9.88	590	59.0	2.90
Reference cell on PET	8.95	567	43.0	2.20
Reference cell on PEN	9.01	570	45.0	2.31
OPV cell made on DC01/SU8	9.54	546	54.6	2.42
OPV cell made on DX51D+AS/SU8	9.01	540	47.3	2.30
OPV cell made on DX51D+Zn/SU8	8.90	546	47.1	2.29
OPV cell made on AISI430/SU8	8.94	540	48.6	2.35

OPV on SiO_x

The results, summarised in Table XXVII, reports the PCE achieved on the four steel substrates (OPV cells of 1cm²). All the different steel substrates produced working devices with PCE above 2%. The results further highlight the compatibility of OPV onto steel/sol-gel IL prototypes.

Table XXVII. OPV device performance onto steel sample coated with SiO_x sol-gel. Jsc: short circuit current density, Voc: open circuit voltage, FF: fill factor

Sample	Jsc (mA/cm ²)	Voc (mV)	FF	PCE (%)
DX51+AS/SiO _x sol-gel	8.70	0.55	0.466	2.23%
DC01/SiO _x sol-gel	8.46	0.56	0.454	2.15%
DX51D+Z/SiO _x sol-gel	8.21	0.55	0.443	2.00%
AISI430/SiO _x sol-gel	9.20	0.53	0.48	2.40%

c) CZTS (Kesterite) TFSC

Kesterites are second generation of TFSC derived from work on Copper indium, gallium and selenide (CIGS) and related material, with the assumption that replacing scarce elements such as Indium and Gallium by Tin and Zinc will reduce photovoltaic modules cost and reduce the environmental impact. This technology has demonstrated good results by some researchers, for instance CZTSSe cell efficiency of 12.6% reported by Mitzi et al in 2003 [17], but there are no reports of depositing kesterite solar cells on IL/barrier layers or on rough metallic substrates.

CZTS TFSC were only deposited on the hybrid SiO_x tri-layer as this was the only stable IL layer developed for high temperatures.

The Mo deposition process, back contact, was optimized by using a modified Thornton model, whereby several parameters of the magnetron sputtering process were tuned. Mo deposition was modified to be successfully compatible with barrier layer and rough metallic substrate.

Different alternative processes are available to create the CZTS photosensitive part, but neither of them has demonstrated for their scalability yet. The well-known sequential process to create the CZTS semiconductor was followed. It is based on a first step where precursors (Cu-Zn-Sn) are deposited by magnetron sputtering at DC mode. Then, second step consists to introduce these precursors into a Selenium atmosphere at approximately 550°C. Selenium diffuses into precursor materials and system crystallizes into kesterite phase.

Samples were characterized by XRF, SEM, XRD and Raman Spectroscopy. The results (XRF) indicate that most of the samples prepared so far were Cu poor/Zn rich or Cu poor/Sn poor. Further optimisation of the process parameters could yield a sputter deposition process that reaches the optimal conditions for TFSC deposition.

Raman microscopy (Figure 70) can be used to determine if absorber layer created has a CZTS phase, and if there are any undesired component or defects within their structure. Comparing with literature resonance modes of the spectrum obtained when samples are excited with green laser sources, we can conclude that samples match the expected phases closely.

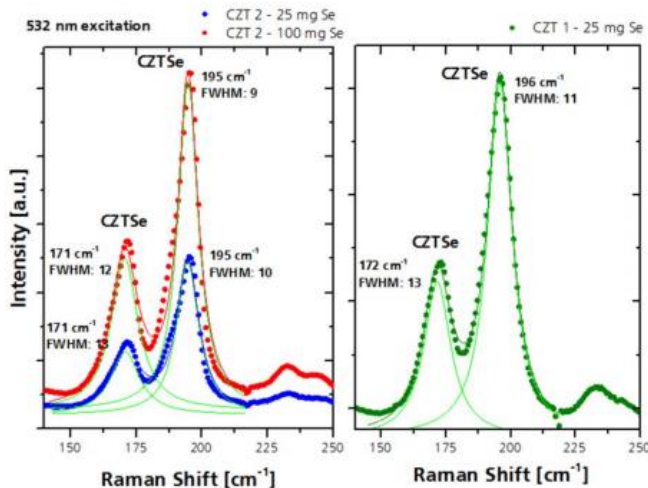


Figure 70 Raman spectrum obtained for CZTS samples excited with 532nm laser source.

d) Perovskite TFSC

An additional highly promising TFSC technology (perovskite solar cells_PSCs) was tested for the STEELPV project. Current PCE is over 22% (lab-scale). The rapid rise compared to most other TFSC technologies over a relatively short period of time has meant that in the space of three years PSCs have managed to achieve PCE comparable to all other TFSC technology, which has been around for nearly 40 years. PSCs are based on organometal-halide based perovskite materials [18,19]. For illustration, an image of perovskite based solar cell on steel is shown in Figure 71.

The IV curve of the PSC measured under 1 Sun irradiation shows a PCE of 3.8%, which indicates that IL-coated DC01 steel can successfully be applied for the fabrication of PSC. This was not expected as part of the project, but provides supplementary results to the project.

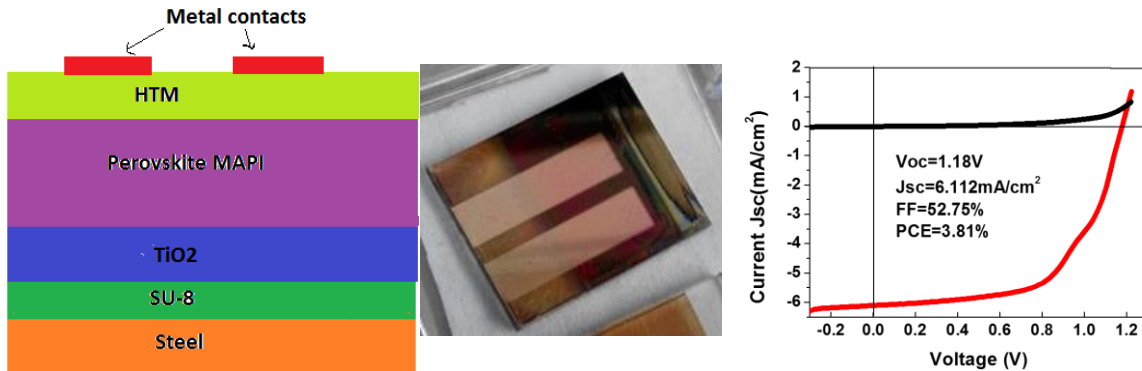


Figure 71. Schematic of perovskite solar cell fabricated on steel, an image of perovskite device on steel, and IV curve of PSC on DC01 (DC01/IL(SU-8)/TiO₂/MAPI/HTM/MoO₃/Au).

2.3.2. Steel/ILs protection during the storage (01/01/2016-31/12/2016_Task3.2)

After the IL deposition, the steel back side is oil free and, depending on the steel grade, it is plausible that some corrosion can appear during the storage prior to the PV device manufacturing. After TFSC deposition, the whole steel and solar cell sample will be subjected to an encapsulation process, thus avoiding further corrosion. Moreover, it is important to verify that the IL does not suffer any degradation during the storage period, what would be dramatic for the TFSC manufacture. This section summarises the work reported in the deliverable D3.2 'Steel/ILs protection during storage'.

In this line, first tests were performed considering SiOx sol-gel. As this layer was not developed as anti-corrosion layer, and due to its relatively low thickness (about 3 microns), conventional standard accelerated aging tests were not considered. The evaluation was taking into account more softened aging analysis that could give much more data related to the SiOx behavior.

Two different aging conditions were considered; Indoor (23°C – 45°HR) and outdoor real atmospheres (12°C-30°C - >70°HR [20]). As the deterioration of the sol-gel could be difficult to be detected visually or by optical microscopic analysis, it was decided to evaluate it through the breakdown voltage test. Initially on the indoor sample and after each months (on both indoor and outdoor samples) an Al (1.5x1.5cm) pad was deposited and the samples tested in terms of breakdown voltage.

Figure 72 shows reference steels (without sol-gel) and steel samples (with sol-gel) at different exposing times; 0 and 3 months. As expected, indoor conditions are more benign than the outdoor ones and only a very low red oxidation of the DC01 steel was starting after 2 months. Sol-gel aspect look apparently unchanged after 3 months. Related to the outdoor conditions, the uncoated DC01 steel was quickly oxidized (first month) followed by the DX51D+Z reference steel (white Zn(OH)₂ products) after 2 months. Concerning sol-gel layer, the DC01 is affected after 3 months. The other coated steels seem to be unchanged.

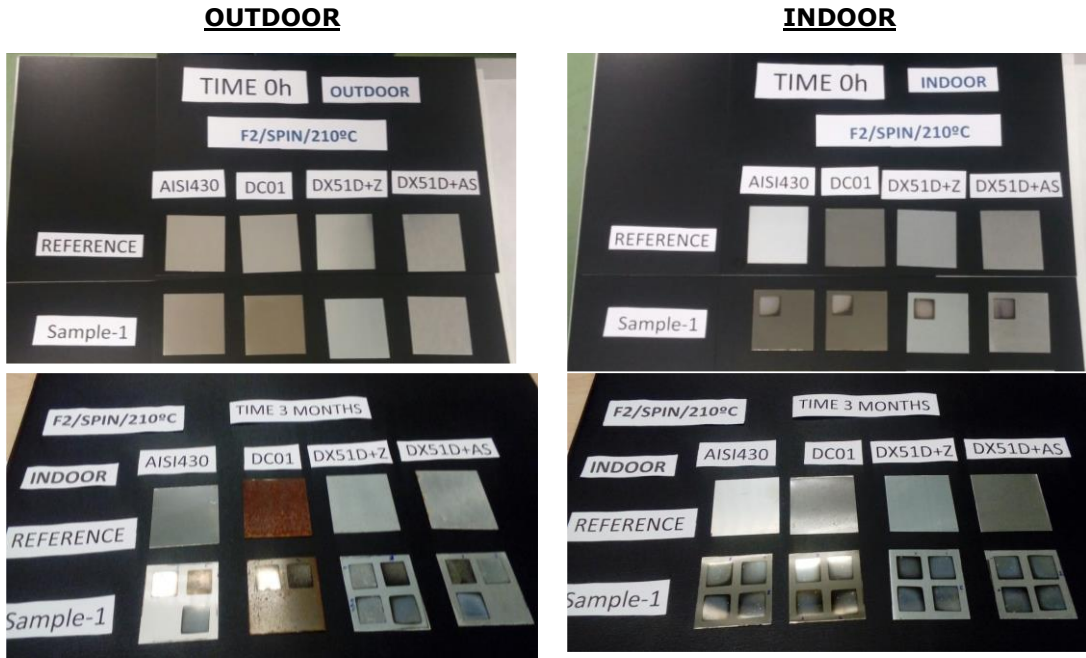


Figure 72. Visual aspect of the four steels with and without sol-gel_ Outdoor: time 0 and 3 months. Indoor: time 0 and 3 months.

Table XXVIII reports the breakdown voltage values of the four steels/SiO_x IL exposed to the indoor and outdoor real atmosphere. Results are in agreement with the visual surface study (Figure 72) as the DC01/IL sample shows a deterioration in outdoor conditions since the second months (shorts at 37V). The breakdown voltage evaluation also shows a deterioration of steel/IL systems at the third month in outdoor conditions (DX51D+AS and DX51D+Z).

Table XXVIII. Steels/SiO_x sol-gel IL. Evaluation of integrity through the breakdown voltage

	INDOOR			OUTDOOR	
	0	2	3	2	3
AISI430+IL	>53 V	>53 V	>53 V	>53 V	>53 V
DC01+IL	>53 V	>53 V	50 V	37 V	---
DX51D+Z+IL	>53 V	>53 V	>53 V	>53 V	36 V
DX51D+AS+IL	>53 V	>53 V	40 V	>53 V	30 V

Based on these first tests, storage experiments (including some protections) were performed on different steel/ILs candidates; steels/SiO_x sol-gel for the wet strategy, steels/polymeric 'blue ink' for the commercial dielectric inks and AISI430/SiO_x tri-layer for the hybrid approach. Considering the necessity to avoid the corrosion process but also to propose cost effective steel/IL products, different solutions for the storage were first discussed:

- **Application of anticorrosion commercial protecting oils.** This approach should have the highest grade of effectiveness for the back side steel protection. However, its main drawback comes from the covering, in the same process, of the IL and it is expected a possible deterioration of the IL in the cleaning stages to remove the oil previous to the TFSC deposition. So, this approach was discarded.
- **Commercial polymeric adhesive films.** This strategy is pertinent for the STEELPV project as it enables its application only on the steel back side avoiding to damage the IL. However, this film will have to be removed before the TFSC process and the steel back side has to be cleaned in order not to contaminate TFSC deposition vacuum chambers. During this cleaning process, the IL could be deteriorated. So, this approach was not initially considered.
- **Specific anti-corrosion storage papers.** This strategy seems to be the least effective but has the advantage that only a very light steel/IL cleaning will be needed before the TFSC

manufacture. From an economic point of view, this approach is also the most cost effective and is considered in this section.

Two different storage configurations were set up simultaneously; One samples group was enveloped in a VCI paper (volatile corrosion inhibitor) and the other one was protected by the use of a paper without any anti-corrosion protection. An anti-scratch paper was introduced between each steel/IL samples. In a same configuration, each specimens (steel+IL) were produced twice.

The storage tests were performed in the head locations of both CSM and ITMA, respectively in Rome (Italy) and in Aviles (Spain). The tests were carried out indoor in order to reproduce real storage conditions of IL coated steel sheets with a duration of 3 months: this time was considered compatible with the mean storage time waiting for an industrial production of PV cells. It is to remind that storage time represent undesired costs in the industrial production, so they have to be minimized.

The samples were evaluated after each month, visually (superficial aspect) and studying the dielectric property of the IL (First procedure). Moreover, defects were observed by SEM analysis. Table XXXII and Table XXX show the results of the breakdown voltage measurements. In ITMA, the tests were performed after each month and in CSM at the end of the experiment.

Table XXIX. Results of the breakdown voltage measures performed respectively after one, two and three months of storage in ITMA head location (Aviles, Spain). Before the storage tests all the coated sample support 53V.

Sample	1 month		2 month		3 month	
	VCI	NO VCI	VCI	NO VCI	VCI	NO VCI
All steels/Blue ink	> 53	> 53	> 53	> 53	> 53	> 53
AISI430 + sol-gel	> 53	> 53	47	53	> 53	> 53
DX51D+Z+sol-gel	> 53	> 53	49	47	48	49
DX51D+AS + sol-gel	> 53	> 53	42	45	44	49
DC01 + sol-gel	50	37	47	40	45	37
AISI430 + hybrid SiOx	36	36	39	28	> 53	35

Table XXX. Results of the breakdown voltage measurements performed by ITMA of the samples used by CSM for the storage test. Before the storage tests all the coated sample support 53V.

After 3 months of storage test in CSM		
Sample	VCI	No VCI
All steels/Blue ink	> 53V	> 53V
AISI430 + SiOx sol-gel	41V	41V
DX51D+Z + SiOx sol-gel	37V	35V
DX51D+AS + SiOx sol-gel	40V	50V
DC01 + SiOx sol-gel	50V	51V
AISI430 + hybrid SiOx	42V	33V

Comparing the results of the breakdown voltage tests on samples stored and considering the results of visual qualitative and SEM analysis, the following conclusions are made:

- Polymeric 'blue ink', independently from the steel substrate, shows the best performances.
- Differences were observed between AISI430+hybrid SiOx stored in the no VCI and in the VCI paper. The samples stored in the VCI paper showed better performances respect to those stored in the no VCI paper; this behaviour could be explained with VCI absorption on the layer of SiOx, filling the holes observed on the surface by SEM analysis and consequently bettering the breakdown voltage properties.
- The majority of tested samples showed breakdown voltage properties higher than the lower limit requested in the ambit of STEELPV after the three months. AISI430/hybrid SiOx shows

the worst results with a clear deterioration of the electrical isolation. The lack of stability of this IL could be due to the steel oxidation during the annealing treatments. As this drawback was explained/solved, a clear improvement of this IL will be expected

- Some differences at the end of the three months of storage were also observed between samples stored in CSM and in ITMA, especially as regards DC01 + sol-gel and DX51D+Z+ sol-gel. However, these differences falls within the statistical fluctuations of the estimated values and moreover measures performed each month by ITMA show the stability of electrical properties for all the tested samples.
- DC01, even if breakdown voltage properties are satisfactory, could determine instability of the electrical properties. In fact, SEM analysis gave evidence of local detachment of the coating. However, as the IL integrity seems stable, the deposition of TFSC should not be affected

2.3.3. Encapsulation of the steel and aging tests (01/01/2016-31/12/2016_Task3.3)

This section summarises the work reported in the deliverable D3.3 '*Encapsulation of the steel/IL and degradation tests*'.

Steel samples are known to corrode with even benign weather conditions [21,22,23]. Therefore, the encapsulation materials over steel surfaces are needed to prevent or minimize the process of corrosion [24,25]. There are a number of well-known coating materials and methodologies for inhibiting steel degradation and to ensure over 20 years' stability in most outdoor environments, for example in building applications. However, for PV applications, these coatings need to be highly transparent (>85% needed in the visible spectrum) and need to be coated at low temperature so to not cause degradation to the PV module. The different steels considered in STEELPV were encapsulated considering several standard transparent polymeric films of Ethylene tetrafluoroethylene (ETFE), polyvinyl butyral (PVB) and Ethylene-vinyl acetate (EVA). Moreover, polyethylene napthalate (PEN) and polyethylene terephthalate (PET) were considered to ensure an extra barrier against humidity and oxygen.

Initially, the effectiveness of the polymeric films was tested by laboratory-based accelerated UV light degradation test (QUV test) according to IEC guidelines. Before and after QUV test transparency (%T) and yellow index (YI) were determined for the sets of polymers (ETFE, PVP, EVA, PEN, PET) and their combination as multiple polymeric films. %T of over 80% was observed after QUV test. Films containing PEN as one of the component was found to cause maximum discolouration after QUV test, as results showed the highest change in yellowing index. PEN was consequently not considered as encapsulation material for the subsequent experiments where steel was encapsulated.

Next, encapsulation at two different temperature settings of 100°C and 135°C of the two most corrosion sensitive steels, DX51D+Z and DC01, with four different combinations of polymer films were carried out (S1 to S8). The lower temperature was used thinking to OPV technology.

- S1** (ETFE/PVB/PET/PVB/ DX51D+Z/PVB/PET/PVB/ ETFE),
- S2** (ETFE/EVA/ the PET/EVA/ DX51D+Z/EVA/PET/EVA/ ETFE),
- S3** (ETFE/PVB/ DX51D+Z/PVB/ETFE),
- S4** (ETFE/EVA/DX51D+Z/EVA/ ETFE),
- S5** (ETFE/PVB/PET/PVB/DC01/PVB/PET/PVB/ETFE),
- S6** (ETFE/PVB/DC01/PVB/ETFE),
- S7** (ETFE/EVA/PET/EVA/DC01/EVA/PET/EVA/ETFE),
- S8** (ETFE/EVA/DC01/EVA/ETFE)

Thermal cycling test of encapsulated samples (S1-S8) were carried out in the range -40°C to 85°C for 670h. By visual inspection, only moderate discolouration, delamination and corrosion was observed.

Thermal-humidity test of encapsulated samples (S1-S8) was carried out with RH=85% and T=85°C for 1000h hours. High levels of degradation and corrosion were observed after thermal-humidity testing.

- The configuration **S1** (ETFE/PVB/PET/PVB/ DX51D+Z/PVB/PET/PVB/ ETFE) was found as the best encapsulation type for the protection of steel DX51D-Z. The configuration **S8** (ETFE/EVA/DC01/EVA/ETFE) was found to be the most effective protection for DC01. Both the (ETFE/PVB/PET/PVB/ steel type/PVB/PET/PVB/ ETFE) and the (ETFE/EVA/steel type/EVA/ETFE) configurations were considered for experiments on the other two steels; AISI430 and DX51D+AS.
- Corroded surface after thermal-humidity cycling of encapsulated samples were studied by combination of microscopy, Raman spectrum and XRD pattern. The identified metal oxides are Goethite (α -FeOOH), magnetite (Fe_3O_4) and Lepidocrocite (γ -FeOOH), which are to be expected for these forms of steel substrates.
- As corrosion was noticed, DX51D+AS and AISI430 were also encapsulated at 135°C considering the two best encapsulation configurations from **S1** and **S8**. After 1000 hours of thermal-humidity cycling, it can be concluded that no obvious surface degradation is observed from either encapsulation strategy on either DX51D+AS or AISI430.
- Considering the two best encapsulation configurations, a higher encapsulation temperature of 150°C (max. for a-Si TFSC) was applied on the four steel. After the thermal-humidity tests, the results show no DC01 samples possess moderately improved stability by using the elevated temperature, but no change in the stability of DX51D+Z samples is observed.

From those results it can be concluded that a more robust encapsulation system should be needed to avoid both steel back side corrosion and obviously the TFSC degradation. Related to the back side protection, other back sheet systems such as Tedlar, Tedlar/Al, Tedlar/Polyester/Tedlar, etc. could be experimented.

Concerning the front encapsulant sheet, other materials in substitution of ETFE (e.g. polyvinylidene fluoride_PVDF, polyisobutylene_PIB based polymer sealant, etc.) as well as high performance inorganic barrier films deposited under vacuum could be explored.

2.4. WP4: Up-scaling of steel/ILs at pilot line level: validation and viability (WP leader_ SU)

From the developments and results achieved in WP2 (*Intermediate layers developments at lab-scale level*) and WP3 (*Direct thin film PV depositions on steel/IL*), the ILs and deposition processes reported in Table XXXI have been explored at the up-scale pilot plant level. For each IL/process, Table XXXI also reports which steel was used and its size.

Table XXXI. ILs, deposition processes and steels' size considered at the up-scale pilot plant level.

IL	Successful Lab-scale process	Up-scale process considered	Steels considered	Steel sizes
SiO _x sol-gel F1	Dip, roll, spray	spray	All	30cm x 30cm
SiO _x sol-gel F3	K-bar	K-bar	All	30cm x 30cm
Blue ink	Screen printing	Screen printing	All	30cm x 30cm 30cm width coil
Hybrid Si ₃ N ₄ /SiO _x	Hybrid (PVD/sol-gel)	Hybrid (PVD/sol-gel)	AISI430 DX51D+AS	10cm x 180cm
Hybrid SiO _x / SiO _x / SiO _x	Hybrid (sol-gel/PVD/sol-gel)	Hybrid (sol-gel/PVD/sol-gel)	AISI430 DX51D+AS DC01	10cm x 10cm
Hybrid SiO _x / SiO _x / SiO _x	Hybrid (sol-gel/PECVD/sol-gel)	Hybrid (sol-gel/PECVD/sol-gel)	AISI430 DX51D+AS DC01	10cm x 10cm
Hybrid SiO _x / SiO _x		Hybrid (sol-gel/PECVD)	AISI430 DC01	10cm x 10cm

This section summarises the work reported in the deliverables D4.1 'Development processes to up-scale ILs at pilot plant level and characterization tests' and D4.2 'Technical feasibility'.

2.4.1 In-house SiO_x sol-gel

Up-scaling of SiO_x F1 sol-gel by spray coating

Based on the tests and results achieved at lab-scale level, it was decided to work with the F1 SiO_x sol-gel formulation due to its good shelf life, compatibility with ethanol (in case a dilution is necessary) and stability at high temperature (500°C).

The trials were performed considering a commercial spray gun (Spraying system) (Figure 73a). The nozzle cone angle of 60° was used to ensure the homogeneity and the reproducibility of the SiO_x sol-gel coating. It was mounted on an automatized spray system and moved transversely with respect to the sample movement (Figure 73b). The trials were carried out varying i) the F1 SiO_x sol-gel liquid pressure (from 0.2bar to 0.6bar), ii) considering a sol-gel dilution of 1:0.5 in ethanol, iii) a holder speed of 1.6m/min, iv) a nozzle/sample distance of 8cm and v) **a one scan spray**. The coated steels were dried and cured using a home-made hotplate of 50cm x 50cm up to 210°C (Figure 73c) and 30cm x 30cm formats were considered.



Figure 73. a) Spray gun, b) spray system and c) Hotplate

As it can be observed in Figure 74 using this automatized spray system and the experimental conditions previously described, it was possible to reach a thick IL (above 3 μ m) only with one. Considering the bare low carbon steel substrate (DC01), a thickness of 3.1 μ m and 4.0 μ m were reached for the respective sol-gels sprayed at liquid pressures of 0.5bar and 0.6bar. It is also important to note that the samples were crack free in all cases. Related to the 0.2bar liquid pressure condition, the lowest thickness (2.3 μ m) is the result of one scan and the highest thickness (4.2 μ m) the result of three scans.

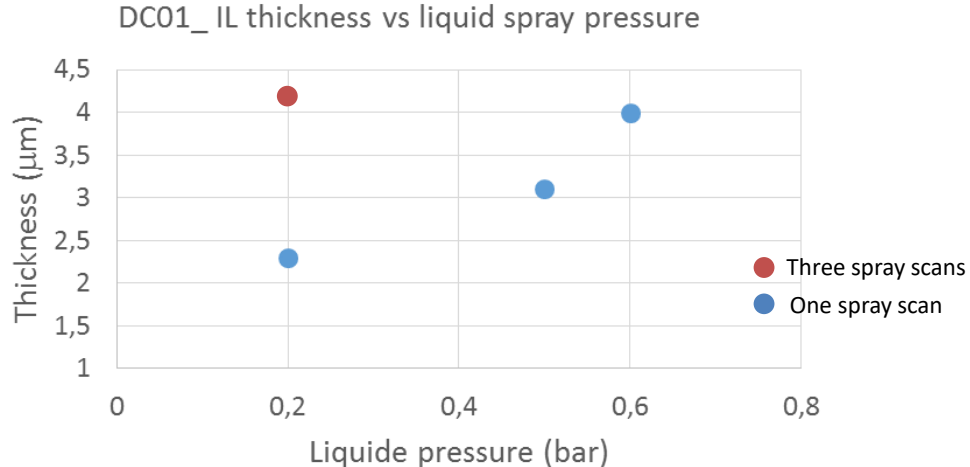


Figure 74. Influence of the spray liquid pressure and spray scan's number on the SiO_x thickness. Sol-gel dilution 1:0.5. Steel substrate: DC01. Samples of 30cm x30cm.

Regarding the sol-gel IL roughness, Figure 75 shows that the liquid pressures of 0.5bar and 0.6bar enable to drastically decrease the native roughness (reported in the y-axis at the 0bar liquid pressure), fulfilling the levelling requirement ($R_a < 40\text{nm}$ and $R_z < 350\text{nm}$). Related to the 0.2bar liquid pressure, the experimental condition that enables to reach a thickness above 3 μ m (three spray scans) shows a not affordable roughness for the purpose of the project ($R_a = 54\text{nm}$ and $R_z = 510\text{nm}$).

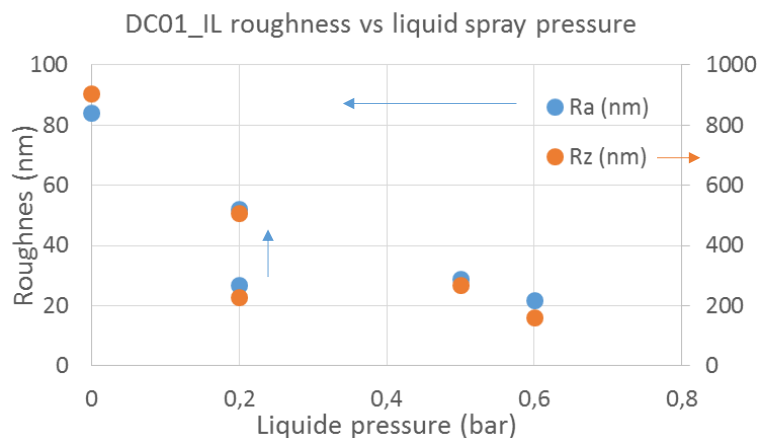


Figure 75. Influence of the spray liquid pressure and spray scan's number on the DC01/SiO_x IL roughness. Sol-gel dilution 1:0.5. Steel substrate: DC01. Samples of 30cm x30cm

From those experiments and tests, it was decided, for the other steel substrates, to consider F1 SiO_x sol-gel dilution of 1:0.5 in ethanol, liquid spray pressure around 0.5bar, a nozzle/sample distance of 8cm and one spray scan.

Taking into account the above results, AISI430, DX51D+Z and DX51D+AS (30cm x 30cm) were processed. Figure 76 shows the visual aspect of the SiO_x F1 sol-gel (after the curing step up to 210°C) applied on the AISI430 steel, depending on the sol-gel spray liquid pressure (0.5bar and 0.4bar). It can be clearly observed that the 0.5bar sol-gel liquid pressure is a wrong condition. The thickness achieved is not particularly high but the cracks show that 4.2 μ m is too high for the critical thickness. The 0.4bar sol-gel liquid pressure shows a much better result. No crack is observed and

the thickness slightly higher than the $3\mu\text{m}$ required is reached (inductive probe meter and according to the magnetic induction method standard ISO2178:2016-3).

It is important to note that the gap of the process condition to reach a thickness above $3\mu\text{m}$ without any crack seems to be very narrow. As already commented in the ‘steel substrates delivered’ section, the AISI430 steel delivered for up-scale experiments has a native roughness quite low $R_z=493\text{nm}$ (and much lower than the one used for lab-scale experiments $R_z=927\text{nm}$) and may be a reason why the cracks happened at a relative low thickness (for instance, using the DC01 steel, the critical thickness is much higher and the native steel roughness is also much higher $R_z=892\text{nm}$)

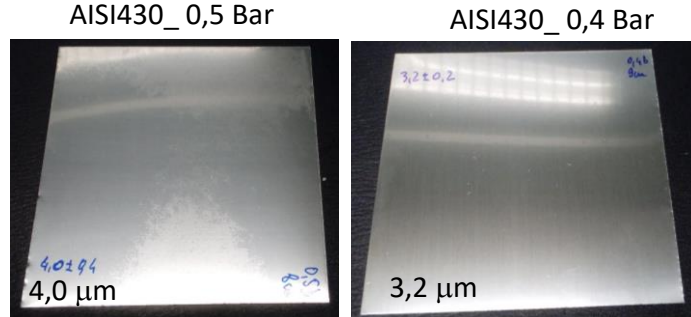


Figure 76. Visual aspect of the F1 SiO_x sol-gel depending on the sol-gel liquid pressure (0.5bar and 0.4bar).

In the case of the DX51D+Z and DX51D+AS steels, the highest successful sol-gel liquid pressures were 0.4bar and 0.5bar with respective thicknesses of $3.4\mu\text{m}$ and $4.1\mu\text{m}$.

Figure 77 reports the roughness of the native steels and the levelling grade after the application of the F1 SiO_x sol-gel. It can be observed that in all cases the R_a and R_z are below the values required in the STEELPV project ($R_a<40\text{nm}$ and $R_z<350\text{nm}$).

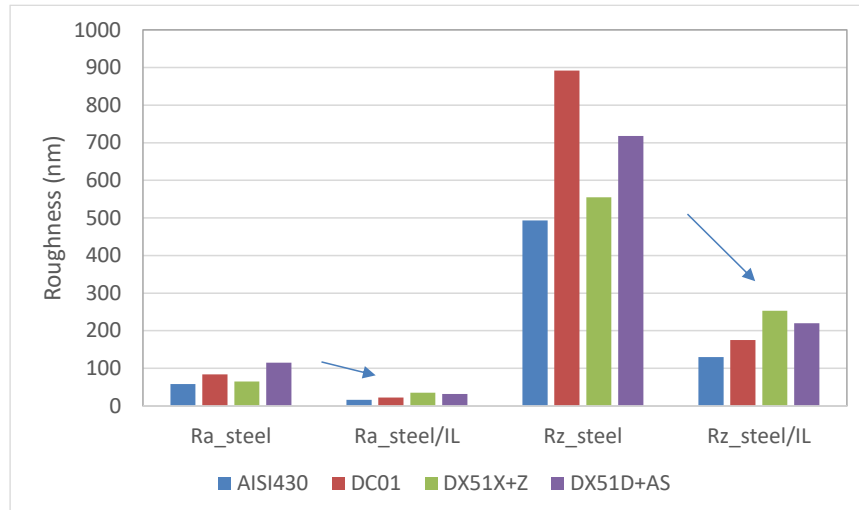


Figure 77. Roughness of the native steels (30cm x 30cm format) and after the F1 SiO_x sol-gel application.

Figure 78 shows a scheme and a picture explaining the procedure followed to carry out the dielectric tests. For each 30cm x 30cm prototype (steel/IL), three 10cm x 10cm samples were extracted and different Ag pad sizes (1cm^2 , 6.25cm^2 and 12.5cm^2) were deposited by thermal evaporation. The dielectric behaviour was determined following the ‘First procedure’.

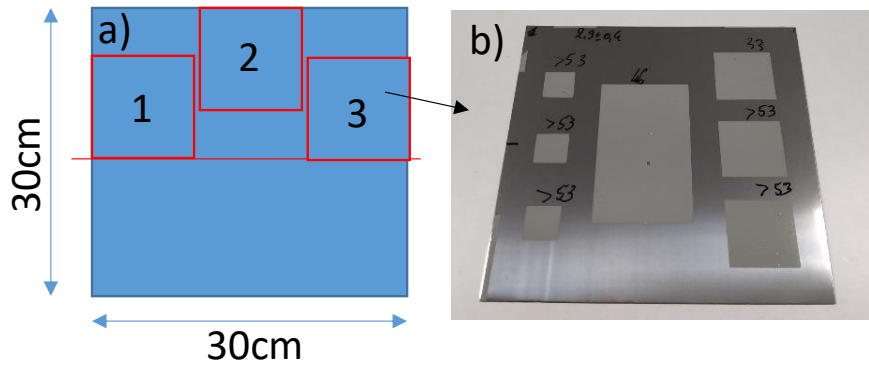


Figure 78. Dielectric test on 30cm x 30cm steel/F1 SiO_x sol-gel prototypes. a) three 10cmx10cm tested, b) Ag pads for each 10cmx10cm samples.

Table XXXII reports the percentages of Ag pads that passed the dielectric tests, taking into account 9 Ag pads of 1cm², 9 pads of 6.25 cm² and 3 Ag pads of 12.5cm². The results are better for the smallest size pad and progressively worsen (except for the DX51D+Z/IL) with the increase of the pad size. A first possible reason to explain Table XXXII results could be due to a higher probability to find defects in the sol-gel IL when the pad size is larger. However, and only looking at the 1cm² size, not in all case the percentage is 100% when it was the case at lab-scale level.

A possible reason could come from to the F1 SiO_x sol-gel spray application process and experimental conditions used at pilot plant level. Indeed, the spray application process was carried out in normal atmosphere and ambient dust could be easily caught by the liquid spray and be deposited at the same time than the sol-gel. Moreover, this phenomena could be magnified by the spray nozzle/steel substrate distance that was optimised to 8cm in order to reach an homogenous sol-gel coating. If an ambient dust is deposited, the sol-gel coating will definitely be thinner at this local zone and the electric insulation lower what could explain the shorts.

In order to avoid dust contamination of the sol-gel layer, it is recommended to carry out the spray coating process in a clean atmosphere tunnel at industrial level.

Table XXXII. Percentage of pads that passed the dielectric tests (First procedure)

Prototype	1cm ²	6.25cm ²	12.5cm ²
AISI430/IL	67%	44%	0%
DC01/IL	100%	78%	67%
DX51D+Z/IL	100%	56%	100%
DX51D+AS/IL	89%	44%	33%

The glow discharge technique coupled to a time of flight mass spectrometer (GD-TOF-MS) was used for the elemental in-depth analysis, which purpose was to evaluate the anti-diffusion behaviour of the F1 SiO_x sol-gel coating. The tests were performed before and after the simulation of an amorphous silicon (a-Si) TFSC process (2h30-210°C in vacuum chamber).

Figure 79 shows, as example, qualitative in-depth elemental profiles of a DC01/IL covered by a Ag layer before and after the annealing treatment. Following the Fe elemental line (brown one), it can be observed that no diffusion is registered. The large substrate interface (from 200s to 350s) comes from the DC01 roughness and that the steel is sputtered at the same time than the SiO_x layer in this range time. Those results are in concordance with the one achieved at lab-scale level where a proper anti-diffusion behaviour of the SiO_x IL was concluded for all the steels substrates.

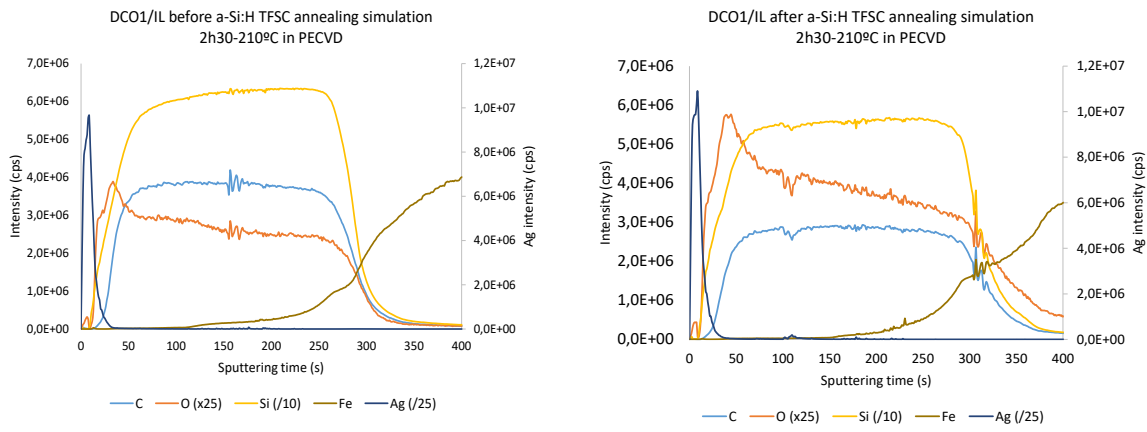


Figure 79. In-depth profiles (GD-TOF-MS) of DC01/IL prototypes before and after the simulation of a a-Si TFSC (2h30-210°C in PECVD).

It can be concluded that the F1 SiO_x sol-gel was successfully up-scaled by spray coating on the 4 steels substrates (size 30cm x 30cm). A levelling below 30nm (R_a) and 300 nm (R_z), an electrical insulation above 40V and a good anti-diffusion behaviour were achieved. However, further works have to be carried out to improve the quality of this IL in terms of defects (e.g. dust) and propose reproducible prototypes.

Another aspect explored of the up-scaling F1 SiO_x IL step was related to the optimization of the drying/curing process. Annealing sol-gel step was firstly carried out by using a standard hot-plate increasing progressively the temperature; 60°C-30min, 100°C-15min, 150°C-15min and 210°C-30min.

In order to optimise this curing process and propose a more feasible technical solution for an hypothetic industrial step (closely to the SiO_x IL application up-scaling), a fast curing step, by means of a near infra-red (NIR) technique, was explored. This fast heating of the steel substrate, combined with the relative transparency of the sol-gel film to NIR radiation (Figure 80) allows a rapid, indirect annealing of the sol-gel [26]; the curing is carried out from the inner to the outer part of the coating and enable a correct extraction of the solvents.

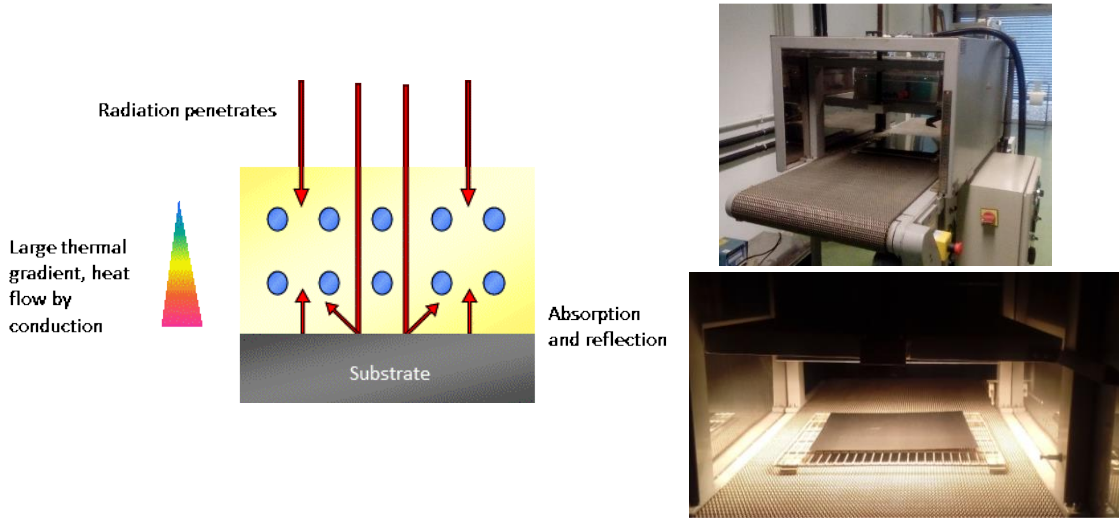


Figure 80. NIR principal and real steel/IL curing

The experiments were performed using a NIR equipment (AdPhos, model 336-250). It is composed of eight NIR lamps (0.8kW each) of 250mm x 42mm, which input a maximum power density of 76kW/m². For the trials, the irradiation power was varied from 85% to 100% and the irradiation time from 1' to 8'. The distance between the NIR lamps and the steel/IL prototypes were kept constant (20cm). The experiments were carried out in static mode considering the DC01 steel. The sol-gel IL curing grade was evaluated in terms of micro-hardness and desorption behaviour in high vacuum

PECVD chamber. The results were compared with a reference sol-gel coating cured using a hotplate and following the standard annealing procedure.

Figure 81 reports the influence of the NIR curing time on the sol-gel hardness (HV), considering a constant power of 85%. The first column shows the native DC01 hardness and the second one the sol-gel hardness after the standard curing by hotplate. It can be observed that there is no significant increase of the hardness between 1' and 9' of NIR curing. Moreover, the hardness achieved by NIR is in the same order that the one reached by hot-plate.

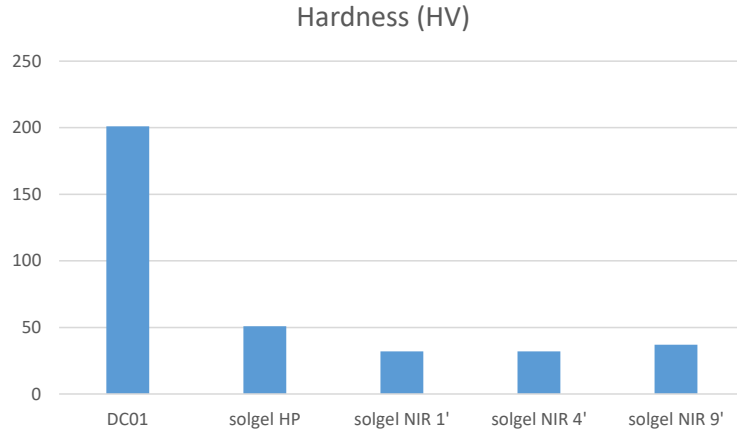


Figure 81. Influence of the NIR curing time on the sol-gel hardness (power of 85%). Comparison with sol-gel cured by hotplate_ HP (used as reference)

Figure 82 reports the results of the influence of the NIR power on the sol-gel hardness considering a NIR curing time of 2'. The first column shows the DC01 hardness and the second one the sol-gel hardness after the standard curing by hotplate. The vacuum values are the one registered in a high vacuum chamber after 1' of the introduction of the DC01 and the DC01/sol-gel IL. It can be observed that all the NIR power enable to reach a satisfactory hardness of the SiO_x sol-gel, similar to the one achieved after the hot-plate curing. Related to the desorption sol-gel grade in high vacuum chamber, it is important to note that all the three NIR powers enable a similar vacuum value than the one reached with the DC01/IL hotplate prototype. However, it seems that the highest the NIR power is, the best is the vacuum reached. In all case, the vacuum values reached demonstrated that no significant desorption is registered.

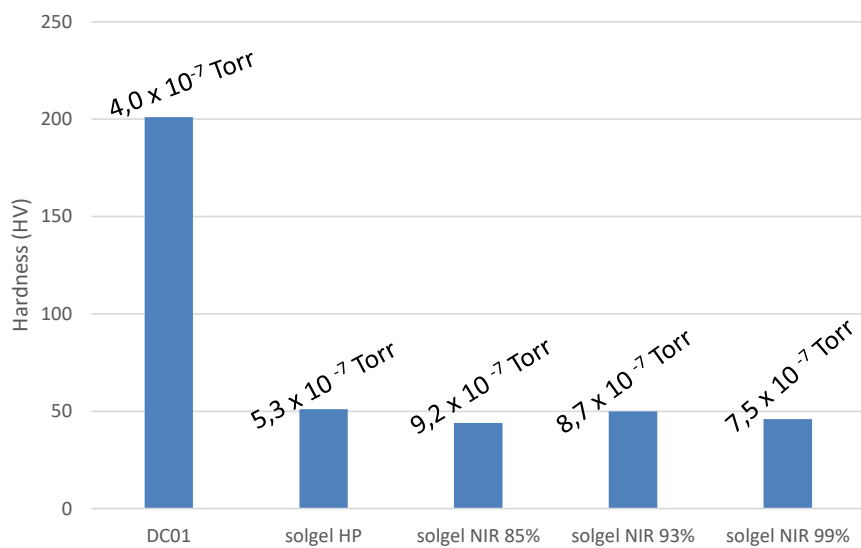


Figure 82. Influence of the NIR power on the sol-gel hardness and desorption in high vacuum chamber (NIR curing time of 2'). Comparison with sol-gel cured by hotplate (HP).

It can be concluded that the NIR annealing is a suitable technique to optimise the Steel/F1 SiO_x sol-gel curing process, showing that curing times of 2' and curing powers around 90%

enable to achieve successful F1 SiO_x sol-gel hardness and lack of desorption in high vacuum chamber.

As conclusion of this section, a SWOT (Strengths, Weaknesses, Opportunities, Threats) analysis has been performed of the steels/IL prototypes (IL= F1 SiO_x sol-gel).

STRENGTHS	WEAKNESSES
<ul style="list-style-type: none"> 1. Simple system (single and thin IL) 2. Non-vacuum manufacturing 3. Very high levelling effect 4. Compatible with rigid, semi-rigid and flexible steels 5. Compatible with S2S and R2R processes 6. Suitable for the 4 steels substrates (AISI430, DX51D+Z, DX51D+AS and DC01) 7. Suitable for a-Si:H and OPV thin film solar cells 8. No modification of the steels' appearance 	<ul style="list-style-type: none"> 1. The IL must have a high defect free quality to run properly 2. Risk of failure due to shocks (brittle IL) 3. Conformability limitations 4. Some prototypes (e.g. bare DC01/IL) might be difficult to pass the building certification
OPPORTUNITIES	THREATS
<ul style="list-style-type: none"> 1. BIPV growing market 2. In-line with the European efficiency directives 3. Promote the increase of steel use for façade/BIPV 4. Prototypes suitable for other applications; biocide, hydrophobic, tribologic, etc. (some specific modifications/nanoparticles additions should be carried out) 	<ul style="list-style-type: none"> 1. New organic coatings (supporting high temperatures, chemically stable, etc.) 2. New sol-gel formulation with improved properties 3. Overall system performance 4. Regulatory requirements for BIPV application

It can be concluded that the steels/F1 SiO_x prototypes seems to be a great solution to match structural low cost steels with low temperature thin film solar cells. Several steel's format are suitable and sheet to sheet (S2S) and roll to roll (R2R) processes are compatible to ensure a low cost manufacturing. Moreover, these prototypes could be used in the growing BIPV market but also be part of structures for other applications. Indeed, if some small changes are carried out in the SiO_x sol-gel formulation a hydrophobic property could be reached. In this case, the steel/IL will not be employed as TFSC direct substrate but could be used for improving the corrosion resistance aspect or/and for better cleaned façades.

Furthermore, if some metallic nanoparticles (e.g. Ag nanowires) are included in the SiO_x sol-gel matrix, a biocide effect could be reached. In this case the steel/IL could have an application for anti-bacterian surfaces.

However, at this stage, the highest risk comes from the necessity to offer a very low defect quality of the single F1 sol-gel SiO_x IL. This could oblige to carry out the deposition process under clean atmosphere what would increase the industrial final cost of the prototypes.

Up-scaling of SiO_x F3 sol-gel by K-bar coating

In-house F3 SiO_x sol-gels were developed with a wide range of viscosities (3 orders of magnitude). Newtonian and shear thinning sol-gels were developed to suit all printing and coating processes. A high speed curing method (NIR) was also successfully developed at lab-scale level and thicknesses of about 3 µm (2.88 ± 0.1 µm for F3_PEG200000 sol-gel) for crack free sol-gel ILs were achieved. This was sufficient to ensure a good insulation (>53V using ITMA procedure) and, therefore, compatible with TFSC technologies.

Up-scaling experiments were performed curing the F3 SiO_x sol-gel ILs with the stand-alone Heraeus NIR unit at the pilot line (Figure 83). This equipment combines power density of the NIR lamps 10 times higher than that of the lab NIR unit (250 kW).



Figure 83. R2R pilot line with stand-alone Heraeus NIR unit (denoted by red rectangle)

K-bar 3 was used to give a dry film thickness of about 3 µm using the F3_PEG200000 sol-gel. After the initial experiments which identified the minimum NIR lamps intensity capable of curing the F3_PEG200000 sol-gel layer, the intensity of the lamps was varied between 50 and 100%. Best results were achieved exposing the IL to NIR (100%) in two steps of 5 s and 10 s with an interval of 60 seconds. Figure 84 shows six samples prepared using these process parameters. However, cracks appeared during further post-processing (deposition of Ag pads by thermal evaporation) and it was concluded that the stand-alone Heraeus NIR unit at the pilot line was not the feasible up-scaling curing technique.



Figure 84. Six AISI430/ F3_PEG200000 sol-gel samples: NIR (100%); 2 steps - 5 s and 10 s with an interval of 60 s.

To mitigate the bottleneck in sol-gel IL processing the lab scale Pulse Forge 1200 Photonic curing system (Figure 84a) was used to cure F3 SiOx sol-gels deposited onto the steel substrates using a K-bar coater (Figure 84b). Photonic curing allows a very quick thermal treatment (in about 10 milliseconds) which makes it compatible with the production process.

For the experiments, the F3_PEG200000 and F3_PEG400000 sol-gel were used, the intensity of the lamp was varied between 70% and 90%. Best results were achieved with a duty cycle of 80%, 10 micro-pulses, one repetition and an interval of 60s. Figure 85 displays AISI430, DC01, DX51D+Z, and DX51D+AS steel samples coated with either F3_PEG200000 or F3_PEG400000 sol-gels using either K-Bar 3 (24 µm wet film deposit_ about 3 µm cured film) and K-Bar 4 (40 µm wet film deposit_ about 5-6 µm cured film) after photonic curing.

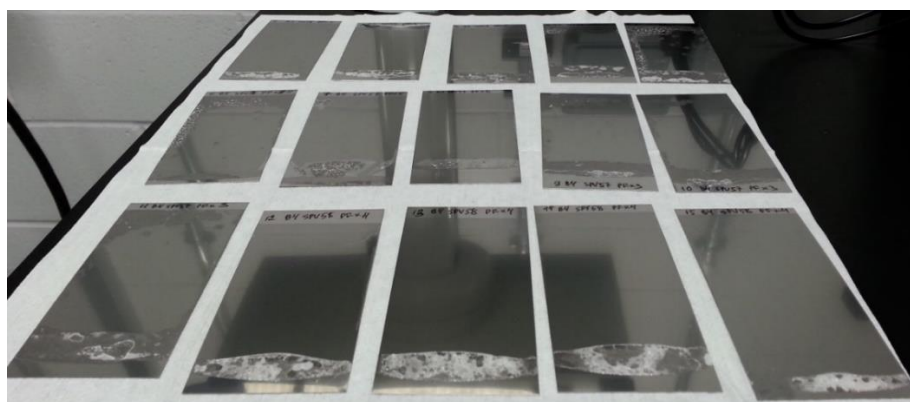


Figure 85. AISI430/F3_PEG200000 IL and AISI430/F3_PEG400000 IL after photonic curing using different process parameters

No cracks were registered after the photonic curing but cracks developed during Ag pad deposition by thermal evaporation, Figure 86. Both sol-gels F3_PEG200000 and F3_PEG400000 failed the dielectric test for all steel types and K-bars used. Although, F3 SiOx sol-gel ILs were successfully cured using the Pulse Forge 1200 at the lab level, cracks developed during post-processing by thermal evaporation most likely due to thickness being above CCT and therefore they were not suitable for TFSC technologies.

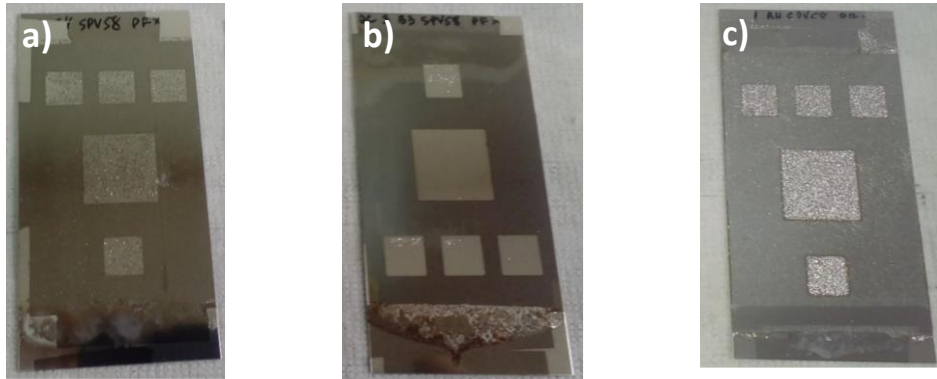


Figure 86. Cracks in F3 SiOx sol-gel IL after Ag pad deposition by thermal evaporation: a) AISI430/F3_PEG400000 IL using K-bar 4, b) DC01/F3_PEG400000 IL using K-bar 4, c) DX51D+AS/F3_PEG400000 IL using K-bar 3

2.4.2. Commercial Blue ink IL up-scaling

Experiments were performed to evaluate the up-scaling of combined planarising and insulating ILs by both sheet to sheet (S2S) and R2R processes at pilot plant level using commercially available dielectric denominated blue inks (D2140114D5_GEM, UK).

Sheet-to-sheet screen printing

Figure 87a) is an illustration of the typical S2S screen printer (DEK 248) used in this study suitable for handling 35cm x 35cm thick (up to 6 mm) steel sheets. The optimum process parameters obtained through lab scale experimentation were successfully used to manufacture 30cm x 30cm prototypes (Figure 87b). Although the optimum levelling effect was reached after applying two dielectric blue ink layers at lab-scale level, it was decided to apply only one layer at pilot plant level for an obvious productive reason. Thicknesses of $8.1\mu\text{m}\pm0.1$, $8.2\mu\text{m}\pm0.2$ and $6.8\mu\text{m}\pm0.2$ for the AISI430, DC01, DX51D+Z, respectively were determined by magnetic induction method (average of nine measurements).



Figure 87. a) Flatbed screen printer, b) 30cmx30cm prototypes and c) Batch 1 after curing.

Figure 88 reports the roughness of ten steel/Blue ink IL prototypes from Batch 1 in terms of R_a and R_z . Clearly, as shown in this statistical process control (SPC), the steel/Blue ink IL printed prototypes are smoother than the corresponding native steels (Figure 15) reflecting the levelling ability of the Blue ink IL due to its Newtonian nature and its surface tension levels. However, as it is reported in Figure 88, the levelling does not reach the expected values to be compatible with the TFSC.

The roughness of native steels (Figure 15) is: AISI430 ($R_a=58\text{nm}$, $R_z=493\text{nm}$), DC01 ($R_a=84\text{nm}$, $R_z=892\text{nm}$), DX51D+Z ($R_a=65\text{nm}$, $R_z=555\text{nm}$), DX51D+AS ($R_a=115\text{nm}$, $R_z=718\text{nm}$).

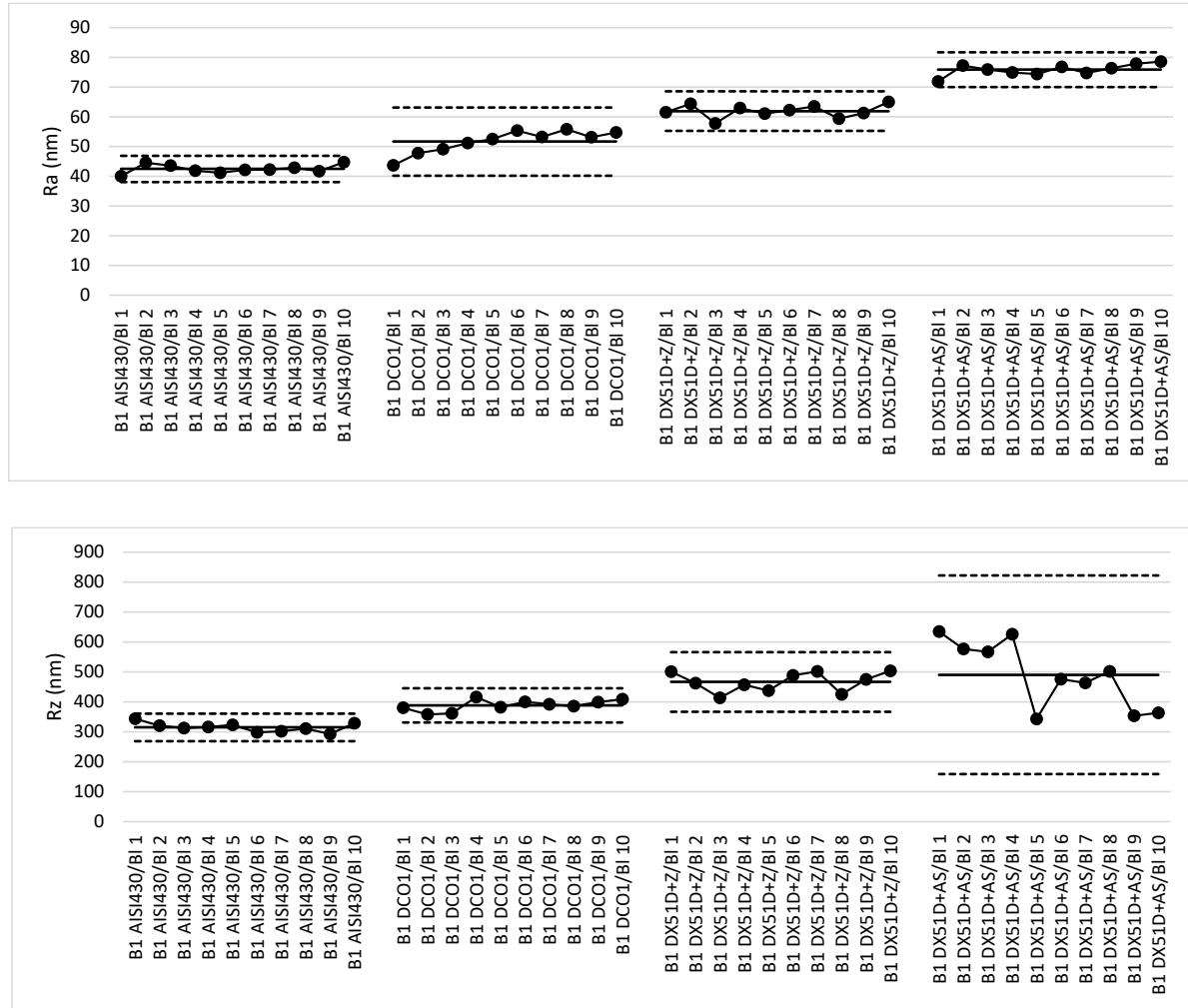


Figure 88. Roughness SPC_ Steel/Blue ink IL prototypes for four steels

In order to achieve further reduction in surface roughness two researches lines were explored; i) same previous experiments but after the improvement of the samples' flatness and ii) increase of the amount of ink transferred using a coarser polyester mesh. In this case, a coarser polyester mesh (SEFAR PET 1500 90/40, MCI precision screens, UK) was used to increase the amount of ink delivered by the screen to the steel substrate. In order to assess capability of the S2S screen printing process, 80 prototypes (20 prototypes for each steel type) and 24 prototypes (6 prototypes for each steel type) were respectively printed.

Figure 89 shows the results of the SPC after the steel sheets were flattened. It can be seen that the process was stable and only random variations were present based on the control chart rules, BS 5702 standard. It can be seen that the levelling property was significantly improved related to the first up-scaling strategy for all steels. This confirmed the importance of the steel substrate quality in terms of flatness.

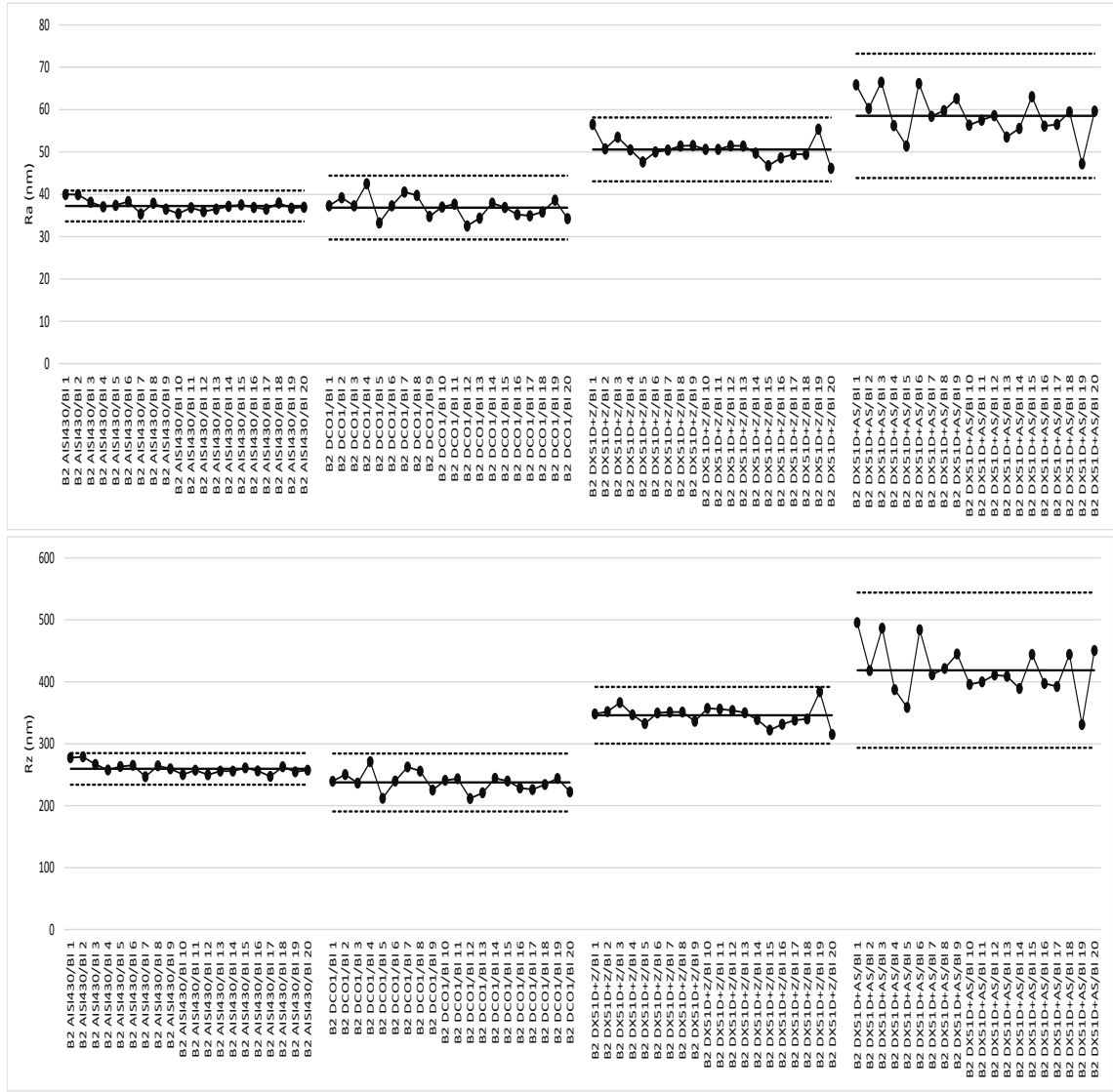


Figure 89. Roughness SPC_Ra and Rz control charts for steel/Blue ink IL prototypes for four steels after the improvement of the steels' flatness.

Figure 90 reports the SPC results after the increase of ink through the coarser polyester mesh. It can be seen that the process enables to improve the first up-scaling results for all steels, especially for the DX51D+Z and DX51D+AS steels. Concerning AISI430 and DC01 steels, very similar results are reported after the steels' flatness and the increase of the ink applied improvements. This indicates that the amount of ink delivered by the thinnest mesh was sufficient to achieve the levelling required for the STEELPV project.

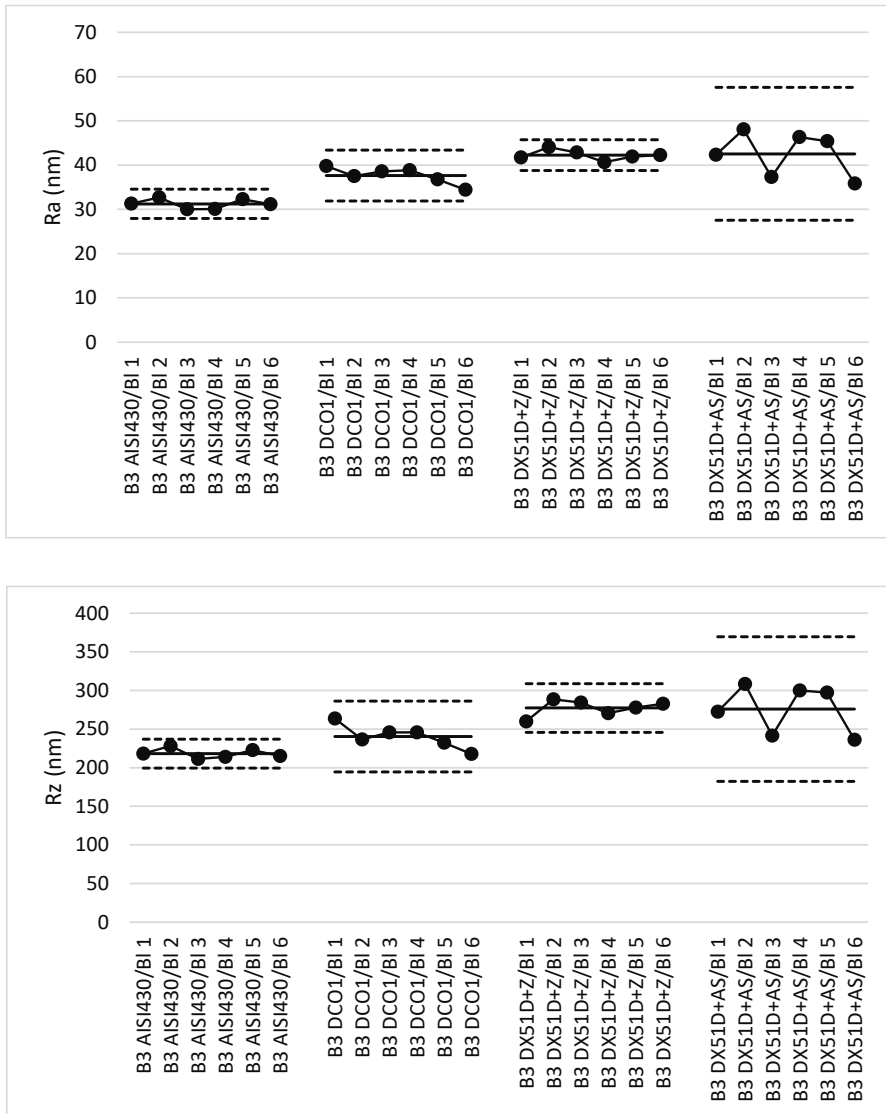


Figure 90. Roughness SPC_ Ra and Rz control charts for steel/Blue ink IL prototypes for four steels. Coarser polyester mesh used

The dielectric behavior of the blue ink prototypes was measured through the breakdown voltage test and following the ITMA procedure. Figure 91 shows the different Ag pads sizes deposited by thermal evaporation on the dielectric blue ink. All the samples analyzed passed the test.

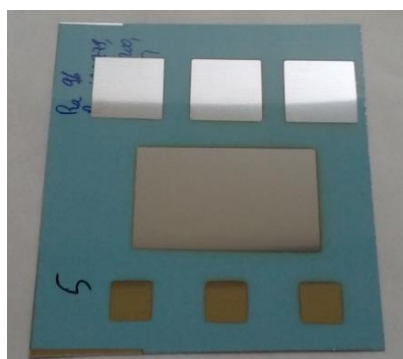


Figure 91. Blue ink prototype with Ag pads for breakdown voltage measurements.

It can be concluded that the commercial dielectric ink (Solvent Resistant Blue Dielectric Ink) was successfully up-scaled by sheet-to-sheet screen printing process on the 4 steels substrates (size 30cm x 30cm). A levelling below 40nm (R_a) and 350 nm (R_z) was achieved. An electrical insulation above 40V was achieved for all steels.

To conclude this section, a SWOT analysis was performed for the steel/Blue ink IL prototypes.

STRENGTHS	WEAKNESSES
<ul style="list-style-type: none"> 1. Simple system (single layer) and opportunity for failure mitigation by a double layer 2. Non-vacuum manufacturing 3. High levelling effect 4. Compatible with rigid, semi-rigid and flexible steels 5. Compatible with S2S processes and volume up-scaling 6. Cost effective coating system to deliver required properties for application 7. Suitable for all Steelpv steels 8. Suitable for a-Si:H TFSC 	<ul style="list-style-type: none"> 1. Conformability limitations 2. In single IL, the layer must not have defect 3. The bare low carbon steel/ blue ink IL might be difficult to pass the building certification 4. Coating must be formulated to assure rheology for levelling
OPPORTUNITIES	THREATS
<ul style="list-style-type: none"> 1. BIPV growing market 2. In-line with the European efficiency directives 3. Promote the increase of steel use for façade/BIPV 4. Compatible with rigid, semi-rigid and flexible steels 5. Suitable for other applications such as protective coatings having superior barrier and dielectric properties (this is relevant to a diversity of end applications for functional devices manufactured over large areas using printing/coating processes) 	<ul style="list-style-type: none"> 1. Decrease in vacuum IL process costs 2. New dielectric ink formulations with improved properties 3. Emergence of new organic materials with appropriate electrical and levelling properties

It can be concluded that the steels/Blue ink IL prototypes seems to be a great solution to match structural low cost steels with low temperature thin film solar cells. Several steel types are suitable for sheet-to-sheet screen printing process to ensure a low cost manufacturing. Moreover, these prototypes are suitable for the growing BIPV market but also can be used for other applications.

Roll-to-roll screen printing

The commercial blue dielectric ink (D2140114D5, GEM, UK) was applied by rotary screen print onto the 30 cm wide AISI430 coils. Figure 92 displays the coil prototype in the pilot plant line and after the application.



Figure 92. AISI430 30 cm wide coil in the pilot plant line and after the application

The non-contact White Light Interferometry (WLI) measurement method was used for the steel/Blue ink IL surface topography and roughness measurements. Surface parameters of the rotary screen printed 'blue dielectric ink' ILs were determined using the WYKO NT9300 interferometer in the vertical scanning mode.

As shown in Table XXXIII, the IL failed the levelling test. Moreover, air bubbles were generated in the rotary screen under constant shear, Figure 93. They were transferred onto the AISI430 steel

coil with the ink during ink transfer step. They subsequently bust during drying step in the oven leaving behind large deep craters Figure 93a) and Figure 93b).

Table XXXIII. Roughness of dielectric ink ILs at pilot plant level

Ink description	Target roughness	R _a (nm) (4 steels)	R _z (nm) (4 steels)
Solvent Resistant Blue Dielectric Ink	fail*	≥ 2000	≥ 13000

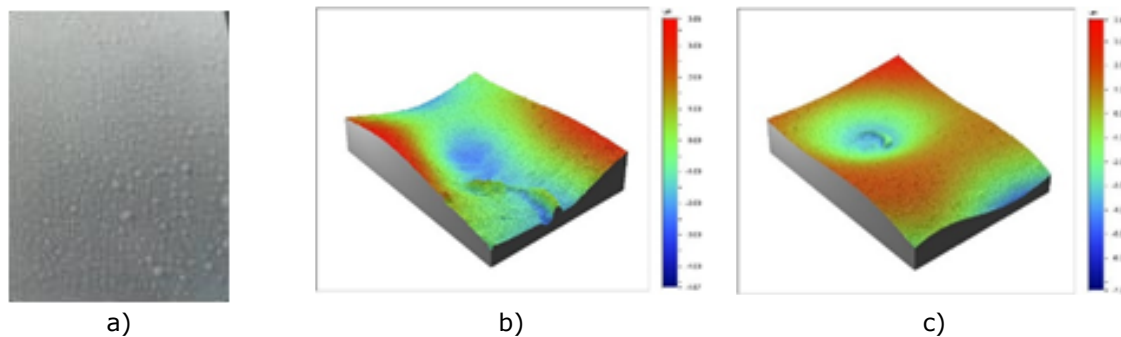


Figure 93. Solvent Resistant Blue Dielectric Ink (D2140114D5): a) air bubbles generation in the rotary screen under constant shear, b) 3D-representation of craters left by bubbles burst during drying, c) 3D-representation of an individual crater left by a bubble burst during drying

To further benchmark these results SPGPrints (Netherlands) was approached and five more rotary screen printed samples using ink A, B, C, D, and E were tried. SPGPrints is a world leader in rotary screen printing and have claimed experience of printing numerous dielectric inks for a range of applications. Table XXXIV itemises the roughness parameters (R_a and R_z) for five inks: A, B, C, D, and E. Clearly the ink E is smoother than the A, B, C and D inks although the levelling reached is not sufficient for the purpose of the project.

Table XXXIV. Summary of surface parameters for all samples

Sample	R _a (μ m)	R _z (μ m)
A across	0.38	2.35
B across	0.45	2.25
C across	0.46	5.23
D across	0.31	3.03
E across	0.17	0.84

The main finding is that the shear thinning inks were not able to achieve the levelling target most likely due to mesh marking and ink film splitting instabilities as well as limited levelling time in R2R processing. These results point to further needs to explore more fully the rotary screen printing process.

2.4.3. ILs based on hybrid sol-gel/ vacuum

Si₃N₄/SiO_x sol-gel

The up scaling of the Si₃N₄ rf-sputtering PVD process was obtained by coating long strips within the PVD equipment shown in Figure 94. The set up of the PVD chamber was modified so that a cylinder with a diameter of 72cm was used to sustain the steel strips as shown in Figure 94. This solution allowed the production of coated specimens on strips 10cm x 176cm.



Figure 94. Sample configuration for strip PVD coating

The samples were processed at 450°C, using Ar as sputtering gas. The working pressure was 0.5×10^{-3} bar and the forward RF power 1300W.

Figure 95 shows the two coated strips (AISI430 and DX51D+AS). The different color between the AISI430/Si₃N₄ and DX51D+AS/Si₃N₄ prototypes is possibly due to interference lines after the Si₃N₄ depositions. The difference of color in a same sample probably comes from very slight difference of Si₃N₄ thickness.



Figure 95. Si₃N₄ PVD coated strips

The characterization of the Si₃N₄ was performed by scanning electronic microscopy (SEM). A good quality of the coating and a thickness around 0.6 micron was found as it can be observed in Figure 96.



Figure 96. SEM-EDS characterization of coating (Si₃N₄ on AISI430 sample)

The SiO_x layer was achieved using the F1 SiO_x sol-gel and the pilot spray plant. The F1 SiO_x sol-gel dilution was 1:0.5 in ethanol. The annealing treatment was carried out by hot-plate up to two final temperatures; 210°C focused on low temperature TFSC (a-Si and OPV) and 500°C for high temperature TFSC (CIGS/CZTS).

Although the two steels covered by the Si₃N₄ layer were up-scaled to the 10cm x 180 cm size, it was not possible to process this format using the spray pilot plant. First experiments were carried out on

10cm x 20cm samples but, as it can be observed in Figure 97, the significant lack of flatness disabled homogeneous annealing treatments. So, it was decided to finally process 10cm x 10cm samples.

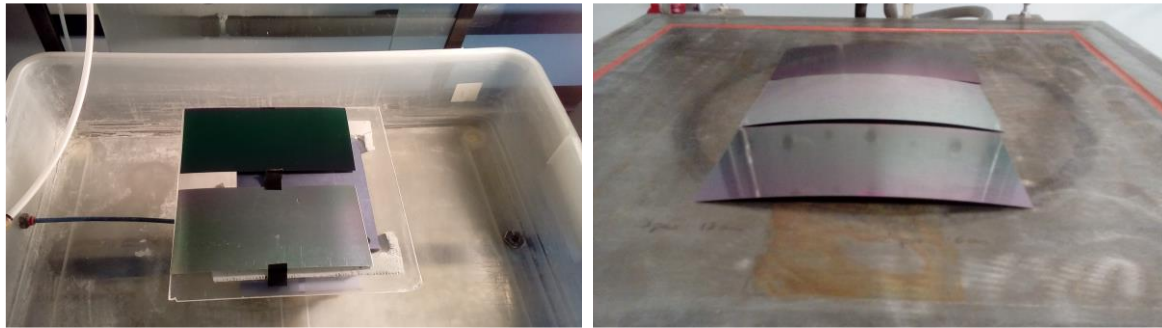


Figure 97. 10cm x 20cm steels/ Si_3N_4 during the SiO_x sol-gel spray application and hot plate curing.

Table XXXV and Figure 98 show the visual aspect, the levelling effect and the dielectric behaviour of the hybrid $\text{Si}_3\text{N}_4/\text{SiO}_x$ layer after the application of the F1 SiO_x sol-gel (curing temperature of 210°C). Related to the visual aspect, no cracks were registered. The different color between the AISI430 and DX51D+AS steels was already noticed after the Si_3N_4 layer, possibly due to interference lines after the Si_3N_4 depositions.

Regarding the influence of the F1 SiO_x liquid pressure it can be observed a real difference in terms of thickness between 0.2bar and 0.3bar, what is also confirmed by the dielectric behaviour of the $\text{Si}_3\text{N}_4/\text{SiO}_x$ stack. Considering the 0.3bar liquid pressure it is demonstrated the levelling effect with values compatible with both the a-Si and OPV TFSC.

Related to the dielectric behaviour, several Ag pads (1cm^2 and 4cm^2) were deposited by thermal evaporation and the tests were carried out following the 'First procedure'. As reported in Table XXXV and Figure 98, the 0.3bar liquid pressure enables to reach successful results for both steels.

Table XXXV. Steel/ Si_3N_4 -F1 SiO_x sol-gel prototypes depending of spraying conditions

Substrate (10cm x 10cm)	SiO_x Spray pressure (bar)	R_a (nm)	R_z (nm)	SiO_x Thickness (μm)	Dielectric behaviour
AISI430+ Si_3N_4	0.2			2.3	3/5 > 40V
AISI430+ Si_3N_4	0.3	33	215	3.4	5/5 > 53V
DX51D+AS+ Si_3N_4	0.3	24	164	---	5/5 > 40V

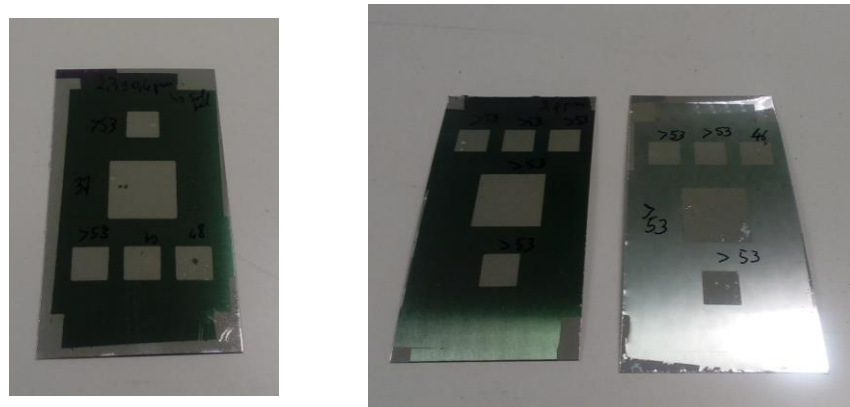


Figure 98. AISI430 processed at 0.2bar (liquid pressure) and AISI430 and DX51D+AS processed at 0.3bar (liquid pressure)

The F1 SiO_x sol-gel was then applied by using the spray pilot plant and cured up to 500°C in order to match with the temperature process of CIGS/CZTS TFSC. First experiments showed superficial small cracks, possibly due to coating internal strengths or because of the steel/IL bending at 500°C (effect not registered at 210°C). In order to try to avoid the cracks, the thickness of the F1 SiO_x sol-gel was reduced, working at the 0.2bar liquid pressure. Figure 99 shows a processed 10cm x 10cm AISI430 sample. The thickness measured (taking into account the Si_3N_4 layer) was 2.1 μm and, as

it can be shown in Figure 99, the dielectric behaviour of the $\text{Si}_3\text{N}_4/\text{SiO}_x$ is satisfactory. However, the visual aspect is still not perfect and an improvement of the F1 SiO_x sol-gel formulation should be necessary. Nevertheless, it is demonstrated the great potential of the $\text{Si}_3\text{N}_4/\text{SiO}_x$ hybrid layer for the CIGS/CZTS TFSC.

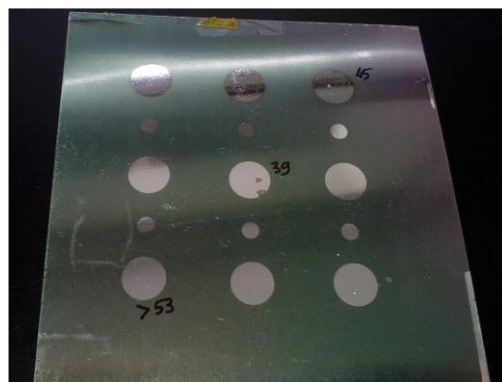


Figure 99. Visual aspect of the AISI430/ Si_3N_4 - SiO_x prototype; the SiO_x was cured at 500°C

As both Si_3N_4 and SiO_x layer were processed at 500°C , in-depth elemental analysis (GD-TOF-MS spectrometric technique) were performed in order to evaluate the anti-diffusion behaviour of this hybrid stack. Figure 100 shows the result considering the AISI430/ Si_3N_4 - SiO_x prototype. It can be observed that no Fe and Cr have diffused in the hybrid stack what demonstrate a satisfactory anti-diffusion behaviour.

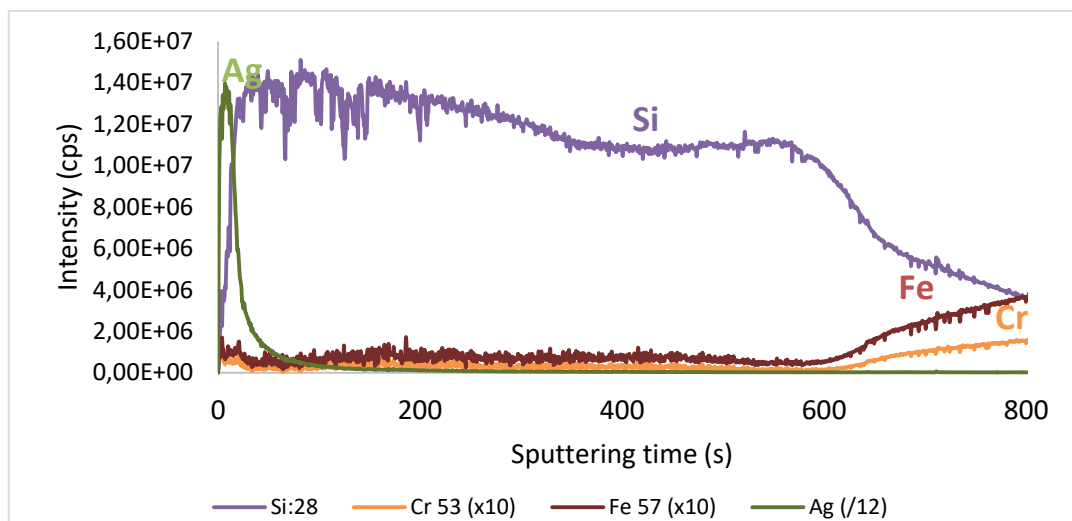


Figure 100. In-depth qualitative element profile (GD-TOF-MS) of the AISI430/ Si_3N_4 - SiO_x prototype. Si_3N_4 and SiO_x were deposited/cured at 500°C

It can be concluded that the hybrid strategy considering the Si_3N_4 (PVD deposition) and F1 SiO_x sol-gel stack is technically suitable to fulfil the requirements of STEELPV project. However, further work is necessary to better explore this hybrid approach, in terms of i) improvement of the vacuum PVD deposition time and ii) improvement of the F1 SiO_x sol-gel curing time.

As conclusion of this section, a SWOT analysis of the Si₃N₄/SiO_x hybrid IL has been performed.

STRENGTHS	WEAKNESSES
<ol style="list-style-type: none"> 1. Very high levelling effect 2. Compatible with rigid, semi-rigid and flexible steels 3. Compatible with S2S and R2R processes 4. Suitable for low (a-Si:H, OPV) and high (CIGS, CZTS) temperature thin film solar cells 5. High density due to the PVD RF sputtering coating 6. Very low contamination due to the PVD RF sputtering layers 7. Good adhesion and high dielectric quality 	<ol style="list-style-type: none"> 1. Relative long and costly process 2. Risk of failure due to shocks (brittle IL) 3. Conformability limitations 4. Not relevant for Galvanized steel 5. Some prototypes (e.g. bare DC01/IL) might be difficult to pass the building certification
OPPORTUNITIES	THREATS
<ol style="list-style-type: none"> 1. BIPV growing market 2. In-line with the European efficiency directives 3. Promote the increase of steel use for façade/BIPV 4. Prototypes suitable for other applications; biocide, hydrophobic, tribologic, etc. (some specific modifications/nanoparticles additions should be carried out) 5. Possible integration into steel coating line 	<ol style="list-style-type: none"> 1. Wet IL processes; sol-gel formulation with improved properties 2. New organic coatings (supporting high temperatures, chemically stable, etc.) 3. Higher efficiency of other PV technologies could limit the development of this solution 4. Overall system performance 5. Regulatory requirements for BIPV application

It can be concluded that the steels/Si₃N₄-SiO_x prototypes seems to be a great solution to match structural low cost steels with TFSC. Although the vacuum process enables to give a high quality of the final IL, the IL cost should also be much higher than the wet IL approaches. Moreover, these prototypes could be used in the growing BIPV market but also be part of structures for other applications. Indeed, if the sol-gel is applied as outer layer, some small changes in its formulation could confer it a hydrophobic property. In this case, the steel/IL will not be employed as TFSC direct substrate but could be used for improving the corrosion resistance aspect or/and for better cleaned façades.

Furthermore, if some metallic nanoparticles (e.g. Ag nanowires) are included in the SiO_x sol-gel matrix, a biocide effect could be reached. In this case the steel/IL could have an application for anti-bacterian surfaces.

SiO_x IL

Based on the results achieved at lab-scale level, it was initially decided to carry out up-scale experiments considering the hybrid SiO_x tri-layer stack. The below two configurations were explored and three steels (DC01, DX51D+AS and AISI430) were used:

- SiO_x sol-gel/ SiO_x PVD/ SiO_x sol-gel
- SiO_x sol-gel/ SiO_x PECVD/ SiO_x sol-gel
- To solve some drawbacks, mainly related to the oxidation of the DC01, an hybrid SiO_x bi-layer approach was also developed.
- SiO_x sol-gel/ SiO_x PECVD

Finally, some work using the NIR curing technique was carried out in order to optimize the SiO_x sol-gel annealing time (respecting to hotplate curing). All the annealing treatments (by hotplate or NIR) were carried out in air atmosphere).

Based on the results achieved with the different sol-gel formulations, the F1 SiO_x sol-gel one was chosen for the trials and the spray pilot plant used as wet up-scaling technique.

As the purpose of this IL is to be used for all kind of TFSC, the SiO_x hybrid stack has to support a maximum process temperature of 500°C. An IL thickness about 3µm was established as sufficient for single SiO_x sol-gel IL to match the steels selected in the project and the TFSC. Following this result, the thicknesses targets were about 1-1.5µm for the F1 SiO_x sol-gel layer of about 500nm for the SiO_x vacuum layer. For the SiO_x bi-layer prototype, the SiO_x vacuum coating was increased to

1 μ m. As the curing process was carried out up to 500°C the galvanized steel (DX51D+Z) was not considered.

Hybrid SiO_x tri-layer

The first layer (SiO_x sol-gel) was deposited by spray coating and initially cured up to 500°C by hotplate following these steps: 30min_60°C, 15min_100°C, 15min_210°C, 15min_350°C and 30min_500°C. The experimental conditions for the F1 SiO_x sol-gel depositions were i) a sol-gel dilution of 1:1 in ethanol, ii) a liquid pressure of 0.3bar, iii) a holder speed of 2.5m/min, iv) a nozzle/sample distance of 8cm and v) a one scan spray. 10cm x 10cm samples were processed as it is the maximum size for the vacuum PVD and PECVD steps.

After this process, a thickness range of 1.0-1.3 μ m on the three substrate was determined by inductive probe meter. Very thin cracks were visually detected and Figure 101 shows optical microscopic images of those cracks defects. It can be observed that the cracks are very thin and start from a local impurity probably deposited at the same time than the SiO_x sol-gel.

These thin cracks were not registered when the F1 SiO_x sol-gel was deposited in similar conditions but only cured up to 210°C. Possible explanations could be that i) the steel substrate has to support much stronger strengths and bending at 500°C than at 210°C or/and ii) the F1 SiO_x sol-gel layer cured at 210°C is much more elastic due to the no-degradation of its releasing agent (PEG) at this temperature. At 500°C, the F1 SiO_x sol-gel layer is much closer to the SiO₂ structure and also much more compact and brittle.

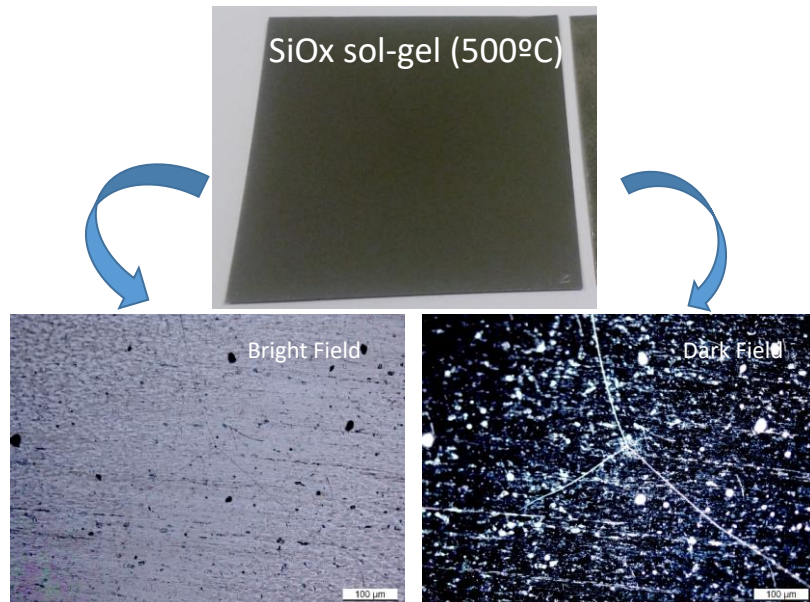


Figure 101. 10cm x 10cm AISI430 sample covered by F1 SiO_x sol-gel and cured up to 500°C. Bright field and dark field optical micrographs (magnification x100) of cracks defects.

The next steps (SiO_x by PVD or PECVD and the final SiO_x sol-gel layers) were carried out in order to evaluate the impact of those thin cracks on the final SiO_x tri-layer stack behaviour. The PVD experiments were carried out by using the magnetron sputtering physical vapour deposition of the Figure 102a (AJA International, model ATC Orion 8HV) and a 3" SiO_x material as target (CathayMaterials_99.99% purity). Initially, the depositions were carried out without applying any temperature to the substrate, an Ar (sputtering gas) flow of 20sccm (standard cubic centimeter per minute), a working pressure of 3mTorr and a working power of 90W (RF source). The duration of the experiments was 20000s and a thickness of 380nm was measured.

The PECVD trials were carried out by using the cluster system of the Figure 102b (Elettronrava, model V0714). In this case, and following a previous background, a temperature of 500°C (heater 700°C) was applied. The following gas mixture was considered: SiH₄ (Silane) and N₂O (Nitrogen monoxide) with 6sccm and 113sccm flows, respectively. The optimum homogeneity of the deposition was found at a working pressure of 800mTorr and a working power of 3W (RF source at the frequency

of 13.56 MHz) was applied. The duration of the experiments was 4min and a thickness of 280nm was measured.

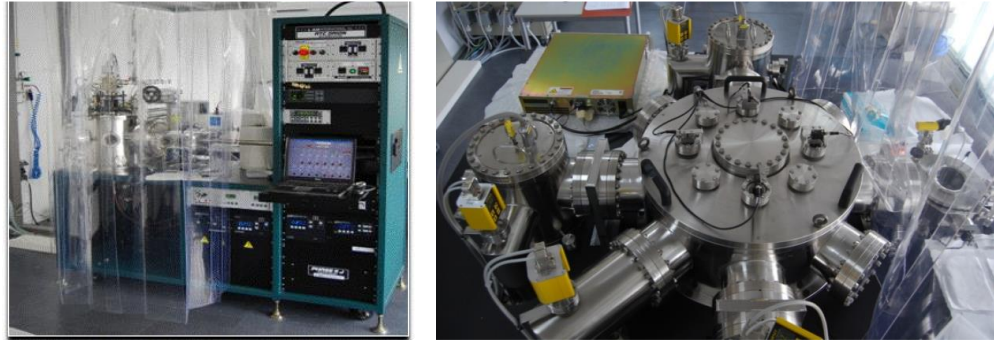


Figure 102. Magnetron_Sputtering PVD and PECVD used for the vacuum SiO_x depositions.

After the trials, as no increase of the cracks was visually detected, the third SiO_x layer was deposited by spray coating in a similar way as the one described for the first SiO_x layer. Figure 103 shows a visual aspect of two SiO_x tri-layer prototypes deposited on AISI430 steel; sol-gel/PVD/sol-gel (Figure 103a) and sol-gel/PECVD/sol-gel (Figure 103b) configurations. It can be clearly observed an increase of the coating degradation in the case of the sol-gel/PVD/sol-gel system as macro cracks are now registered (comparing with the first sol-gel layer_Figure 101). SiO_x tri-layer prototypes including thinner SiO_x PVD (80nm and 160nm) were carried out, but macro cracks were always registered.

Related to the sol-gel/PECVD/sol-gel system, only a very slight increase of the cracks was visually detected and mainly located at the edges of the sample. The tri-layer thickness was 2.5µm and its roughness was R_a =29nm and R_z =280nm.

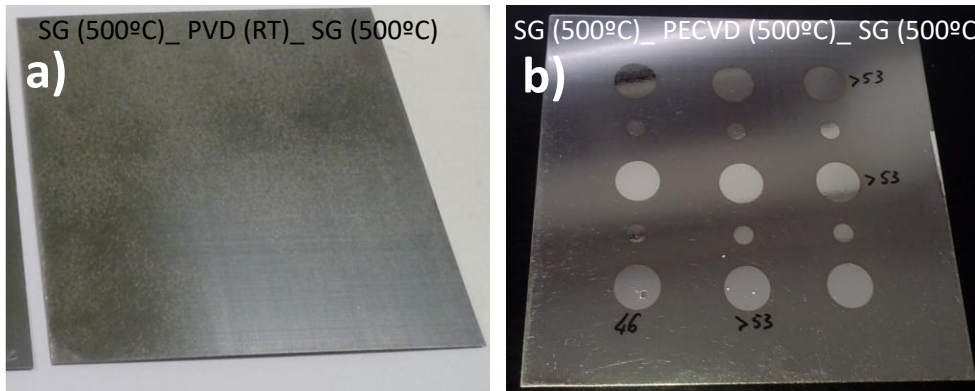


Figure 103. Visual aspect of two tri-layer SiO_x prototypes deposited on AISI430 steel. a) sol-gel/PVD/sol-gel and b) sol-gel /PECVD/sol-gel.

In order to give a possible explanation to this difference, X-ray diffraction (XRD) analysis of both vacuum SiO_x layers were performed. The SiO_x were deposited in the same experimental conditions on a Si wafer substrate (because of its very low roughness). Figure 104 reports qualitative analysis of the SiO_x layers deposited by PVD at room temperature and by PECVD at 500°C (heater 700°C) after removing the Si wafer background. The phase identification was carried out with EVA software [27], using PDF-2 ICDD database (International Centre for Diffraction Data). It can be clearly observed a difference in the amorphous phase intensity much more important in the room temperature experiment.

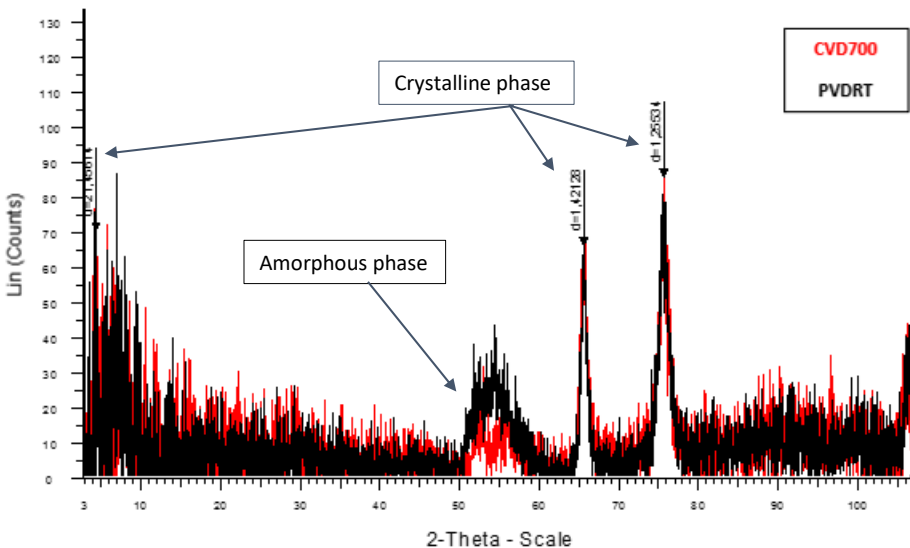


Figure 104. X-ray diffractogram of SiO_x films at different temperature deposition.

Table XXXVI reports the percentage of crystallinity determined through the equation 1. The percentage of crystallinity was calculated by the integration of the intensities (peak area) of the crystalline and amorphous contribution ($I_{\text{crystalline}}$ and $I_{\text{amorphous}}$ respectively) and considering the Rietveld refinement [28] with TOPAS software [29].

$$(1) \quad \% \text{ Crystallinity} = \frac{I_{\text{crystalline}}}{I_{\text{crystalline}} + I_{\text{amorphous}}} \times 100$$

Table XXXVI. Percent crystallinity

Deposition method	Deposition Temperature (°C)	% Crystallinity
PVD	RT	40
CVD	500	55

This difference of crystallinity could be part of the reason why the tri- SiO_x layer is completely cracked in the case of the sol-gel/PVD/sol-gel prototype. Indeed, the higher SiO_x amorphous phase could promote much more instability and strengths of the stack during the curing at 500°C of the last SiO_x sol-gel layer.

The dielectric behaviour of the sol-gel/PECVD/sol-gel IL prototypes was then determined. As shown in Figure 103b, Ag pads (diameter of 1 cm) were deposited by thermal evaporation. Following the 'First procedure' a voltage was swept from 0V to 53V. In Figure 103b, it can be observed that the four Ag pads tested support more than 40V what demonstrate that the thin cracks detected in first SiO_x sol-gel layer cured by hotplate at 500°C do not seem to have influence on the stack final quality.

However, the visual aspect is not satisfactory and new experiments were performed curing the first SiO_x sol-gel up to 220°C by hotplate instead of the 500°C. The following SiO_x layers were deposited in a same way as previously described (vacuum SiO_x by PVD or PECVD and upper SiO_x layer by sol-gel). However, and considering the importance of the temperature during the vacuum step, the PVD SiO_x deposition was carried out at 350°C. Figure 105 shows an improvement of the visual aspect of the AISI430/ SiO_x tri-layer IL prototypes. This time the thin cracks defects were only observed at one edge of the AISI430_PVD sample. In the case of the DC01/IL and DX51D+AS prototypes, the results were satisfactory using both the PVD and the PECVD techniques.

However, a dark colour for DC01/IL prototypes was observed after the upper sol-gel (500°C in air atmosphere) step due to an oxidation process. A possible solution would be to carry out the last SiO_x sol-gel layer under inert atmosphere although it would have influence on the final IL cost. Another approach, described in the following paragraph, would be to consider a SiO_x bi-layer composed by a SiO_x sol-gel and a thicker PECVD SiO_x coating. In this case the PVD technique was not considered as the sputtering rate was extremely long (20000s to reach 380nm) and not viable for an industrial level.

PVD



PECVD



Figure 105. Visual aspect of the three steels covered by the sol-gel (220°C)/PVD or PECVD/sol-gel (500°C).

Concerning the anti-diffusion behaviour of the hybrid SiO_x tri-layer, a qualitative in-depth elemental analysis (by GD-TOF-MS) of the AISI430/IL was performed. As shown in Figure 106, no Fe and Cr diffusion is observed what demonstrate the required behaviour of this IL. The large substrate/IL interface (from 120s to 230s) is due to the AISI430 roughness.

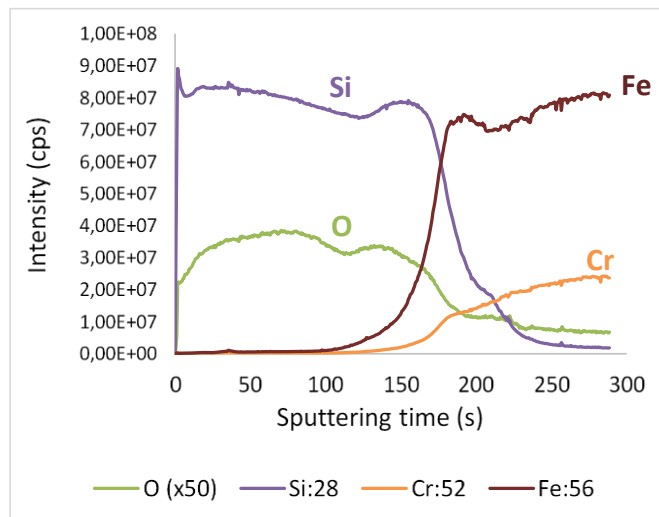


Figure 106. Qualitative in-depth elemental profile of the AISI430/hybrid SiO_x tri-layer (vacuum one by PECVD)_GD-TOF-MS spectrometric method.

Hybrid SiO_x bi-layer

The first layer (SiO_x sol-gel) was deposited by spray coating and cured up to 220°C by hotplate. The experimental conditions for the F1 SiO_x sol-gel depositions were identical as the ones previously

described. A thickness range of 1.1-1.2 μm on the substrates was determined, according to the magnetic induction method. The rf-PECVD depositions were carried out at the substrate's temperature of 500°C (heater 700°C), with a gas mixture of SiH₄/N₂O. The duration of the experiments was 14min and a thickness about 1 μm was measured. The roughness measured reports a R_a of 35nm and R_z of 320nm for the AISI430/SiO_x bi-layer and a R_a of 32nm and R_z of 299nm for the DC01/SiO_x bi-layer. Figure 107 shows the visual aspect of the SiO_x bi-layer on AISI430 and DC01 steels. No cracks were detected and decrease of the DC01 oxidation (compared to Figure 105) can be easily observed. The slight brown color is due to the oxidation process during the first SiO_x sol-gel layer cured at 220°C (hotplate_air atmosphere).

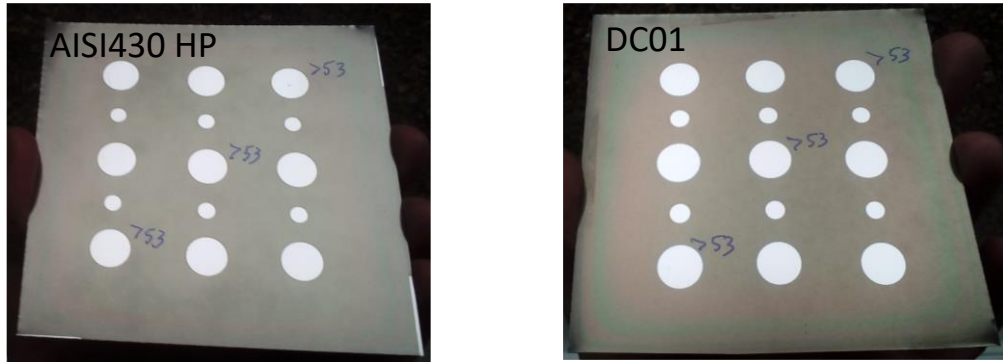


Figure 107. Visual aspect of the AISI430/SiO_x bi-layer and DC01/SiO_x bi-layer prototypes.

The dielectric behaviour of the sol-gel/PECVD IL prototypes was then determined. As shown in Figure 107, Ag pads (diameter of 1 cm) were deposited by thermal evaporation. Following the 'First procedure' a voltage was swept from 0V to 53V. As it can be observed in Figure 107, the three Ag pads tested support more than 53V what demonstrate the stack final quality.

NIR annealing

Finally, a NIR curing process was applied in order to evaluate the SiO_x sol-gel behaviour through the optimization of this annealing time. The experiments were performed considering SiO_x tri-layer and SiO_x bi-layer IL and the AISI430 steel. The NIR equipment (AdPhos, model 336-250) was used and an irradiation power of 90% during an irradiation time of 2' was applied.

In the case of the SiO_x tri-layer, the NIR conditions were only applied on the first SiO_x sol-gel layer as only a maximum temperature of 198°C was reached. The other SiO_x sol-gel coating was cured by traditional hotplate up to 500°C. The vacuum SiO_x layer was grown by PECVD. Figure 108 shows the visual aspect of the SiO_x tri-layer (Figure 108a) and SiO_x bi-layer (Figure 108b) deposited on AISI430. No thin cracks were detected after the sol-gel (cured by NIR) and PECVD steps and very few defect were detected in the bottom part of the sample after the sol-gel cured by hot plate (Figure 108a). The thickness measured was 2.3 μm for the SiO_x tri-layer and 2.2 μm for the SiO_x bi-layer.

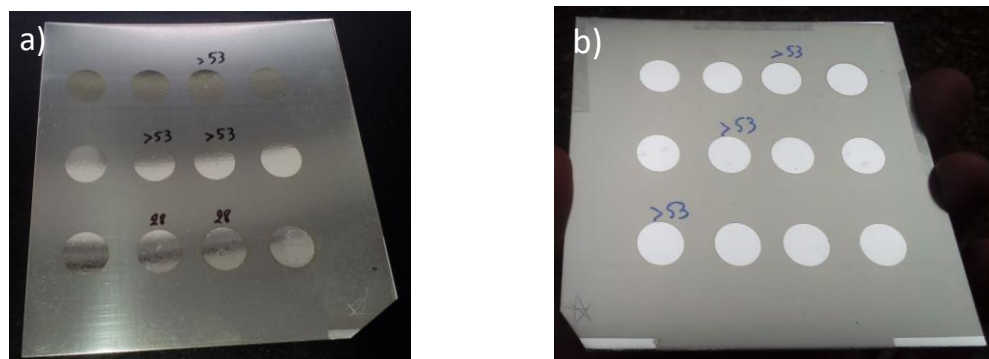


Figure 108. a) SiO_x tri-layer on AISI430 steel. First layer: SiO_x sol-gel cured up to 200°C by NIR, second layer: SiO_x by PECVD at 500°C and third layer: SiO_x sol-gel cured up to 500°C by hotplate, b) SiO_x bi-layer on AISI430 steel. First SiO_x sol-gel cured up to 200°C by NIR and second SiO_x by PECVD at 500°C

The roughness measured reports a R_a of 29nm and R_z of 235nm for the AISI430/SiO_x bi-layer. The dielectric behaviour of both SiO_x tri-layer and SiO_x bi-layer prototypes was then determined. As shown in Figure 108, Ag pads (diameter of 1 cm) were deposited by thermal evaporation. Following the ITMA procedure a voltage was swept from 0V to 53V. As reported by Figure 108, it can be observed that the four Ag pads tested support more than 40V what demonstrate the stack final quality.

A sum up of the experiments for the hybrid SiO_x up-scaling are reported in the Table XXXVII and Table XXXVIII. It can be concluded that:

- **SiO_x grown by PVD at room temperature is not suitable as the final SiO_x tri-layer stack is then fully cracked. Thinner SiO_x PVD layers do not show improvements.**
- **SiO_x grown by PVD under temperature improves the final results of the SiO_x tri-layer although the PVD process time is not compatible with an industrial manufacture (too long).**
- **The thin cracks detected in first SiO_x sol-gel layer cured by hotplate at 500°C do not seem to have influence on the hybrid IL stack stability. However, the bad visual aspect of the first SiO_x sol-gel layer makes this approach difficult to propose at industrial level.**
- **The NIR treatment enables to reach a good SiO_x sol-gel quality in terms of visual aspect and stability during the PECVD vacuum process. Moreover, the short process time makes this approach technically viable at industrial level.**
- **SiO_x grown by PECVD under temperature enables to achieve successful results in terms of visual aspect and stability. This process is relatively fast (4' for the SiO_x tri-layer and 14' for the SiO_x bi-layer) and makes it technically viable at industrial level.**
- **The SiO_x bi-layer is particularly interesting for DC01 substrate as the oxidation process is drastically reduced.**

Table XXXVII. Hybrid SiO_x tri-layer prototypes_ Evaluation of the technical feasibility

	First SiO _x layer			Second SiO _x layer			Third SiO _x layer
	SG_HP_500°C	SG_HP_220°C	SG_NIR_200°C	PVD_RT	PECVD_350°C	PECVD_500°C	SG_HP_500°C
AISI430	=	+	No crack, long process	---	IL fully cracked after the third SiO _x layer	=	=
DX51D+AS		+	No crack, long process				
DC01	Thin cracks	=	No crack, slight oxidation, long process	+++ No crack, very fast process	=	++ No crack, fast process	+ long process
							--- Strong oxidation, long process

Table XXXVIII. Hybrid SiO_x bi-layer prototypes_ Evaluation of the technical feasibility

	First SiO _x layer		Second SiO _x layer
	SG_HP_220°C	SG_NIR_200°C	PECVD_500°C
AISI430	+ No crack, long process	+++ No crack, very fast process	++ No crack, fast process
DC01			

As conclusion of this section, a SWOT analysis has been performed of the steels/IL prototypes (IL= SiO_x bi and tri-layer with PECVD as vacuum technique).

STRENGTHS	WEAKNESSES
<ol style="list-style-type: none"> 1. Very high levelling effect 2. Compatible with rigid, semi-rigid and flexible steels 3. Compatible with S2S and R2R processes 4. Suitable for low (a-Si:H, OPV) and high (CIGS, CZTS) temperature thin film solar cells 5. No modification of the steels' appearance 	<ol style="list-style-type: none"> 1. Relative long and costly process 2. The IL must have a high defect free quality to run properly 3. Risk of failure due to shocks (brittle IL) 4. Conformability limitations 5. Not relevant for Galvanized steel 6. Some prototypes (e.g. bare DC01/IL) might be difficult to pass the building certification
OPPORTUNITIES	THREATS
<ol style="list-style-type: none"> 1. BIPV growing market 2. In-line with the European efficiency directives 3. Promote the increase of steel use for façade/BIPV 4. Prototypes suitable for other applications; biocide, hydrophobic, tribologic, etc. (some specific modifications/nanoparticles additions should be carried out) 	<ol style="list-style-type: none"> 1. Wet IL processes; sol-gel formulation with improved properties 2. New organic coatings (supporting high temperatures, chemically stable, etc.)

It can be concluded that the steels/SiO_x bi and tri-layers prototypes seems to be a good solution to match structural low cost steels (except the galvanised one) with all kinds of thin film solar cells. Sheet to sheet and roll to roll processes could be compatible to ensure a low cost manufacturing. Moreover, these prototypes could be used in the growing BIPV market but also be part of structures for other applications. Indeed, if the sol-gel is applied as outer layer, some small changes in its formulation could confer it a hydrophobic property. In this case, the steel/IL will not be employed as TFSC direct substrate but could be used for improving the corrosion resistance aspect or/and for better cleaned façades.

Furthermore, if some metallic nanoparticles (e.g. Ag nanowires) are included in the SiO_x sol-gel matrix, a biocide effect could be reached. In this case the steel/IL could have an application for anti-bacterian surfaces.

However, at this stage, the highest risks identified comes from the increase of cost respecting to a wet IL approach.

3. Exploitation and impact of the research results

3.1. Actual applications

The main niche for steel/IL/TFSC products is directly related to BIPV, BIPVT (Building Integrated Photovoltaic Thermal system) and BAPV, proposing multifunctional PV façade that provide active and passive benefits to new and retrofitted buildings such as i) in-situ electricity generation, ii) thermal envelope solutions (e.g. pre-heating flow for winter seasons), iii) acoustic benefits, iv) aesthetical added value and v) atmospheric protection of the internal structure.

In particular, and because the STEELPV prototypes use steel as substrate, a concrete application could be for BIPVT as shown in Figure 109. In this case, the ventilated façade would have benefit for improving the electricity generation (by cooling the solar panel what enables an increase the PV efficiency) and producing heated air useful for a pre-heating of the building.

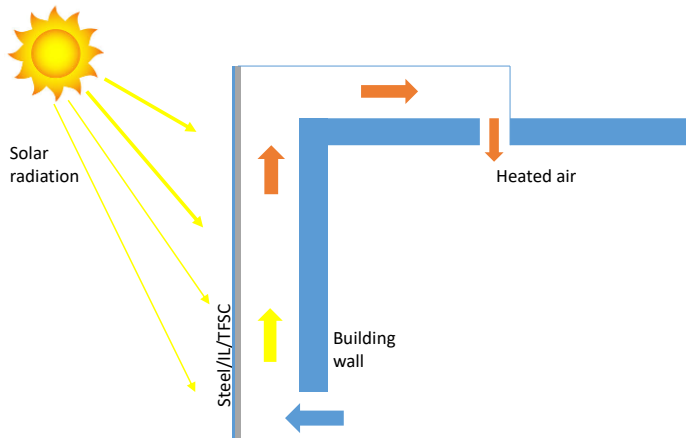


Figure 109. Scheme of a BIPVT system.

3.2. Technical and economic potential for the use of the results

Technical potential

The successful developments of ILs and their applications at pilot plant scale level are reported in *Table XLIV* (Conclusions_ p105), showing the STEELPV portfolio. Two IL strategies were successful; i) wet approach and ii) hybrid (combining wet and vacuum processes) and four different steels considered. The depositions were achieved through industrial techniques (Spray coating, Screen printing, PVD and PECVD). It can be concluded that:

Wet intermediate layer prototypes:

- The in-house F1 SiO_x demonstrated a great potential as it was successfully up-scaled by spray coating on the four steels substrates (size 30cm x 30cm). Moreover, it seems compatible with fast curing process (NIR technique). However, further researches have to be performed to improve the final quality of this IL in terms of defects (e.g. dust), reproducibility of the prototypes (through a statistical process control) and stability of the sol-gel industrial volumes.
- The commercial dielectric blue ink was successfully up-scaled by sheet-to-sheet screen printing process on the four steels substrates (size 30cm x 30cm) and seems to be a great solution to match structural low cost steels with low temperature TFSC. One important strength of this IL is to work with an already commercial product what enabled the achievement of a statistical process control. Another advantages are its highly dielectric behaviour and corrosion protection. As main weakness, it can be mentioned that this IL was not able to be applied by R2R process.

Hybrid intermediate layer prototypes:

- The hybrid strategy based on a bi-layer composed by the Si₃N₄ (PVD deposition) and F1 SiO_x sol-gel (Spray coating) is technically suitable (except for the galvanised steel) to fulfil the requirements of STEELPV project and seems to be compatible with low and high temperatures TFSC. However, further work is necessary to better explore this hybrid approach, in terms of i) improvement of the vacuum PVD deposition time, ii) improvement of the F1 SiO_x sol-gel curing time, iii) the deposition of all kind of TFSC and iv) the reproducibility of the prototypes through a statistical process control.
- The steels/SiO_x bi and tri-layers prototypes seems to be a good solution to match structural low cost steels (except the galvanised one) with all kinds of TFSC. The F1 SiO_x sol-gel seems to be compatible with NIR fast curing and SiO_x grown by PECVD under temperature enables to achieve successful results in terms of visual aspect and stability. This process is relatively fast (4' for the SiO_x tri-layer and 14' for the SiO_x bi-layer) and makes it technically viable at industrial level. Moreover, the SiO_x bi-layer is particularly interesting for DC01 substrate as the oxidation process is drastically reduced. Sheet to sheet and roll to roll processes could be compatible to ensure a low cost manufacturing.
- However, further work is necessary to better explore this hybrid approach, in terms of i) improvement of the F1 SiO_x sol-gel final quality and curing time and ii) the deposition of all kind of TFSC and iii) the reproducibility of the prototypes through a statistical process control.

The technologies analysed within the STEELPV project highlight the potential for the development of products oriented toward the BIPV market. By utilising the different steel thickness and IL options, STEELPV could potentially cater for a number of BIPV and Business to Business (B2B) interim product categories as shown in Figure 110.

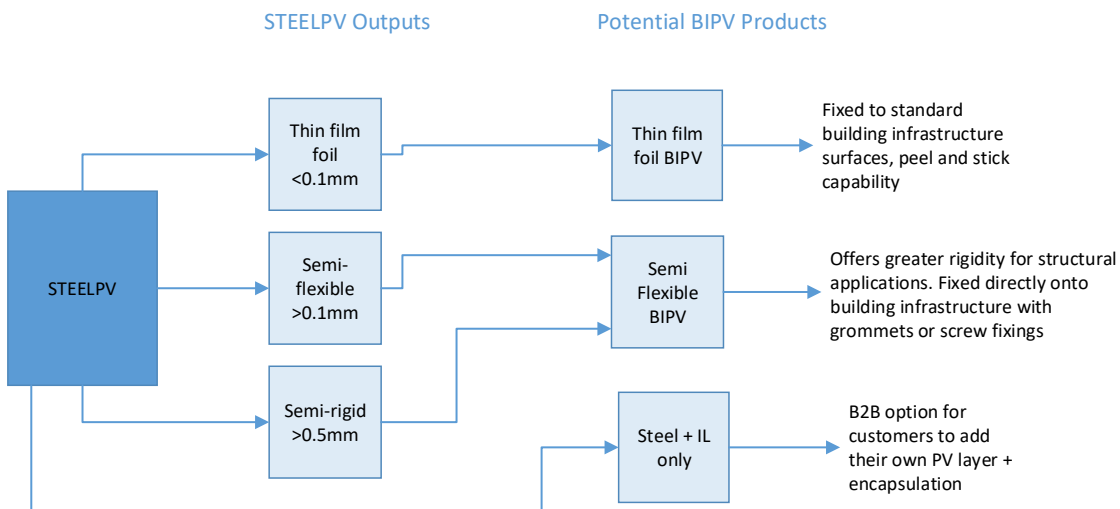


Figure 110. Potential STEELPV products

Economic potential

This section summarises the work reported in the deliverable D4.3 'Economic viability'.

Market study and evaluation

European directive 2010/31/EU [30] states that all buildings occupied by public authorities built after 31st December 2018 should be NZEB. The 2010/31/EU directive also states that all other new buildings must be NZEB by 31st December 2020 and that 3% of all public buildings have to be renovated. Moreover, a EuroAce work shows that if all existing buildings in Europe could be submitted to a retrofit until 2050, at least 5 million of annual buildings would be involved [31]. Cost effective BIPV, BIPVT and BAPV have the potential to provide an important component of this transition and enable organisations to comply with 2010/31/EU utilising the existing building infrastructure. The

market is currently supplied by three PV product categories: c-Si semi flexible, thin film on glass and thin film foil products. Thin film BIPV products offer a number of advantages over competing product categories namely: weight, flexibility and ease of installation. Furthermore these advantages open up the potential for BIPV, BIPVT and BAPV within the retrofit market where existing building materials have come to the end of their useful life or need replacing with an energy producing product. Retrofit projects impose restrictions on the choice of PV product in that many buildings may have weight restrictions for roof structures or possess limitations with regard to available surface areas for PV. Thin film BIPV can offer a cost effective solution to these types of projects where their inherent flexibility and light weight can work within the restrictions of the building infrastructure.

Many of the thin film BIPV manufacturers such as Hanergy/Miasole, Flisom and LQ Solar, incorporate R2R manufacturing processes that are deemed to offer the most cost effective method of manufacture with minimal levels of waste. This method of manufacture is key to any new market entrant. Currently, solar grade stainless steel substrates are used by a number of PV manufacturers such as Hanergy/Global Solar, Hanergy/Miasole, Sopray Solar and Flisom and UK based thin film manufacturer BIPVco. This aligns with the potential product offering from STEELPV and the opportunity to deliver cost savings against competing products via effective use of cheaper steel products incorporating an IL, in place of solar grade steel.

Cost analysis

The process followed to ascertain the costs involved in manufacturing a new BIPV product are set out in Figure 111. The process entailed the development of a cost model that adopted a bottom up approach in alignment with Anderson, where each of the individual cost elements were identified and included within the model [32]. The cost analysis was performed at the up-scaling stage of the IL coating processes where the technical viability of each of the IL options was established. The cost analysis assumes the utilisation of a modern R2R production facility to assure the most efficient and cost effective means to develop the BIPV products.

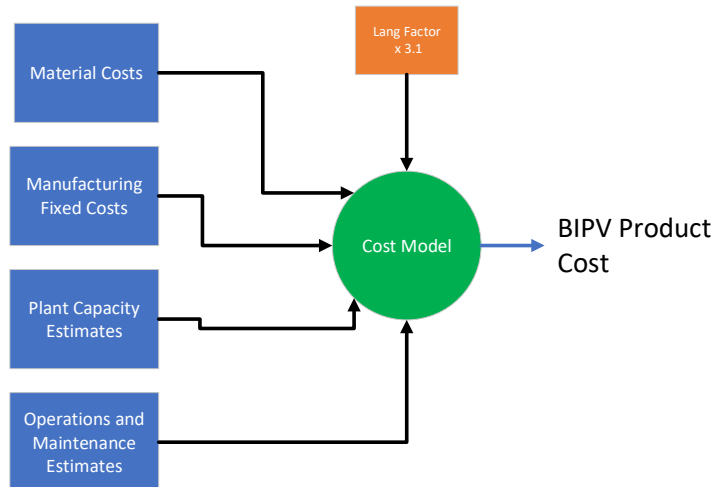


Figure 111. Cost model development process.

Manufacturing plant capacity calculations are based on a facility that can accommodate minimum BIPV production volumes of 30 MW/year [33,34]. This aligns with capacities of peer group manufacturers such as: Energy Conversion Devices Inc, (traded as Uni-Solar) that produced a-Si PV on flexible stainless steel substrates using a R2R process. Energy Conversion Devices operated a 30MW plant in 2003 [35,36]. At 10% efficiency 30 MW/year equates to approximately 1500m²/day of production (assuming 4 production days per week and 1 day of maintenance). This equates to 300,000 m² of annual production. Production line throughput is dependent on feed rate. Assuming a web width of 30 cm and a roll area of 500 m² (length≈1700 m), a feed rate of 5 m/min would take nearly six hours to process the roll, compared to approximately 1 hour at a feed rate of 30 m/min. For the IL coating processes, feed rate is largely determined by curing time and it is assumed that only one R2R line would be required for the coating process.

Raw steel pricing

Solar grade stainless steel is an established material for PV substrates but is expensive due to the high quality of steel used. Costs for this grade of steel are quoted as high as €36/kg at a thickness of 25 µm, equivalent to €8/m² [37]. The STEELPV project analysed the potential of a number of less refined rough steels as substrates for PV modules (AISI430, DX51D+Z, DX51SD+AS, and DC01 structural steels). The prices of each of the steel types in the context of €/kg and €/m² are presented in Figure 112.

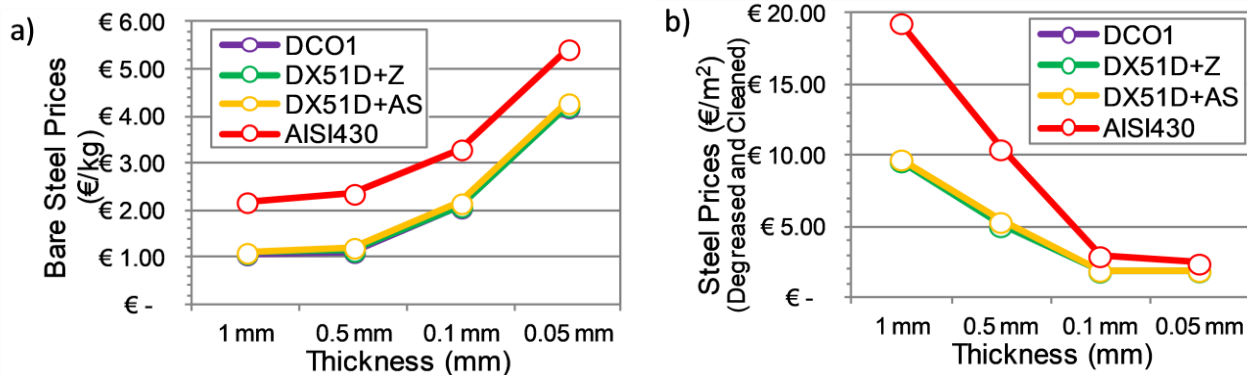


Figure 112. Steel prices: a) €/kg for bare steel; and b) €/m² for prepared steel ready for IL processing.

Intermediate Layer material costs

A number of different ILs were considered during the STEELPV project. Following detailed analysis at both laboratory and pilot-scale the two best candidates were: polymeric Blue Ink (D2140114D5, Gwent Electronic Materials Ltd) and SiO_x deposited by sol-gel to an in-house F1 formulation.

Table XXXIX presents the material costs and usage of Blue Ink and Sol-gel F1. Blue Ink is an expensive commercial product (although good volume discounts are available) whereas Sol-gel F1 is an in-house option. Blue Ink is applied by screen printing and has a low wastage, whereas Sol-gel F1 is applied by spray coating, which can be a wasteful process. Sol-gel F1 has a high proportion of volatile solvents, equating to a loss factor of 93%. The final materials costs are calculated as 1.80€/m² for Blue Ink and 0.33€/m² for Sol-gel F1.

Table XXXIX. IL material costs and usage.

IL Material	Coating thickness (µm)	Raw Material Cost (€/kg)	Wastage (coating process)	Volatile Loss	Material Usage (g/m ²)	Material Cost (€/kg) ^b	Material Cost (€/m ²)
Blue Ink	8	52.14	4%	30%	35.7	50.31	1.80
SolGel F1	3	3.04 ^a	45%	93%	79.8	4.13	0.33

^a including material processing costs (estimated at €1/kg).

^b including waste treatment costs (€1.18/kg, based on high temperature incineration of hazardous waste).

The feed rate for both IL materials has been estimated at 12m/min, taking 6.9 hours to process a 1500m² roll, or 2.3 hours for a 500m² roll (roll size dependant on material thickness). Table XL shows the processing costs for the ILs, including capital investment, labour and electricity and gives total processing costs (including materials) of 2.60€/m² for Blue Ink and 1.24€/m² for Sol-gel F1.

Table XL. IL processing costs.

IL Material	Capital Investment (€M)	Capital Investment (€/m ²)	Labour Cost (€/m ²)	Electricity Cost (€/m ²)	Processing Cost (€/m ²)	Total Processing Cost (including materials) (€/m ²)
Blue Ink	2.8	0.12	0.52	0.15	0.80	2.60
Sol-gel F1	5.3	0.23	0.52	0.15	0.91	1.24

Steel+IL Substrate Price – Comparison with the Stainless steel solar grade

Figure 113 presents the processed Steel+IL prices for Blue Ink and Sol-gel F1 for the different steel types and thicknesses. The SSSG target prices (8€/m²) is also shown, which gives an indication of which thicknesses would be financially viable. It is interesting to conclude that the steel/IL considered enable to significantly increase the thickness (up to 0.75mm if the IL is sol-gel F1) respecting to the stainless steel solar grade (0.025mm)

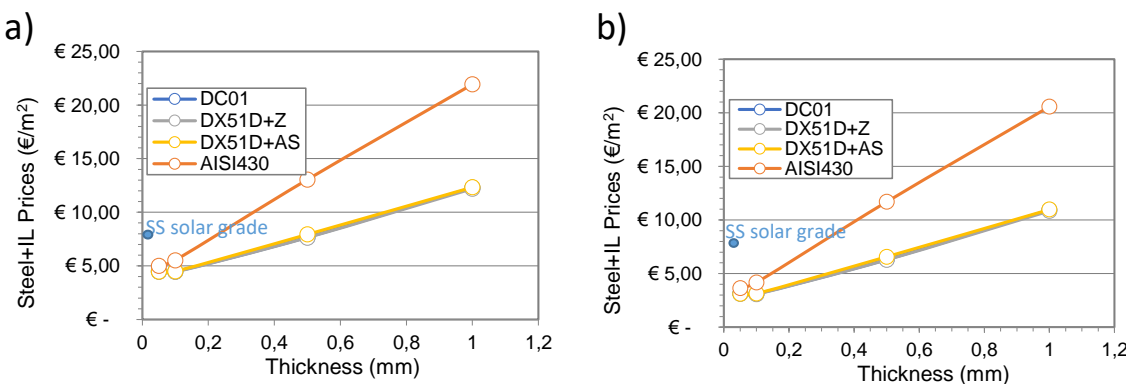


Figure 113. Steel+IL substrate prices showing the target prices for the stainless steel solar grade: a) Blue Ink and b) Sol-gel F1.

Steel+IL Substrate Price – Comparison with the maximum affordable Substrate Price depending on the TFSC technology

Prices for BIPV products cover a wide range depending on the product category and technology. The representative prices for thin film BIPV foil products obtained directly from PV manufacturers ranges between 1.05 – 3.74 (€/W_P) [38]. The range in prices reflect the different product specifications offered and the potential variance in prices depending on order quantities and discounts. The price for the FLEX01 thin film BIPV product from Switzerland based Flisom is representative, in that at 1.05 (€/W_P) this potentially fits the price point for STEELPV due to the product's similar characteristics and European manufacturing base.

From this price, PV manufacturing costs were estimated 0.5€/W_P with the substrate contributing (16-25%) [39]. The other 0.5€/W is mainly due to the balance of system (BoS), installation and power electronic [5]. Considering average PCEs for OPV and a-Si TFSC (6% and 10%, respectively) [40] and a global AM1.5 spectrum (1000 W/m²) at 25°C (IEC 60904-3:2003), maximum affordable substrate costs (Steel+IL) would be €6/m² for OPV and €10/m² for a-Si technologies.

Figure 114 presents the range of thickness of the steels+IL (IL= Blue Ink and Sol-gel F1) affordable for the OPV and a-Si TFSC technologies. Blue Ink is not suitable for OPVs as the roughness is too high (R_a =35-60nm, R_z =320-450nm).

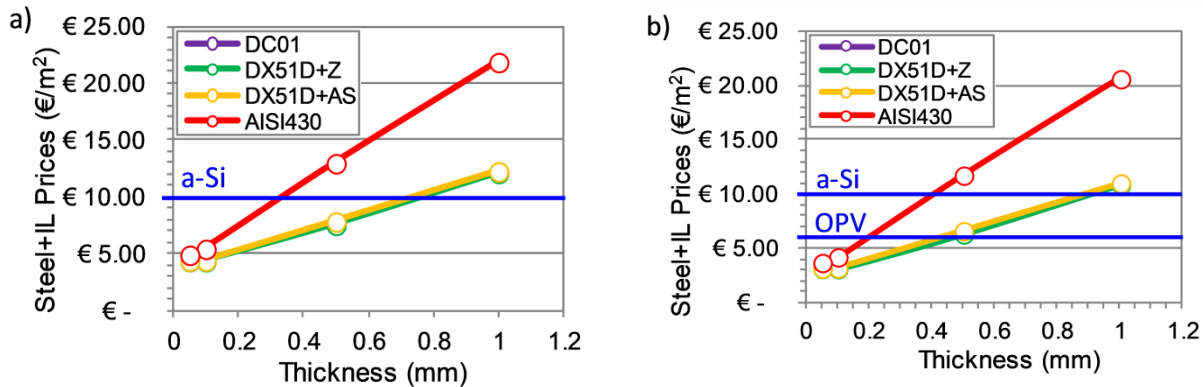


Figure 114. Steel+IL substrate prices showing the maximum substrate prices for PV technologies: a) Blue Ink (a-Si only); b) Sol-gel F1 (OPV & a-Si).

Table XLI summarises the maximum viable steel thicknesses for each steel/IL prototypes and PV technologies (based on a target PV module price of 1€/W_P and substrate/PV price of 0.5€/W_P).

Table XLI. Maximum viable steel thicknesses for the different IL coatings and suitable PV technologies

IL Material	PV Technology	Steel Type			
		DC01	DX51D+Z	DX51D+AS	AISI430
Blue Ink	a-Si (€10/m ²)	0.75 mm	0.75 mm	0.75 mm	0.35 mm
Sol-gel F1	OPV (€6/m ²)	0.45 mm	0.45 mm	0.45 mm	0.2 mm
	a-Si (€10/m ²)	0.9 mm	0.9 mm	0.9 mm	0.45 mm

The steel substrate thicknesses of STEELPV lend themselves to a number of categories of BIPV applications. As presented in Table XLII, Blue Ink and Sol-gel F1 IL coatings on all steel types are suitable for flexible foil (thickness $\leq 0.1\text{mm}$) and semi-flexible modules (thickness $>0.1\text{mm}$, $\leq 0.5\text{mm}$) for all suitable PV technologies and IL materials (Blue Ink: a-Si, Sol-gel F1: OPV & a-Si). For the DC01, DX51D+Z & DX51D+AS steels types both ILs with a-Si PV were suitable for semi-rigid modules (thickness $>0.5\text{mm}$).

Table XLII. STEELPV Suitability of different IL coatings for BIPV module production

IL Material	PV Technology	Steel Type			
		DC01	DX51D+Z	DX51D+AS	AISI430
Blue Ink	a-Si	flexible foil semi-flexible semi-rigid	flexible foil semi-flexible semi-rigid	flexible foil semi-flexible semi-rigid	flexible foil semi-flexible
Sol-gel F1	OPV	flexible foil semi-flexible	flexible foil semi-flexible	flexible foil semi-flexible	flexible foil semi-flexible
	a-Si	flexible foil semi-flexible semi-rigid	flexible foil semi-flexible semi-rigid	flexible foil semi-flexible semi-rigid	flexible foil semi-flexible

Business case and plan - The industrial viability of STEELPV can be further enhanced by exploring a number of potential business models that can exploit the use both the interim and final PV technologies. Figure 115 presents three potential options for STEELPV: Option A: Full lifecycle thin film BIPV manufacturer; Option B: Production of steel substrate and IL bonded to 3rd party supplied PV layer to form complete BIPV product; Option C: Manufacture of steel + IL for sale to 3rd party for thin film PV product manufacture. (Option C could in practice be a sub product of either option A or B).

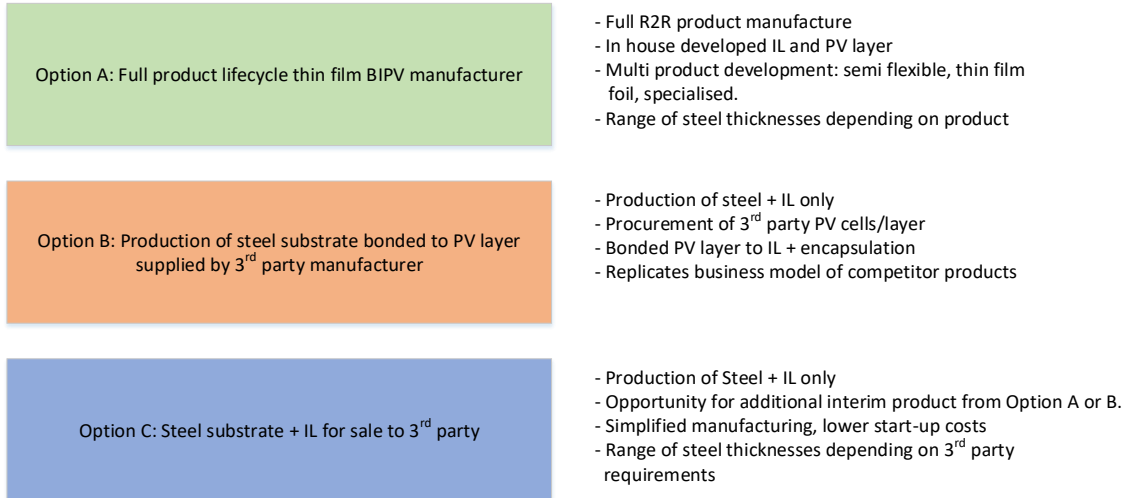


Figure 115. STEELPV business model options

Option A: Full lifecycle thin film BIPV manufacturer:

STEELPV products could offer cost efficiencies over competing BIPV manufacturers, assuming that full R2R product manufacturing was undertaken in house. The key innovation in the driving down of costs is the use of non-solar grade steel in the development of STEELPV products. This range of alternative steel substrates offers significant cost savings when compared to competing manufacturers that utilise more expensive solar grade steel types costed as high as 8€/m². This innovation could provide greater opportunity for more efficient cost control and greater scope to sustain downward market pressures over the short and medium term. The STEELPV cost model is based on the fit out and availability of a modern R2R manufacturing facility. This would entail a manufacturing process, whereby selected grade of coiled steel (AIS430, DX51D+Z, DX51D+AS and DC01) is processed/cleaned and effectively fed in at the start of the R2R process, then covered by an IL and finally a thin film PV product is directly deposited on the steel/IL following the TFSC industrial manufacturing (vacuum deposition steps for the a-Si:H and CIGS/CZTS solar cells and combination of wet and vacuum stages for OPV). The assumption here is that this process is managed in-house and that the STEELPV manufacturing facility is structured to perform all the necessary functions required for thin film product production. Ad-hoc photovoltaic panels size can be cut at the end of the TFSC deposition (so, until the end of the TFSC deposition, a coil is managed) or the steel/IL substrate could be cut just before the TFSC deposition.

Option B: Production of steel substrate and IL bonded to 3rd party PV

This option entails procuring the PV layer from a 3rd party manufacturer that would be bonded to the steel + IL to form the completed product. In this case the PV manufacturer does not apply the IL in its manufacturing plant. The PV manufacturer receives the steel/IL in coil or flat format and directly processes it as direct substrate in his TFSC manufacturing line. STEELPV would be utilising cheaper grades of steel, the additional cost of the procured PV layer could be mitigated whilst still producing a competitive product. The opportunities in this area and assessment of potential demand would require further analysis to ascertain the cost/benefit of this specific route to market. This business model option is currently used by PV product manufacturer BIPVco. BIPVco currently process their own substrate within their manufacturing facility and procure its PV cells from Hanergy subsidiary Miasole that are bonded to the substrate to form a complete PV product. The advantage to BIPVco is the utilisation of a known and industry tested technology and a simplified manufacturing process. Option B could present less risk for a new PV manufacturer with reduced costs and potentially faster time to market. However, the ability to control cost within the value chain in a very competitive market could be a significant constraint as PV prices continue to fall. The Option A model would be better able to compete in a cost constrained market but is likely to require higher initial investment than Option B for the additional components of the manufacturing process and resulting time to market.

Option C: Manufacture of steel + IL for sale to 3rd party Manufacturer

This business model options entails producing an interim manufactured steel + IL product for 3rd party PV organisations. PV manufacturers would procure the STEELPV interim product under license and add their own PV layer and encapsulation to complete the product manufacture. The benefit to 3rd party PV manufacturers could be a reduced R&D spend, simplified manufacturing process and more timely route to market. Adequately protecting IPR would need to be considered during the feasibility analysis of this option, but could offer an alternative funding stream for STEELPV. Option C could potentially be an alternative product offering for Options A and B as long as the manufacturing process is not unnecessarily complex, the technology can be adequately protected and the market exists for this interim type of product.

3.3. Publications/conferences

Publications already accepted and published

Z. Ding, V. Stoichkov, M. Horie, E. Brousseau, J. Kettle, "Spray coated silver nanowires as transparent electrodes in OPVs for Building Integrated Photovoltaics applications", Solar Energy Materials & Solar Cells, 157 (2016) 305–311.

Carmen López-López, Mari-Fe Menendez, Luis Andres Menendez, Armando Menendez, Pascal Sánchez, Maria D. Alba, Emilio Sánchez-Cortezon, Jose-Maria Delgado-Sanchez, "Enhancement of dielectric barrier layer properties by sol-gel and PECVD stacks", Surface & Coatings Technology, 305 (2016) 36–40.

Publication sent to peer reviews

S. Ghosh, L. Haponow, V. Stoichkov, Zhengfei Wei, T.M. Watson, A.L. Martinez, P. Sanchez, D. Gomez, J Kettle "New strategy for large area deposition of magnetite coating onto low carbon steel using polymeric encapsulating for solar absorber coatings", Thin solid films.

Publications in the phase of redaction

"Development of intermediate layer systems for direct deposition of thin film and organic solar cells onto low cost steel substrates" Possible review: Solar Energy Materials & Solar Cells.

Mari-Fe Menendez, Luis Andrés, Pascal Sanchez, Pablo García, David Gómez, Yun Lan "A path towards the use of new steels as direct substrates for TFSC; roll-to-roll functionalization", Possible review: Solar Energy Materials & Solar Cells.

L. Hughes, N. Bristow, P. Sanchez, D. Gómez, J. Kettle, D.T. Gethin "Assessing the potential of steel as a substrate for BIPV applications".

Conference presentations resulting from the project

STEELPV project and results achieved during the 42 months were disseminated in several European events (Table XLIII). Details of the disseminations are reported in the deliverables of WP5.

Table XLIII. Disseminations of STEELPV

Event	Date	Title	Author
Workshop: 'Steel Innovation for the Energy Sector' Spanish Steel Platform (Platea)	 Dec 2014	Thin Film in Photovoltaic Metallic substrates_ Oral presentation	ASNT
Workshop:'Printed Photovoltaics: from Materials to Manufacture' Sêr Solar_Specific	Apr 2015	SteelPV Sustainable Steels for Direct Deposition of Photovoltaic Solar Cells_ Poster presentation	BU

Event	Date	Title	Author
31 st EUPVSEC	 Sept 2015	A path towards the compatibility of flexible metallic substrate and thin film solar cells through intermediate layer ceramic stacks_ Poster presentation	ITMA
11 th Annual Technical conference _ Welsh Center for Printing and Coating	 Nov 2015	Formulation and Deposition of Intermediate Layers on Rough Steel Substrates for Large Area Solar Cells_ Oral presentation	SU
Innovative manufacturing in large area electronics	 Feb 2016	Electrode development for transparent OPVs and applications in BIPVs._ Poster presentation	BU
European Materials Research Society	 May 2016	Novel concept of barrier layer for OPV solar cells with optical performance enhancement. _ Poster presentation	ASNT
Progress in Photovoltaics, Materials and nanotechnology during H2020: EU PV clusters 3 rd work shop and general assembly	 May 2016	Sustainable steels for direct deposition of photovoltaic solar cells (STEELPV). _ Oral presentation	ITMA
32 nd EUPVSEC	 Jun 2016	Dielectric barrier layer: alternative materials and processing comparison for scalable PV technologies on rough steel substrates_ Poster presentation	ASNT
European conference on nanofilms	 Oct 2016	How to use commercial steels for direct solar application? A smart solution based on SiO _x sol-gel_ Oral presentation	ITMA
12 th Annual Technical conference _ Welsh Center for Printing and Coating	 Nov 2016	Challenges in printing smooth functional layers_ Oral presentation	SU
eGOPV conference	 Apr 2017	Application of flexible OPVs for building integration application_ Invited talk	BU
13th Photovoltaic Science Applications and Technology Conference (<u>PVSAT-13</u>)	 Apr 2017	Transparent Encapsulate on Steel Substrate" for BIPV application_ Poster presentation	BU
13 th Annual Technical conference _ Welsh Center for Printing and Coating	 Nov 2017	Up-scaling of combined planarizing and insulating layers on rough steel substrates for large area solar cells_ Oral presentation	SU

Organization of Workshops

Workshop session (Figure 116) took place at the 12th Photovoltaic Science, Application and Technology Conference (PVSAT) organised by the Solar Energy Society in Liverpool.

The figure shows two panels. The left panel is the conference program for PVSAT-12, organized by the Solar Energy Society (SES) and the University of Liverpool. It includes logos for IET Journals, SUPERGEN SuperSolar, and IOP Institute of Physics. The right panel shows a slide for 'Session 6 Chair: Stuart Irvine, Glyndwr University' from 16:15 – 17:45, titled 'STEEL PV Workshop'. A table lists five presentations:

Time	Session No.	Talk	Speaker	Title	Affiliation
16:15	6.1	Invited	Yulia Galagan	Thin film PV for Building Integration	TNO Holst, Netherlands
16:45	6.2	PVSAT-12_85	Joel Troughton	Efficient, flexible & low temperature perovskite solar cells on industrially applicable metal foils	SPECIFIC, Swansea University
17:00	6.3	Steel PV	Pascal Sanchez	Compatibility of 'rough' commercial steels with amorphous silicon solar cells; a smart solution based on SiO _x sol-gel	Fundacion ITMA, Spain
17:15	6.4	Steel PV	Maria del Carmen Lopez Lopez	Surface and electrical characterisation of dielectric thin films for barrier layer applications in CIGs solar cells	Abengoa Research, Spain
17:30	6.5	Steel PV	Jeff Kettle	Application of flexible OPVs for building integration applications	Bangor University

Figure 116. Oral presentations at the 12th Photovoltaic Science, Application and Technology conference (Liverpool_ April 2016). <http://www.pvsat.org.uk/>

Workshop session (Figure 117) took place at the European Materials Research Society (E-MRS) fall meeting 2017 in Warsaw.

The figure shows the E-MRS website interface. The top navigation bar includes 'My EMRS', 'Log-in / Create account', and links for 'About', 'Meetings', 'News & Events', 'Networking & Project'. Below the navigation is a menu for '2017 Spring', 'ICNS' 12', and '2017 Fall'. On the left, there's a sidebar with links for 'Symposia & program', 'Plenary session', 'Exhibition & Workshop', 'Satellite events', 'EMMC Workshop', 'NFFA Europe Workshop', 'STEELPV Workshop', 'Hotel reservation', and 'Practical information'. The main content area features a 'STEELPV Workshop' section with a diagram of a steel PV cell and text about the 'WORKSHOP: 'SUSTAINABLE STEELS CELLS' (STEELPV)'. To the right is a box titled 'Agenda' listing the workshop schedule:

Time	Event	Speaker
16:00	Welcome and presentation of the workshop (ITMA)	Dr. D. Gómez, ITMA Materials Technology, Spain
16:10	Short introduction to STEELPV	Dr. P. Sanchez, ITMA Materials Technology, Spain
16:20	Preparation of metallic substrates for BIPV	Dr. Y. Lan, MK Metallfolien GmbH, Germany
16:40	Development of intermediate layers for based on vacuum strategies	Dr. A. Belluci, CSM, Italy
17:00	Development of intermediate layers for based on SiO _x sol-gel	Dr. P. Sanchez, ITMA Materials Technology, Spain
17:20	Coating/printing techniques on steel substrates	Prof. D. T. Gethin, University of Swansea, UK
17:40	Applying OPVs/PSCs directly to steel	Dr. J. Kettle, University of Bangor, UK

At the bottom of the agenda box, there are logos for the European Union and the Research Fund for Coal and Steel (RFCS), with the text: 'The research leading to these results has received funding from the European Union's Research Fund for Coal and Steel (RFCS) research programme under grant agreement n° RFSR-CT-2014-00014'.

Figure 117. Oral presentations at the E-MRS 2017 fall meeting (Warsaw_ September 2017). <https://www.european-mrs.com/meetings/2017-fall-meeting>

3.4. Other aspects concerning the dissemination of the results

Created at the beginning of the project, the public and private part of the website (www.steelpv.eu) was regularly updated to disseminate project results and events as well as to promote an easy exchange between partners (technical and administrative data and documents). Figure 118 shows an overview of the final state of the public and private parts, displaying as example the presentations of the final STEELPV workshop.

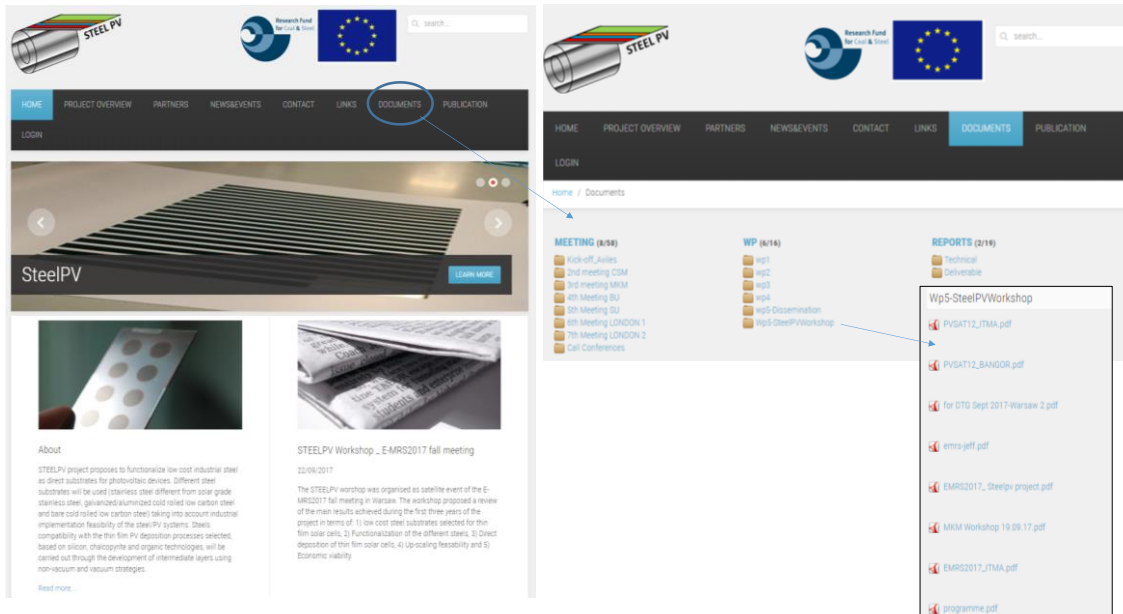


Figure 118. Picture of the STEELPV public and private parts (Final STEELPV workshop pdf presentations are displayed).

4. Conclusions

The aim of STEELPV was to develop steel/ILs prototypes to be used as direct substrates for TFSC. The main purpose of these steel/ILs prototypes are to offer lower cost alternatives to the current solar grade stainless steel substrate and to promote new steels for TFSC applications. *Table XLIV* shows the technically feasible STEELPV portfolio (pilot plant level).

Table XLIV. Pilot plant level STEELPV portfolio. *Theoretically as the IL have fulfilled all the STEELPV requirements. No TFSC has been deposited. **Deposition of a-Si TFSC and CZTS individual layers

	AISI430	DX51D+Z	DX51D+AS	DC01	Comments
F1 SiO_x sol-gel	✓	✓	✓	✓	<ul style="list-style-type: none"> • 30cm x 30cm prototypes • In-house formulation • Spray coating • Fast curing NIR • Low temperature TFSC
Blue ink	✓	✓	✓	✓	<ul style="list-style-type: none"> • 30cm x 30cm prototypes • Commercial formulation • Screen printing • Low temperature TFSC • Statistical process control
Hybrid Si₃N₄/SiO_x	✓	✗	✓	✗	<ul style="list-style-type: none"> • 10cm x 176cm prototypes • In-house formulation • PVD/Spray coating • All temperature TFSC*
Hybrid tri-SiO_x (PECVD)	✓	✗	✓	✓	<ul style="list-style-type: none"> • 10cm x 10cm prototypes • In-house formulation • Spray coating/ PECVD/ Spray coating • Fast curing NIR (1st layer) • All temperature TFSC**
Hybrid bi-SiO_x (PECVD)	✓	✗	✓	✓	<ul style="list-style-type: none"> • 10cm x 10cm prototypes • In-house formulation • Spray coating/PECVD • Fast curing NIR • All temperature TFSC*

Related to the economical aspect, a simulation of cost has been carried out considering the two best steel/IL candidates (IL= F1 SiO_x sol-gel and Blue ink). Maximum affordable substrate costs (Steel+IL) would be €6/m² for OPV and €10/m² for a-Si technologies.

Figure 119 presents the range of thickness of the steels+IL (IL= Blue Ink and Sol-gel F1) affordable for the OPV and a-Si TFSC technologies. It can be notified that, at the SSSG thickness, the steels/sol-gel prototypes enable to decrease the substrate cost in a 50% and the steels/blue ink prototypes in a 40%.

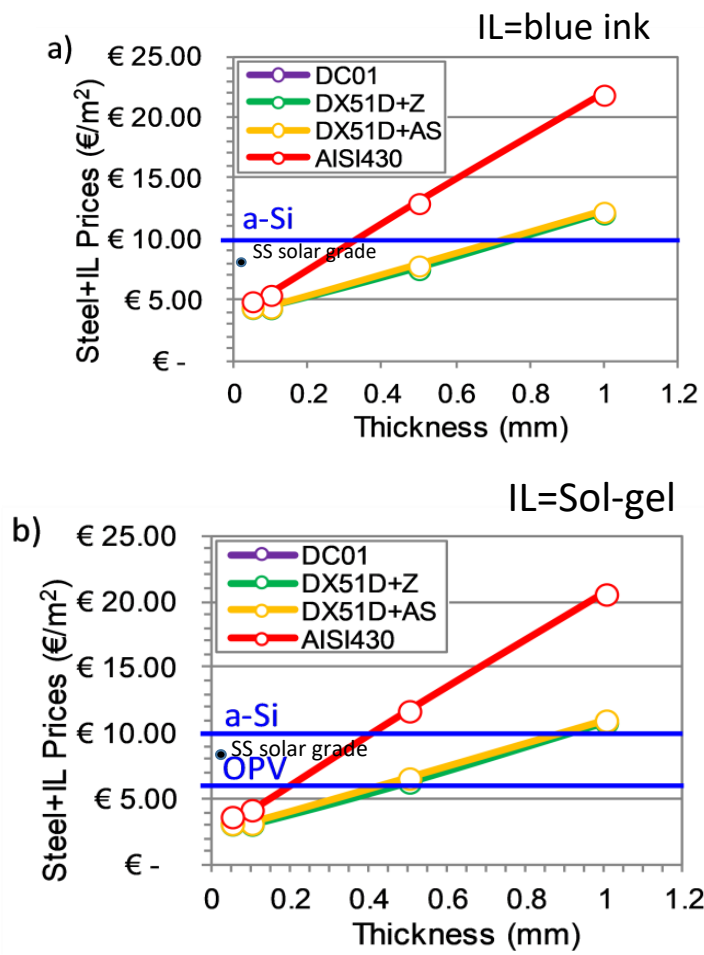


Figure 119. Steel+IL substrate prices showing the maximum substrate prices for PV technologies: a) Blue Ink (a-Si only); b) Sol-gel F1 (OPV & a-Si).

Table XLV summarises the maximum viable steel thicknesses for each steel/IL prototypes and PV technologies (based on a target PV module price of 1€/W_P and substrate/PV price of 0.5€/W_P).

Table XLV. Maximum viable steel thicknesses for the different IL coatings and suitable PV technologies

IL Material	PV Technology	Steel Type			
		DC01	DX51D+Z	DX51D+AS	AISI430
Blue Ink	a-Si (€10/m ²)	0.75 mm	0.75 mm	0.75 mm	0.35 mm
Sol-gel F1	OPV (€6/m ²)	0.45 mm	0.45 mm	0.45 mm	0.2 mm
	a-Si (€10/m ²)	0.9 mm	0.9 mm	0.9 mm	0.45 mm

List of figures

Figure 1. Steel substrates costs (€/m²) depending on the rolling final thickness. Comparison with the SSSG cost (at 25µm) and the maximum affordable substrate cost depending on the TFSC technology

Figure 2. Comparison of the levelling effect depending on the wet IL applied on AISI430 substrate

Figure 3. Comparison of the levelling effect depending on the hybrid IL applied on AISI430 substrate

Figure 4. Efficiency (%) of a-Si TFSC deposited on a reference substrate (Glass) and on different steel/IL systems.

Figure 5. Efficiency (%) of OPV TFSC deposited on a reference substrate (Glass, PET) and on different steel/IL systems.

Figure 6. Influence of the NIR power on the sol-gel hardness and desorption in high vacuum chamber (NIR curing time of 2'). Comparison with sol-gel cured by hotplate (HP).

Figure 7. Steel+IL substrate prices. Comparison with the SSSG price and the maximum affordable substrate prices for PV technologies: a) Blue Ink (a-Si only); b) Sol-gel F1 (OPV & a-Si).

Figure 8. Cost €/Ton and €/m² as function of the HSS rolling process for different types of steels. Evolution of price between Oct. 2014 and Jun. 2017. Prices include the rolling and degreasing and cleaning (15%) of the steels

Figure 9. Estimated substrate cost with different qualities

Figure 10. Dependence of substrate cost €/Wp on surface roughness/working rolls for different types of steels

Figure 11. Evolution of surface roughness of DC01 with firstly Cr-coated and then polished ASP-rolls

Figure 12. Metallic coatings homogeneity. 500x magnification optical microscopy images. a) DX51D+Z steel coil_outer side, b) DX51D+AS steel coil_outer side.

Figure 13. Macroscopic visual aspect of the AISI430 and DC01 steels after the annealing treatments.

Figure 14. Visual aspect of the AISI430. a) Initial materials; Small sample was rolled, b) after the thermal treatment (425°C – 30min_air), c) after the thermal treatment (425°C – 30min_air), sample 3 is rolled and annealed under reductive atmosphere.

Figure 15. Comparison of the steel substrates roughness between the lab-scale and up-scale formats.

Figure 16. Surface roughness comparison with 50 identical samples, each of them measured at 10 points.

Figure 17. Examples of roughness profiles of the four steel substrates.

Figure 18. Hydrolysis-condensation_sol-gel mechanisms.

Figure 19. Effect of PEG concentration and molecular weight on viscosity of PEG solutions _shear rate of 230 1/s.

Figure 20. Maximum IL SiO_x thickness with no delamination/crack and good homogeneity in 5cmx5cm samples: Influence of the coating technique

Figure 21. Roughness measured before and after the application of the F1 sol-gel IL by dip and spray coating.

Figure 22. Visual aspect of IL sol-gel single layer applied by K-Bar 3 coating onto AISI430: SPV38: F3-PEG10000, SPV39: F3-PEG200000, SPV40: F3-PEG400000.

Figure 23. Roughness measured before and after the application of the F3_PEG200000 sol-gel by K-Bar3 coating

Figure 24. Lab scale flexo tester IGT F1 and flexo prints of F1 and F3 sol-gel IL on four steel substrates.

Figure 25. Roughness (R_z) of flexo printed F1 sol-gel IL.

Figure 26. Roughness measured before and after the application of the F3 sol-gel by offset gravure printing

Figure 27. Roughness measured before and after the application of the F3 sol-gels by screen printing

Figure 28. Cracks developed during annealing for screen printed IL: a) F3_PEG200000 and b) F3_PEG400000 sol-gels.

Figure 29. Qualitative depth profiles of not annealed and annealed steels/SiO_x sol-gel samples.

Figure 30. P1 laser scribing considering a-Si and OPV TFSC back contacts.

Figure 31. Influence of the current intensity on the P1 scribe (a-Si TFSC back contact).

Figure 32. Influence on the current intensity on the P1 scribe (OPV TFSC back contact).

Figure 33. Roughness (Ra) determined after applying the different dielectric inks

Figure 34. Screen prints of blue dielectric IL on AISI430.

Figure 35. Visual aspect of the four AISI430 and DX51D+Z with blue ink _ Outdoor test after 3 months.

Figure 36. P1 scribe aspect and mechanical profile (a-Si back contact).

Figure 37. P1 scribe aspect and mechanical profile (OPV back contact)

Figure 38. White light interferometry measurements of (a) AISI430 before and (b) after application of SU-8 IL, (c) DC01 before and (d) after application of SU-8 IL, (e) DX51D+Z before and (f) after application of SU-8 IL and (g) DX51D+AS before and (h) after application of SU-8 IL. Area size is 6x8mm, with a z-axis scale of -50 to 50um

Figure 39. P1 scribe aspect and mechanical profile (a-Si back contact).

Figure 40. P1 scribe aspect and mechanical profile (OPV back contact)

Figure 41. Illustrations of the PVD and PECVD machines

Figure 42. Surface roughness after Al_xN_y deposition with different thickness on AISI430

Figure 43. Surface roughness of SiO_x on AISI430 deposited by PECVD

Figure 44. Comparison of R_z and R_a before and after PVD reactive and non reactive modes.

Figure 45. Surface roughness after TiO_x and AlN_x deposition on AISI430

Figure 46. Surface roughness reduction when SiO_x by PVD is deposited on 300nm of SiO_x/AISI430 deposited by PECVD

Figure 47. Proposed structures to study combined SiO_x layers deposited from sol-gel and PVD

Figure 48. On the left, surface roughness reduction obtained with sandwich structure (sol-gel/PVD/sol-gel) and visual inspection revealing cracks on the surface; on the right, surface roughness measured during the stacking of layers, as function of SiO_x thickness deposited by magnetron sputtering

Figure 49. Qualitative in-depth profiles of not annealed and annealed AISI430/hybrid SiO_x samples.

Figure 50. Influence of the current intensity on the P1 scribe.

Figure 51. Overlapping study. From left to right, 355nm, 532nm and 1064nm

Figure 52. SEM/EDX characterization of P1 scribes: Mo/barrier layer/SS using different laser wavelengths

Figure 53. P1 scribe aspect and mechanical profile (OPV back contact)

Figure 54. Visual aspect of the Si₃N₄/SiO_x hybrid IL. Mechanical profile of the Si₃N₄ coating (left part) and the Si₃N₄/SiO_x hybrid stack (right part).

Figure 55. Roughness measured before and after the application of of Si₃N₄ and the SiO_x F1 sol-gel by spray coating.

Figure 56. Scheme of IL electric insulation property test proposed and example of a real samples with different Al size pad and trial.

Figure 57. Example of breakdown voltage failure. Crater as results of short. DC01 substrate covered by sol-gel (spin coating) _ thickness 1.3±0.2μm.

Figure 58. Current Voltage measurement setup (left) to measure the current leakage across the IL by depositing a back electrode directly onto F2 SiO_x sol-gel-coated AISI430 steel

Figure 59. Mo pads onto the AISI430+SiO_x hybrid IL and scheme of the test.

Figure 60. Two rolls coating technique in a R2R process.

Figure 61. Roughness measured before and after the application of SiO_x sol-gel by two rolls coating in a R2R process. AISI430, DX51D+Z and DX51D+AS are considered.

Figure 62. Visual aspect of Al pads deposited on AISI430/SiO_x after applying 53V.

Figure 63. Visual aspect of the SiO_x F1 and F2 sol-gel coatings after shears cut.

Figure 64. Flexibility test procedure.

- Figure 65.** n-i-p a-Si TFSC developed on the steel/IL prototype
- Figure 66.** a-Si visual aspect and I-V curve achieved on a a-Si TFSC deposited on DX51D+Z/F2 sol-gel.
- Figure 67.** Example of four 1cm² a-Si TFSC grown on steel/polymeric 'blue ink'.
- Figure 68.** Example of four 1 cm² a-Si TFSC grown on AISI430/ hybrid SiOx
- Figure 69** Schematic of the OPV manufactured onto steel and OPV device onto DX51D+Z steel substrate with sol-gel F2
- Figure 70** Raman spectrum obtained for CZTS samples excited with 532nm laser source.
- Figure 71.**Schematic of perovskite solar cell fabricated on steel, an image of perovskite device on steel, and IV curve of PSC on DC01 (DC01/IL(SU-8)/TiO₂/MAPI/HTM/MoO₃/Au).
- Figure 72.** Visual aspect of the four steels with and without sol-gel_ Outdoor: time 0 and 3 months. Indoor: time 0 and 3 months.
- Figure 73.** a) Spray gun, b) spray system and c) Hotplate
- Figure 74.** Influence of the spray liquid pressure and spray scan's number on the SiOx thickness. Sol-gel dilution 1:0.5. Steel substrate: DC01. Samples of 30cm x30cm.
- Figure 75.** Influence of the spray liquid pressure and spray scan's number on the DC01/SiOx IL roughness. Sol-gel dilution 1:0.5. Steel substrate: DC01. Samples of 30cm x30cm
- Figure 76.** Visual aspect of the F1 SiOx sol-gel depending on the sol-gel liquid pressure (0.5bar and 0.4bar).
- Figure 77.** Roughness of the native steels (30cm x 30cm format) and after the F1 SiOx sol-gel application.
- Figure 78.** Dielectric test on 30cm x 30cm steel/F1 SiOx sol-gel prototypes. a) three 10cmx10cm tested, b) Ag pads for each 10cmx10cm samples.
- Figure 79.** In-depth profiles (GD-TOF-MS) of DC01/IL prototypes before and after the simulation of a a-Si TFSC (2h30-210°C in PECVD).
- Figure 80.** NIR principal and real steel/IL curing
- Figure 81.** Influence of the NIR curing time on the sol-gel hardness (power of 85%). Comparison with sol-gel cured by hotplate_HP (used as reference)
- Figure 82.** Influence of the NIR power on the sol-gel hardness and desorption in high vacuum chamber (NIR curing time of 2'). Comparison with sol-gel cured by hotplate (HP).
- Figure 83.** R2R pilot line with stand-alone Heraeus NIR unit (denoted by red rectangle)
- Figure 84.** Six AISI430/ F3_PEG200000 sol-gel samples: NIR (100%); 2 steps - 5 s and 10 s with an interval of 60 s.
- Figure 85.** AISI430/F3_PEG200000 IL and AISI430/F3_PEG400000 IL after photonic curing using different process parameters
- Figure 86.** Cracks in F3 SiOx sol-gel IL after Ag pad deposition by thermal evaporation: a) AISI430/F3_PEG400000 IL using K-bar 4, b) DC01/F3_PEG400000 IL using K-bar 4, DX51D+AS/F3_PEG400000 IL using K-bar 3
- Figure 87.** a) Flatbed screen printer, b) 30cmx30cm prototypes and c) Batch 1 after curing.
- Figure 88.** Roughness SPC_ Steel/Blue ink IL prototypes for four steels
- Figure 89.** Roughness SPC_Ra and Rz control charts for steel/Blue ink IL prototypes for four steels after the improvement of the steels' flatness.
- Figure 90.** Roughness SPC_ Ra and Rz control charts for steel/Blue ink IL prototypes for four steels. Coarser polyester mesh used
- Figure 91.** Blue ink prototype with Ag pads for breakdown voltage measurements.
- Figure 92.** AISI430 30 cm wide coil in the pilot plant line and after the application
- Figure 93.** Solvent Resistant Blue Dielectric Ink (D2140114D5): a) air bubbles generation in the rotary screen under constant shear, b) 3D-representation of craters left by bubbles bust during drying, c) 3D-representation of an individual crater left by a bubble bust during drying
- Figure 94.** Sample configuration for strip PVD coating
- Figure 95.** Si₃N₄ PVD coated strips
- Figure 96.** SEM-EDS characterization of coating (Si₃N₄ on AISI430 sample)

Figure 97. 10cm x 20cm steels/Si₃N₄ during the SiO_x sol-gel spray application and hot plate curing.

Figure 98. AISI430 processed at 0.2bar (liquid pressure) and AISI430 and DX51D+AS processed at 0.3bar (liquid pressure)

Figure 99. Visual aspect of the AISI430/Si₃N₄_SiO_x prototype; the SiO_x was cured at 500°C

Figure 100. In-depth qualitative element profile (GD-TOF-MS) of the AISI430/Si₃N₄_SiO_x prototype. Si₃N₄ and SiO_x were deposited/cured at 500°C

Figure 101. 10cm x 10cm AISI430 sample covered by F1 SiO_x sol-gel and cured up to 500°C. Bright field and dark field optical micrographs (magnification x100) of cracks defects.

Figure 102. Magnetron_Sputtering PVD and PECVD used for the vacuum SiO_x depositions.

Figure 103. Visual aspect of two tri-layer SiO_x prototypes deposited on AISI430 steel. a) sol-gel/PVD/sol-gel and b) sol-gel /PECVD/sol-gel.

Figure 104. X-ray diffractogram of SiO_x films at different temperature deposition.

Figure 105. Visual aspect of the three steels covered by the sol-gel (220°C)/PVD or PECVD/sol-gel (500°C).

Figure 106. Qualitative in-depth elemental profile of the AISI430/hybrid SiO_x tri-layer (vacuum one by PECVD)_GD-TOF-MS spectrometric method.

Figure 107. Visual aspect of the AISI430/SiO_x bi-layer and DC01/SiO_x bi-layer prototypes.

Figure 108. a) SiO_x tri-layer on AISI430 steel. First layer: SiO_x sol-gel cured up to 200°C by NIR, second layer: SiO_x by PECVD at 500°C and third layer: SiO_x sol-gel cured up to 500°C by hotplate, b) SiO_x bi-layer on AISI430 steel. First SiO_x sol-gel cured up to 200°C by NIR and second SiO_x by PECVD at 500°C

Figure 109. Scheme of a BIPVT system.

Figure 110. Potential STEELPV products

Figure 111. Cost model development process.

Figure 112. Steel prices: a) €/kg for bare steel; and b) €/m² for prepared steel ready for IL processing.

Figure 113. Steel+IL substrate prices showing the target prices for the stainless steel solar grade: a) Blue Ink and b) Sol-gel F1.

Figure 114. Steel+IL substrate prices showing the maximum substrate prices for PV technologies: a) Blue Ink (a-Si only); b) Sol-gel F1 (OPV & a-Si).

Figure 115. STEELPV business model options

Figure 116. Oral presentations at the 12th Photovoltaic Science, Application and Technology conference (Liverpool_ April 2016). <http://www.pvsat.org.uk/>

Figure 117. Oral presentations at the E-MRS 2017 fall meeting (Warsaw_ September 2017). <https://www.european-mrs.com/meetings/2017-fall-meeting>

Figure 118. Picture of the STEELPV public and private parts (Final STEELPV workshop pdf presentations are displayed).

Figure 119. Steel+IL substrate prices showing the maximum substrate prices for PV technologies: a) Blue Ink (a-Si only); b) Sol-gel F1 (OPV & a-Si).

List of tables

Table I. Percentage of metallic pad (18 pads tested) that passed the breakdown voltage test before and after flexibility experiments.

Table II. ILs, deposition processes and steels' size considered at the up-scale pilot plant level.

Table III. Pilot plant level STEELPV portfolio. *Theoretically, as the ILs have fulfilled all the STEELPV requirements. No TFSC was deposited.**Deposition of a-Si TFSC and CZTS individual layers

Table IV. Maximum viable steel thicknesses for the different IL coatings and suitable PV technologies

Table V. STEELPV Suitability of different IL coatings for BIPV module production

Table VI. Substrate selected.

Table VII. Chemical composition of steels proposed.

Table VIII. Mechanical and physical properties (first lab-scale delivery)

Table IX. Thermal treatments applied on the four rolled steels before their characterizations_ annealing time: 1 hour.

Table X. AISI430 steel properties considering several process conditions: 1) before the rolling process, 2) after the rolling process, 3) after the rolling and annealing processes.

Table XI. Evolution of the sol-gel viscosity at a speed rate of 100rpm.

Table XII. Compatibility of the different sol-gel solutions depending on the coating/printing techniques experimented at lab-scale level.

Table XIII. Combination of Steel/Polymeric commercial IL/application techniques successful for TFSC depositions and IL up-scaling.

Table XIV. Measure surface roughness (nm) by WLI and mechanical profilometry (MP) of steel grades selected in WP1 before and after IL coating with SU-8.

Table XV. Vacuum deposition techniques and materials considered

Table XVI. Process conditions during SiO_x by PECVD

Table XVII. Example of characterization test by SEM and FIB analyser_ Si₃N₄ IL on AISI430 steel.

Table XVIII. Example of characterization test by SEM and FIB analyser_ Si₃N₄ IL on AISI430 steel.

Table XIX. Vacuum deposition techniques and materials considered

Table XX. Deposition techniques and material considered

Table XXI. Summary of the dielectric tests carried out on the different IL.

Table XXII. Roughness of 0.1mm and 0.3mm steel substrates

Table XXIII. Critical thicknesses achieved taking into account the three steels and F1 and F2 formulations.

Table XXIV. Percentage of metallic pad (18 pads tested) that passed the breakdown voltage test before and after flexibility experiments.

Table XXV. Results of a-Si TFSC PCE on the different steel/ sol-gel IL prototypes. IL deposited by spin, dip and roll coating. Comparison of the influence of the curing method (hot-plate and convection). Comparison with a reference a-Si TFSC deposited on glass. J_{sc}: short circuit current density, V_{oc}: open circuit voltage, FF: fill factor.

Table XXVI. Comparison of OPV performance made on a range of competing substrates. J_{sc}: short circuit current density, V_{oc}: open circuit voltage, FF: fill factor.

Table XXVII. OPV device performance onto steel sample coated with SiO_x sol-gel. J_{sc}: short circuit current density, V_{oc}: open circuit voltage, FF: fill factor.

Table XXVIII. Steels/SiO_x sol-gel IL. Evaluation of integrity through the breakdown voltage

Table XXIX. Results of the breakdown voltage measures performed respectively after one, two and three months of storage in ITMA head location (Aviles, Spain). Before the storage tests all the coated sample support 53V.

Table XXX. Results of the breakdown voltage measurements performed by ITMA of the samples used by CSM for the storage test. Before the storage tests all the coated sample support 53V.

Table XXXI. ILs, deposition processes and steels' size considered at the up-scale pilot plant level.

Table XXXII. Percentage of pads that passed the dielectric tests (First procedure)

Table XXXIII. Roughness of dielectric ink ILs at pilot plant level

- Table XXXIV.** Summary of surface parameters for all samples
- Table XXXV.** Steel/Si₃N₄_F1 SiO_x sol-gel prototypes depending of spraying conditions
- Table XXXVI.** Percent crystallinity
- Table XXXVII.** Hybrid SiOx tri-layer prototypes_ Evaluation of the technical feasibility
- Table XXXVIII.** Hybrid SiOx bi-layer prototypes_ Evaluation of the technical feasibility
- Table XXXIX.** IL material costs and usage.
- Table XL.** IL processing costs.
- Table XLI.** Maximum viable steel thicknesses for the different IL coatings and suitable PV technologies
- Table XLII.** STEELPV Suitability of different IL coatings for BIPV module production
- Table XLIII.** Disseminations of STEELPV
- Table XLIV.** Pilot plant level STEELPV portfolio. *Theoretically as the IL have fulfilled all the STEELPV requirements. No TFSC has been deposited.**Deposition of a-Si TFSC and CZTS individual layers
- Table XLV.** Maximum viable steel thicknesses for the different IL coatings and suitable PV technologies

List of acronyms and abbreviations used in the report

a-Si:	Hydrogenated amorphous silicon
AS	Aluminium/Silicon
BAPV	Building attached photovoltaic
BIPV:	Building integrated photovoltaic
CCT	Critical cracking thickness
CIGS:	Copper Indium Gallium Selenium
CZTS	Copper Zinc Tin Selenium
CTE:	Coefficient of thermal expansion
FF	Fill factor
FIB	Focused ion beam
€/W _p	Watt-peak cost
GD	Glow discharge
HSS	High speed steel
ILs:	Intermediate layers
ITO	Indium tin oxide
Isc	Short circuit current
J _{sc}	Short circuit density
L _n	Evaluation length
MS	Mass spectrometry
MW	Microwave
MTES	Methyltriethoxysilane
NIR	Near infrared
NZEB	Near zero energy building
OPV:	Organic photovoltaic
PCE	Power conversion efficiency
PECVD:	Plasma enhanced chemical vapour deposition
PEG	Polyethylenglycol
PIB	Polyisobutylene
PV:	Photovoltaic
PVD	Physical vapour deposition
PVDF	Polyvinylidene fluoride
PVP	Polyvynilpyrrolidone
PSC	Perovskite solar cells
TCO:	Transparent conductive oxide
TFPV:	Thin film photovoltaic
TFSC:	Thin film solar cell
R _a :	Average arithmetic roughness
R _z :	Average peak-to-valley roughness
rf:	Radio frequency
R2R	Roll to roll
SEM	Scanning electron microscope
SS:	Stainless steel
S2S	Sheet to sheet
SSSG	Stainless steel solar grade
SPC	Statistical process control
SWOT	Strengths, weaknesses, opportunities, threats
TEOS	Tetraethylorthosilicate
VCI	Volatile Corrosion Inhibitor
V _{oc}	Open circuit voltage
WLI	White light interferometry

List of references

- [1] Europe's buildings under the microscope, Buildings Performance Institute Europe (BPIE), 2011
- [2] <https://ec.europa.eu/energy/en/topics/energy-efficiency/buildings>
- [3] EU Commission, Energy performance of building directive, Directive 2010/31/EU
- [4] EuroAce, EuroAce position on the EU efficiency Plan 2011
- [5] U.S. Department of Energy, *Advanced Research Projects Agency-Energy*, 2010
- [6] Horowitz, K, A, W, and Woodhouse, M, "Cost and potential of monolithic CIGS photovoltaic modules," *2015 IEEE 42nd Photovolt. Spec. Conf. PVSC 2015*, 2015.
- [7] Sinke, W, C, et al., "A Strategic Research Agenda for Photovoltaic Solar Energy Technology," No. PV-LAB-CONF-2007-004., 2007
- [8] Guglielmi, M., "Sol-Gel Coatings on Metals", *J. Sol-Gel Sci. Technol.* 8: 443-449 (1997).
- [9] Kozuka, H., "Stress evolution on gel-to-ceramic thin film conversion", *J. Sol-Gel Sci. Technol.* 40: 287-297 (2006).
- [10] Takemori, M., "Crack formation, exfoliation, and ridge formation in 500°C annealed sol-gel silica coatings on stainless steel SUS304: Part I. Microscopic observations and elemental analyses", *Ceram. International* 35: 1731-1746 (2009).
- [11] Innocenzi, P., Abdirashid, M.O., Guglielmi, M., "Structure and properties of Sol-Gel coatings from Methyltriethoxysilane and Tetraethoxysilane", *J. Sol-Gel Sci. Technol.* 3: 47-55 (1994)
- [12] J. Pisonero, B. Fernández, R. Pereiro, N. Bordel and A. Sanz-Medel, Glow-discharge spectrometry for direct analysis of thin and ultra-thin solid films, *Trends in Analytical Chemistry* 25 (2006) 11-18.
- [13] J. Pisonero, B. Fernández, D. Günther, Critical revision of GD-MS, LA-ICP-MS and SIMS as inorganic mass spectrometric techniques for direct solid analysis, *J. Anal. At. Spectrom.* 24 (2009) 1145-1160.
- [14] Löffler, J., et al., 2008. Monolithic series interconnection for thin-film silicon solar cells on steel foil. In: Proceeding at 23th EUPVSEV, Valencia (Spain), pp. 2285-2288
- [15]<http://www.woespana.es/weather/maps/city?LANG=es&WMO=08011&ART=MXMN&CONT=eses&R=0&LEVEL=150®ION=0005&LAND=SP&NOREGION=0&MOD=&TMX=&TMN=&SON=&PRE=&MONAT=&OFFS=&SORT=&MM=08&YY=2016&WEEK=12>
- [16] A. Shah et al, *Thin film silicon solar cell technology*, Progress in photovoltaics: research and applications, 2004, 12, 113-142.
- [17] Wang W, Winkler MT, Gunawan O, Gokmen T, Todorov TK, Zhu Y, Mitzi DB. Device characteristics of CZTSSe thin-film solar cells with 12.6%efficiency. *Advanced Energy Materials* 2013, DOI:10.1002/aenm.201301465
- [18] M. A. Green, K. Emery, Y. Hishikawa, W. Warta and E. D. Dunlop, *Prog. Photovoltaics*, 2015, 23, 1.
- [19] K. T. Butler, "Screening procedure for structurally and electronically matched contact layers for high-performance solar cells: hybrid perovskites," *J. Mater. Chem. C*, 2016, 4, 1149-1158, 2016.
- [20]<http://www.woespana.es/weather/maps/city?LANG=es&WMO=08011&ART=MXMN&CONT=eses&R=0&LEVEL=150®ION=0005&LAND=SP&NOREGION=0&MOD=&TMX=&TMN=&SON=&PRE=&MONAT=&OFFS=&SORT=&MM=08&YY=2016&WEEK=12>
- [21] R. A. Antunes, R. U. Ichikawa, L. G. Martinez, and I. Costa, "Characterization of Corrosion Products on Carbon Steel Exposed to Natural Weathering and to Accelerated Corrosion Tests," *International Journal of Corrosion*, 2014, 1, 2014. [doi: org/10.1155/2014/419570]
- [22] P. Wilhelm, "High-Temperature Corrosion of Steel in an ESEM With Subsequent Scale Characterisation by Raman Microscopy," *Oxid Met.*, 70, 257, 2008. [doi: 10.1007/s11085-008-9119-9]
- [23] R. Altobelli, I. Costa, D. Lúcia, and A. De Faria, "Characterization of Corrosion Products Formed on Steels in the First Months of Atmospheric Exposure," *Material Research*, 6 (3) 403-408, 2003.

-
- [24] G. Grundmeier, W. Schmidt, and M. Stratmann, "Corrosion protection by organic coatings: electrochemical mechanism and novel methods of investigation," *Electrochimica Acta*, 45, 2515–2533, 2000.
- [25] A. Amirudin and D. Thierry, "Application of electrochemical impedance spectroscopy to study the degradation of polymer-coated metals," *Progress in Organic Coating*, 9440 (95), 1–28 1995.
- [26] K. Hooper, et al., "Near Infrared Radiation as a Rapid Heating Technique for TiO₂ Films on Glass Mounted Dye-Sensitized Solar Cells," *Int. J. Photoenergy*, vol. 2014, (2014), 953623.
- [27] "EVA Application 11, 0, 0,3 SOCABIM Copyright © SOCABIM 1996-2005".
- [28] H. M. Rietveld, *Acta Cryst.* 20, 508(1966a). H. M. Rietveld, *Acta Cryst.* 21, A228 (1966b).
- [29] "Bruker AXS, TOPAS, Version 2.0 Copyright © 1999, 2000 Bruker AXS.
- [30] EU Comission, Energy performance of building directive, Directive 2010/31/EU
- [31] EuroAce, EuroAce position on the EU efficiency Plan 2011
- [32] Anderson J. Determining manufacturing costs. *Chem Eng Prog* 2009;105:27–31
- [33] Green MA, Emery K, Hishikawa Y, Warta W, Dunlop E, Levi D, et al. Solar cell efficiency tables (version 49). *Prog Photovolt Res Appl* 2017;25:3–13. doi:10.1002/pip
- [34] Zinßer B, Makrides G, Schubert MB, Georghiou GE, Werner JH. Temperature and irradiance effects on outdoor field performance. 24th EU Photovolt Spec Conf 2009:4083–6
- [35] Shuklar A., Sudhaker K, Baredar P. Recent advancement in BIPV product technologies: A review. *Energy Build* 2017;140:188–95. doi: 10.1016 / j.enbuild.2017.02.015
- [36] Dos-Santos I., Rüther R. The potential of building-integrated (BIPV) and building-applied photovoltaics (BAPV) in single-family, urban residences at low latitudes in Brazil. *Energy Build* 2012;50:290–7. doi:10.1016/j.enbuild.2012.03.052
- [37] MK Metallfolien GmbH. private communication. 2017
- [38] Alibaba n.d
- [39] Schmela M. Global Market Outlook: Solar Power Europe. 2016. doi:http://www.solarpowereurope.org/fileadmin/user_upload/documents/Events/SolarPower_Webinar_Global_Market_Outlook.pdf
- [40] Green MA, Emery K, Hishikawa Y, Warta W, Dunlop ED, Levi D, et al. Solar cell efficiency tables (version 49). *Prog Photovolt Res Appl* 2017;25:3–13. doi:10.1002/pip.2855.

Getting in touch with the EU

In person

All over the European Union there are hundreds of Europe Direct information centres. You can find the address of the centre nearest you at: https://europa.eu/european-union/contact_en

On the phone or by email

Europe Direct is a service that answers your questions about the European Union. You can contact this service:

- by freephone: 00 800 6 7 8 9 10 11 (certain operators may charge for these calls),
- at the following standard number: +32 22999696 or
- by email via: https://europa.eu/european-union/contact_en

Finding information about the EU

Online

Information about the European Union in all the official languages of the EU is available on the Europa website

at: https://europa.eu/european-union/index_en

EU publications

You can download or order free and priced EU publications at:

<https://publications.europa.eu/en/publications>. Multiple copies of free publications may be obtained by contacting Europe Direct or your local information centre (see https://europa.eu/european-union/contact_en).

EU law and related documents

For access to legal information from the EU, including all EU law since 1952 in all the official language versions,

go to EUR-Lex at: <http://eur-lex.europa.eu>

Open data from the EU

The EU Open Data Portal (<http://data.europa.eu/euodp/en>) provides access to datasets from the EU. Data can be downloaded and reused for free, for both commercial and non-commercial purposes.

The aim of STEELPV was to develop steel/intermediate layers prototypes to be used as direct substrates for TFSC. The main purpose of those prototypes are to offer lower cost alternatives to the current solar grade stainless steel substrate (25µm) and to promote new steels thicknesses for TFSC applications.

Four low cost steel substrates were selected and, after a low cost rolling process, several intermediate layers approaches (wet, vacuum and hybrid) were studied at lab-scale and pilot plant levels.

From the Technical feasibility, steel/SiO_x sol-gel and steel/dielectric ink were the two best options to fulfil the levelling, dielectric, anti-diffusion and stability ILs' requirements and matched with the a-Si and OPV TFSC. Spray coating and screen printing were used at pilot plant level and the NIR fast curing technique was explored. The hybrid options are technically more complicated but provide an interesting solution for high temperatures' TFSC (CIGS/CZTS).

Related to the economical aspect, a simulation of costs has been carried out considering the steel/IL wet approach candidates (IL= F1 SiO_x sol-gel and Blue ink).

Considering the reference stainless steel solar grade thickness (30µm), the steel/sol-gel prototypes enable to decrease the substrate cost in a 50% and the steel/blue ink prototypes in a 40%.

Considering the maximum affordable substrate costs of 6€/m² for OPV and 10€/m² for a-Si technologies, a range of thickness from 0.2mm to 0.9mm was determined depending on the steel selected. This range of thickness offers the possibility to propose lower cost as well as flexible (<0.1mm), semi-flexible (<0.5mm) and semi-rigid (>0.5mm) new products.

Finally, through a business case study, several production options were proposed and discussed.

Studies and reports

